UNIVERSITY OF CALIFORNIA,
IRVINE

Advancing Human Skin Equivalents Using Single Cell RNA Sequencing Technologies

DISSERTATION

submitted in partial satisfaction of the requirements
for the degree of

DOCTOR OF PHILOSOPHY

in Biological Sciences

by

Adam Roy Stabell

Dissertation Committee:
Associate Professor Scott Atwood, Chair
Professor Xing Dai
Assistant Professor Dae Seok Eom

2023

DEDICATION

To

my parents and siblings,
for always encouraging and putting up with me

my friends near and far,
for making this journey all the more enjoyable

my extended family,
for all the support and love you've provided

Katie Redford,
without whom none of this would have been possible

This is as much your accomplishment as it is mine.

"The only way to do great work is to love what you do. If you haven't found it yet, keep looking. Don't settle." – Steve Jobs

TABLE OF CONTENTS

LIST OF FIGURES

ACKNOWLEDGEMENTS

To my dissertation advisor, Scott Atwood, Ph.D., thank you for giving me the opportunity to learn and develop as a scientist in your lab. I've been able to develop a lot of life skills that I will now be able to carry into my future career.

To my current and past committee members, Xing Dai, Ph.D., Dae Seok Eom, Ph.D., Maksim Plikus, Ph.D., and Kai Kassenbrock, Ph.D., thank you for your time, support, and guidance on my projects.

To my labmates, past and present, Tuyen Nguyen, Eric Tarapore, Rachel Chow-Gutierrez, Kirsten Wong, Emmanuel Dollinger, Yunlong Jia, Lulu Lai, Gavin Long, Venus Sosa Iglesias, and Nick Bradbury, thank you for all of your support throughout the years. You all have made coming into lab that much more enjoyable. It wouldn't have been as fun without you.

To my undergraduate student mentees, Grace Lee, Alexia Dizon, Haley De Ocampo, and Sandrine Nguyen, thank you for all your help with the various projects I was working on. I wish each of you all the best with your future endeavors.

To my graduate advisor, Christine Süetterlin, Ph.D., thank you for all of your support and guidance through some of the most stressful moments of grad school.

To the love of my life, Kaitlyn Redford, thank you for your unwavering support through all our years together. The past several years have been the best of my life, and I can't wait to see what our future holds.

Chapter 2 of this dissertation is a reprint of the material as it appears in Stabell, A. R., et al. Single-cell transcriptomics of human-skin-equivalent organoids. Cell Rep. 2023, used with permission from Cell Press. Adam Stabell and Scott Atwood conceived the project. Scott Atwood supervised research. Adam Stabell generated and analyzed scRNA-seq libraries. Shuxiong Wang performed SoptSC for lineage and entropy analysis. Adam Stabell, Sandrine Nguyen, Yunlong Jia, Kirsten Wong, and Grace Lee performed imaging experiments. J.L. and George Sen performed xenograft experiments. Yunlong Jia performed hypoxia experiments. Adam Stabell, Qing Nie, and Scott Atwood analyzed and interpreted data. Adam Stabell and Scott Atwood wrote the manuscript. All authors analyzed and discussed the results and commented on the manuscript.

This work was made possible by several sources. S.X.A. is supported by NIH grant R01CA237563 and NSF grant CBET2134916. Q.N. is supported by NIH grants U01AR07315 and R01GM123731, an NSF grant DMS11763272, and a Simons Foundation grant 594598. A.S. is supported by NIH National Institute of Arthritis and Musculoskeletal and Skin Diseases (NIAMS) training grant AR080622. K.W. is supported by NIH National Cancer Institute (NCI) training grant CA009054. I would also like to acknowledge the support of the Chao Family Comprehensive Cancer Center Genomics High-Throughput Facility and Optical Biology Core Shared Resource, supported by the NCI of the NIH under award number P30CA062203, and the UCI Skin Biology Resource Center supported by NIAMS under award number P30AR075047. We also thank Jennifer M. Bates and the UCI Institute for Immunology Flow Cytometry Core Facility for help with cell sorting and Bryan K. Sun for comments on the manuscript.

VITA

Adam Stabell

Education

- Ph.D. in Biological Sciences, University of California, Irvine, 2023
- Data Analytics Bootcamp, University at California, Irvine - DCE, 2021
- B.S. in Biochemistry and Molecular Biology, University at Albany, 2017

Presentations

- UCI Center for Multiscale Cell Fate Research Symposium, Poster Presentation, 10/2022
- UCI P30-funded Skin Club, Oral Presentation, 02/2020, 04/2021, 03/2022
- UCI Center for Multiscale Cell Fate Research Annual Symposium, Poster Presentation, 10/2021
- UCI Dept. of Developmental and Cell Biology RIP talk, Oral Presentation, 06/2021
- Society for Investigative Dermatology Annual Meeting, Oral Presentation, 05/2020
- American Society for Cell Biology, Poster Presentation, 12/2019

Publications

- Wong K.N., **Stabell A.R.**, Lum L., Rafi R., England W. E., Spitale R. C., Atwood S. X. (2023) The role of the immune microenvironment in spontaneously regressing murine basal cell carcinoma. In preparation.
- **Stabell, A. R.,** Wang, S., Lee, G. E., Ling, J., Nguyen, S. D., Sen, G. L., Nie, Q., & Atwood, S. X. (2023) Single cell transcriptomics of human skin equivalent organoids. *Cell Reports*.
- Cang, Z., Zhao, Y., Almet, A. A., **Stabell, A.,** Ramos, R., Plikus, M. V., Atwood, S. X., & Nie, Q. (2023). Screening cell-cell communication in spatial transcriptomics via collective optimal transport. *Nature methods*.
- Wang, S., Drummond, M. L., Guerrero-Juarez, C. F., Tarapore, E., MacLean, A. L., **Stabell, A. R.,** Wu, S. C., Gutierrez, G., That, B. T., Benavente, C. A., Nie, Q., & Atwood, S. X. (2020). Single cell transcriptomics of human epidermis identifies basal stem cell transition states. Nature communications.
- O'Keefe, K. J., DeSantis, K. A., Altrieth, A. L., Nelson, D. A., Taroc, E. Z. M., **Stabell, A. R.,** Pham, M. T., & Larsen, M. (2020). Regional Differences following Partial Salivary Gland Resection. *Journal of dental research*.
- DeSantis, K. A., **Stabell, A. R.,** Spitzer, D. C., O'Keefe, K. J., Nelson, D. A., & Larsen, M. (2017). RARα and RARγ reciprocally control $K5^+$ progenitor cell expansion in developing salivary glands. *Organogenesis*.

Awards and Recognition

- Brian G. Atwood '74 and Lynne H. Edminster Graduate Studies Endowment 05/23
- T32 Training Grant 10/22 – 09/23
- NSF-Simons Center for Multiscale Cell Fate Research Graduate Fellow 07/21 – 06/23
- American Society for Cell Biology (ASCB) Travel Award 09/19
- Graduate Assisstance in Areas of National Need (GAANN) Fellowship 10/18 – 09/19

ABSTRACT OF THE DISSERTATION

Advancing Human Skin Equivalents Using Single Cell RNA Sequencing Technologies

by

Adam Roy Stabell

Doctor of Philosophy in Biological Sciences

University of California, Irvine, 2023

Associate Professor Scott Atwood, Chair

In the study conducted, the histological and cellular characteristics of human skin equivalents (HSEs) were explored. These HSEs were created by seeding primary human keratinocytes on devitalized human dermis, treated with either Matrigel (GelHSE) or primary human dermal fibroblasts (FibHSE). A histological analysis was performed revealing similarities between HSEs and in vivo human epidermis, with notable differences such as a thicker living epidermal layer in FibHSEs and reduced keratinocyte proliferation.

Cellular states of keratinocytes from 28-day old HSEs were identified using droplet-enabled scRNA-seq. These transcriptomes were similar to in vivo states, but unique gene expression patterns were identified, including a novel cell state, HSE-1, primarily in the GelHSE cultures.

Despite the predominantly normal histology of HSEs, abnormalities such as an expansion of KRT14+ cell layers and disrupted epidermal differentiation were present. Evidence of a partial epithelial-to-mesenchymal transition (EMT) state was detected, and the expression of the PSCA gene in the HSE-1 cluster was observed, suggesting a residual embryonic program in the culture medium. An examination of the lineage trajectory of HSE epidermal differentiation was conducted, revealing two abnormalities: differentiated keratinocytes retained much of the basal keratinocytes'

gene expression signature and the GelHSE keratinocytes followed a basal to spinous to HSE-unique lineage. All of these changes were evident at the RNA and protein levels.

To address these abnormalities, HSEs were xenografted onto mice, leading to the emergence of three xenograft-specific clusters alongside the expected keratinocyte clusters. This process was found to partially rectify terminal differentiation, cell-cell adhesion, and basal programs, yet it also revealed two distinct transcriptional paths from basal to granular keratinocytes. Hypoxia was identified as a potential driver of the transcriptional changes observed in the xenograft-specific cells. The conducted research has enhanced the understanding of the cellular states and differentiation paths in HSEs and has suggested potential strategies for their enhancement, such as hypoxic culturing and xenografting.

Chapter 1

Introduction

Summary

Human skin, the body's largest organ, is a complex and multifaceted system that serves as the first line of defense against environmental insults[1–6]. It plays a critical role in various physiological functions, including temperature regulation, sensation, and the synthesis of vitamin D[1,2,6]. The skin is composed of multiple layers, each with distinct cellular compositions and functions. The outermost layer, the epidermis, is primarily composed of keratinocytes but also includes melanocytes and Langerhans cells[3,4]. The dermis, located beneath the epidermis, contains fibroblasts and immune cells as well as nerve endings, blood vessels, hair follicles and sweat glands[1–3]. The deepest layer, the hypodermis or subcutaneous tissue, is primarily composed of adipocytes[1,7]. Several models for studying skin exist such as 2D cell cultures, 3D organoids, and in vivo mouse models, each possessing their own strengths and limitations. These model systems have allowed researchers to study skin development, maintenance, wound repair, and diseases[8,9]. While these skin models have made advances in our understanding of skin biology possible, improving the fidelity of skin models will provide tremendous benefit to researchers and clinicians.

The Epidermis

The epidermis forms the direct barrier between the external environment and the body's internal structures. It is composed of several types of cells, including epithelial cells called keratinocytes, neural-crest derived melanocytes, and resident immune cells called Langerhans cells[3,4]. The epidermis can be further subdivided into layers, arranged from the innermost basal layer followed by the spinous, granular, and finally the outermost cornified layer[3]. Keratinocytes are continuously produced by the epidermal stem cells that reside in the basal layer of the epidermis and gradually move upwards to the surface as they terminally differentiate and ultimately shed as part of the natural skin renewal process[3,10]. Keratinocytes form the majority (over 90%) of the cells in the epidermis and are responsible for the tough and durable nature of the skin.

Within the basal layer, melanocytes are also present. Melanocytes are responsible for the production, storage, and transfer of a pigment called melanin, which determines the color of the skin, hair, and eyes[4]. Melanin helps to protect the skin from the harmful effects of ultraviolet (UV) radiation by absorbing and scattering the radiation and serving as an antioxidant[11]. Melanocytes have a dendritic morphology with long, branching protrusions extending between keratinocytes. Melanin synthesis occurs within the melanocytes' melanogenic organelles, known as melanosomes. These melanosomes are exocytosed by the melanocytes and subsequently endocytosed by the surrounding keratinocytes, transferring melanin between these two cell types.

Langerhans cells, specialized immune cells localized primarily to the suprabasal layers of the epidermis, play a role in the immune response, protecting the body from harmful pathogens and foreign substances that may enter through the skin[12]. Langerhans cells recognize and capture antigens, which are foreign substances from pathogens such as bacteria or viruses, and then

present them to other immune cells, initiating an immune response. Langerhans cells also play a role in regulating the body's immune response to harmless substances, such as allergens, preventing the development of allergies or autoimmune diseases.

Our understanding of the cellular heterogeneity of the skin and the complex interplay of its constituent cell types remains incomplete; however, several studies have found strong evidence to support that many of the skin's cell types are more heterogeneous than previously thought[13–17]. Basal keratinocytes exhibit a high degree of transcriptional and spatial heterogeneity, with at least four distinct populations identified[16]. These populations are located at specific positions within the epidermis: at the top and bottom of structures known as Rete ridges and at transitional positions between the basal and suprabasal epidermal layers. Rete ridges, also known as epidermal ridges or rete pegs, are downward projections of the epidermis into the dermis[18]. Alongside dermal papillae, Rete ridges create an undulating pattern along the dermal-epidermal junction, the interface between the epidermis and dermis, and together increase the surface area for exchange between these two skin layers. The localization of these distinct basal stem cell populations in relation to Rete ridges suggests a spatial organization that may be linked to their specific roles in skin renewal and maintenance.

The differentiation of basal stem cells follows a hierarchical lineage. This lineage, as suggested by pseudotime, RNA velocity, and cellular entropy analyses, supports models of multi-stem cell interfollicular epidermal homeostasis[16]. In these models, a diverse pool of stem cells contributes to the maintenance and renewal of the epidermis, ensuring a constant supply of new cells to replace those that are shed or damaged.

Keratinocytes are not only present in the interfollicular epidermis but also play crucial roles in the structure and function of hair follicles and sweat glands. In hair follicles, keratinocytes are found in the outer root sheath (ORS), inner root sheath (IRS), and the hair shaft[3,14]. The ORS keratinocytes are continuous with the basal layer of the interfollicular epidermis and contain a population of hair follicle stem cells in the bulge region. These stem cells are responsible for the cyclical growth (anagen), regression (catagen), and rest (telogen) phases of the hair follicle. The IRS keratinocytes, on the other hand, provide structural support and help guide the growing hair shaft, which is also composed of keratinocytes that undergo a specialized form of apoptosis to form the hair. Sweat glands, specifically eccrine sweat glands, are also composed of specialized keratinocytes. The secretory portion of the sweat gland, located in the dermis, contains secretory cells that produce the sweat, while the duct portion, which extends to the surface of the skin, is lined with ductal keratinocytes[4]. These ductal cells play a crucial role in modifying the primary sweat produced by the secretory cells, contributing to the final composition of sweat that is released onto the skin surface.

The development of hair follicles and eccrine sweat glands in the skin is a complex process that involves a series of tightly regulated morphogenetic events and signaling pathways[19–22]. Hair follicle development, or folliculogenesis, begins in the embryonic skin with the formation of placodes, which are thickened areas of the epidermis that mark the future sites of hair follicles. These placodes form in response to signaling molecules, such as Wnts and fibroblast growth factors (FGFs), from the underlying dermis[20]. The placodes then invaginate into the dermis, forming a hair germ that continues to proliferate and differentiate into the various components of the hair follicle, including the hair shaft, inner root sheath, and outer root sheath. This process is regulated by a variety of signaling pathways, including the Wnt, FGF, Notch, and Hedgehog pathways[14,20,23].

Sweat gland development begins later in embryogenesis than hair follicle development[24]. Similar to hair follicles, sweat gland development is initiated by the formation of placodes in the epidermis. These placodes invaginate into the dermis to form a sweat gland germ, which then undergoes coiling morphogenesis to form the ductal and secretory portions of the sweat gland. The development of sweat glands is regulated by several signaling pathways, including the Wnt and FGF pathways. Unlike hair follicles, sweat glands do not undergo cyclical changes and are thought to be maintained by a slow-cycling population of stem cells.

Both hair follicles and sweat glands are associated with a specialized population of mesenchymal cells in the dermis, known as the dermal papilla for hair follicles and the dermal sweat gland pad for sweat glands[3,4,24]. These dermal cells play a crucial role in the development and function of hair follicles and sweat glands by providing signals that regulate the behavior of the overlying epithelial cells.

It's important to note that the keratinocytes in hair follicles and sweat glands are distinct from those in the interfollicular epidermis and from each other, both in terms of their gene expression profiles and their functions[3,14,16]. These structures extend into the dermis and interact with the various cell types there, but their cellular components are primarily derived from epidermal cells. This diversity of keratinocytes within the skin underscores the complexity of this organ and the intricate coordination required to maintain its various functions. Understanding the diversity of keratinocytes and their specific roles in different skin structures is crucial for understanding skin biology and for developing treatments for skin diseases.

The Dermis

The dermis, located beneath the epidermis, is a thick layer of connective tissue that provides strength and elasticity to the skin[4]. It plays a crucial role in skin homeostasis, contributing to functions such as temperature regulation, sensation, and the provision of nutrients to the skin. The dermis houses a diverse array of cell types, including fibroblasts, which produce the extracellular matrix, as well as immune cells, endothelial cells forming the blood vessels, nerve cells, and cells of the hair follicles and sweat glands, all of which interact to maintain skin health and functionality.

The primary cell type in the dermis is the fibroblast[1,4,6]. These cells are responsible for the production of the extracellular matrix, a complex network of collagen and elastin fibers that provides structural support and elasticity to the skin. Collagen fibers confer tensile strength, preventing the skin from being torn or otherwise damaged by mechanical stress, while elastin fibers allow the skin to return to its original shape after being stretched or compressed. Fibroblasts also secrete growth factors that regulate the proliferation and differentiation of keratinocytes in the epidermis, thereby influencing the renewal and repair of the skin's outer layer.

Various immune cells, including mast cells, macrophages, and T cells also reside within the dermis[1,4,6]. Mast cells are involved in the skin's immune response, releasing histamines in response to injury or allergens, which leads to inflammation and itchiness. Macrophages are phagocytic cells that engulf and destroy pathogens and cellular debris, playing a crucial role in wound healing and immune defense. T cells, on the other hand, regulate immune responses and can directly kill infected cells, playing a key role in protecting the body from infections.

In addition to fibroblasts and immune cells, the dermis houses nerve endings, blood vessels, hair follicles, and sweat glands[2,4]. Nerve endings in the dermis provide sensation, allowing us to feel touch, pressure, heat, cold, and pain. Blood vessels in the dermis supply nutrients and oxygen to both the dermis and the epidermis and help regulate body temperature by dilating or constricting to release or conserve heat. Hair follicles and sweat glands, which originate from the epidermis but extend into the dermis, are involved in protection, sensation, and thermoregulation.

Separating the dermis and the epidermis is the basement membrane, a thin layer of extracellular matrix produced by both epidermal keratinocytes and dermal fibroblasts[25]. This membrane anchors the epidermis to the dermis and acts as a selective barrier, regulating the exchange of cells and molecules between the two layers.

The dermis influences the behavior of the epidermis through the secretion of growth factors and cytokines[26]. For instance, fibroblasts in the dermis secrete growth factors that promote the proliferation and differentiation of keratinocytes in the epidermis. Conversely, keratinocytes in the epidermis can influence the behavior of dermal cells through the secretion of cytokines and other signaling molecules.

The dermis is traditionally divided into two regions: the papillary and reticular dermis[4,27]. The papillary dermis, the uppermost layer of the dermis, just beneath the epidermis, is characterized by its papillae–small, finger-like projections that increase the surface area of the dermis and secure the attachment of the epidermis. It is composed of loose connective tissue--rich in thin

collagen and elastin fibers arranged in a loose, mesh-like network--conferring flexibility and resilience to the skin. The papillae also house capillaries and nerve endings, crucial for nutrient supply to epidermal cells and sensation of touch and temperature. In contrast, the reticular dermis is a deeper, thicker layer of the dermis, characterized by its dense, irregular connective tissue. This layer contains thick, more densely packed collagen fibers in a relatively parallel alignment, providing the skin with tensile strength and resistance to tearing. The reticular dermis also accommodates larger blood vessels, sweat glands, sebaceous glands, and hair follicles, contributing further to skin function.

Fibroblasts, like keratinocytes, are not a homogeneous population but exhibit significant heterogeneity in terms of their functions, gene expression profiles, and locations within the dermis[27]. While fibroblasts are responsible for the production of the extracellular matrix, not all fibroblasts produce the same types or amounts of extracellular matrix components. Some fibroblasts specialize in the production of collagen, while others specialize in the production of elastin or other extracellular matrix components. This functional heterogeneity allows the dermis to adapt to the specific mechanical needs of different areas of the skin.

In addition to their functional heterogeneity, it should come as no surprise that fibroblasts also exhibit heterogeneity in their gene expression profiles[27]. Recent studies using single-cell RNA sequencing have revealed distinct subpopulations of fibroblasts with unique gene expression signatures. These subpopulations are thought to represent different functional states or lineages of fibroblasts, although the exact roles of these subpopulations in skin biology are still being explored.

Fibroblast heterogeneity also has a spatial aspect. Fibroblasts in the papillary dermis are different from those in the reticular dermis[27]. Papillary fibroblasts are smaller, have a less developed endoplasmic reticulum, and produce thinner collagen fibers compared to reticular fibroblasts. Reticular fibroblasts, on the other hand, are larger, have a more developed endoplasmic reticulum, and produce thicker collagen fibers. This spatial heterogeneity reflects the different functional needs of the papillary and reticular dermis.

Furthermore, fibroblasts around hair follicles and sweat glands also exhibit unique characteristics, reflecting their specific roles in supporting these structures[3,14]. For example, dermal papilla fibroblasts at the base of hair follicles play a crucial role in regulating hair growth and cycling.

The Hypodermis

The adipose layer of the skin, also known as the hypodermis or subcutaneous tissue, is the deepest layer of the skin[4]. It serves as an energy reserve, provides insulation and cushioning, and contributes to the skin's overall structure and function. The hypodermis is primarily composed of adipocytes, which are cells specialized in the storage of fat. These cells contain large lipid droplets that take up most of the cell volume. The stored fat can be mobilized and used as an energy source when needed. In addition to adipocytes, the hypodermis also contains fibroblasts, macrophages, and blood vessels.

Adipocytes in the hypodermis are not a homogeneous population[28]. There are two main types of adipocytes: white adipocytes and brown adipocytes. White adipocytes are the most common type and are specialized in the storage of fat. They contain a single large lipid droplet and have a small

amount of cytoplasm. Brown adipocytes, on the other hand, contain multiple small lipid droplets and have a large amount of cytoplasm. They are named for their brown color, which is due to the high number of mitochondria in their cytoplasm. Brown adipocytes are specialized in the generation of heat, a process known as thermogenesis.

In addition to white and brown adipocytes, recent research has identified a third type of adipocyte, known as beige or brite (brown-in-white) adipocytes[28]. Beige adipocytes are found within white adipose tissue and can switch between a white-like phenotype and a brown-like phenotype, depending on various signals such as cold exposure or hormonal changes. This ability to switch phenotypes (known as thermogenic plasticity) allows beige adipocytes to contribute to thermogenesis when needed.

The hypodermis also contains a population of adipose-derived stem cells (ASCs), which are capable of differentiating into various cell types, including adipocytes, osteoblasts, chondrocytes, and myocytes[29]. These stem cells play a crucial role in the maintenance and repair of the hypodermis and may also contribute to the repair of other tissues.

The adipose layer of the skin is a complex and dynamic tissue that plays crucial roles in energy storage, insulation, cushioning, and thermogenesis. The heterogeneity of adipocytes in the hypodermis, including the presence of white, brown, and beige adipocytes, as well as adipose-derived stem cells, contributes to the adaptability and functional diversity of this layer.

Human Skin Equivalents

In the realm of dermatological research, the advent of human skin equivalents, also known as skin organoids, marks a significant stride forward[30–32]. Skin organoids are three-dimensional structures that mimic the cellular composition and organization of human skin. They are generated by culturing keratinocytes, often alongside additional skin cell types, in a controlled environment, providing the necessary cues for self-organization and differentiation. These organoids serve as a powerful tool for studying skin biology, disease modeling, and personalized medicine.

At the cellular level, skin organoids typically consist of two main cell types: keratinocytes and fibroblasts[30,32–34]. To generate skin organoids, researchers start by isolating and expanding these cells from human skin samples or using induced pluripotent stem cells (iPSCs) derived from patient cells. iPSCs can differentiate into various cell types, including keratinocytes and fibroblasts, making them a valuable resource for generating organoids. Once a sufficient number of cells are obtained, they are combined and cultured in a specialized medium that contains growth factors, nutrients, and other components necessary for cell growth and differentiation.

The culture conditions for skin organoids are carefully controlled to mimic the microenvironment of native skin[9]. This involves providing the appropriate physical and chemical cues to guide the self-organization and differentiation of the cells. For example, the medium composition and growth factors used in the culture can influence the differentiation of keratinocytes and stratification of the epidermal layers. Additionally, the use of specific scaffolds or substrates, such as collagen or devitalized dermis, can provide a supportive environment for the cells to organize and form tissue-like structures[35].

One of the most compelling strengths of skin organoids lies in their biological relevance. These models closely emulate the structure and function of human skin, making them invaluable tools for studying human skin biology and disease[9,30,32,36]. The ability to generate these organoids from patient-derived cells opens up new avenues for personalized disease modeling and drug testing, bringing us a step closer to the era of personalized medicine.

The complexity of skin organoids is another key strength. Unlike their two-dimensional counterparts, skin organoids recapitulate the intricate 3D architecture of the skin[9,30–32,37]. This includes the interactions between different cell types and the extracellular matrix, providing a more holistic view of tissue-level behaviors. This complexity makes skin organoids a powerful tool for studying the multifaceted nature of skin biology. Despite their complexity, skin organoids remain a simplified model of skin. They often lack many of the systemic factors that influence skin biology in vivo, such as blood flow, immune surveillance, and hormonal regulation. This simplicity makes skin organoids a high-throughput model for conducting research, but it also possesses limitations that researchers must bear in mind when interpreting results from organoid-based studies.

The variability and versatility of skin organoids is a double-edged sword. Several methods for generating them are actively employed across the field, and these different systems can allow researchers to study areas of skin biology that other systems can't.[9,31,32,36] They can be employed for a broad spectrum of applications, ranging from basic research to drug testing and tissue engineering. Moreover, they can be modified to incorporate additional components, such as immune cells or nerve cells, to better mimic the in vivo environment. However, this variability can complicate the comparison of results between studies, posing challenges for the standardization of research findings.

One type of skin organoid is the full-thickness model. Full-thickness organoids aim to replicate the complexity of native skin by incorporating multiple layers, including the epidermis, dermis, and sometimes even the hypodermis[32]. These organoids can be generated using different protocols, which may involve variations in the composition of the culture medium, growth factors, and cytokines used to promote tissue differentiation and maturation[32,38]. Additionally, the choice of substrates for culturing the organoids can vary. Some protocols employ collagen substrates, which provide structural support and mimic the native extracellular matrix (ECM) environment of the skin[39]. In contrast, other protocols may use devitalized dermis, which retains the ECM components but lacks live cells[32]. Some protocols utilizing devitalized dermis will seed the devitalized dermis with human dermal fibroblasts[27]. These differences in protocols can influence the structural organization and functionality of the full-thickness organoids generated.

Spheroids are another type of skin organoid that can be generated[36]. Spheroids are three-dimensional cell aggregates that do not possess distinct layers like full-thickness models. They are typically composed of keratinocytes and fibroblasts, which are the major cell types found in the epidermis and dermis, respectively. Spheroids can be generated using various techniques, such as hanging drop culture or centrifugation, and they can differ in terms of the cell types used, the ratio of cell types, and the culture conditions[9,36]. Variations in the medium composition, growth factors, and substrates utilized in spheroid generation protocols can also influence the spheroid structure and functionality.

Organ-on-a-chip systems represent another approach to generating skin organoids[40,41]. These microfluidic devices aim to mimic the physiological conditions and interactions between different

cell types within an organ. In the case of skin organ-on-a-chip models, they can include layers of keratinocytes, fibroblasts, and endothelial cells, among others. The design and fabrication of organ-on-a-chip devices can differ between labs, leading to variations in the size, shape, and composition of the microfluidic chambers. Additionally, the culture medium and flow conditions within the chip can be customized, potentially affecting the behavior and functionality of the skin organoid.

Apart from the types of organoids described above, there may be additional variations in protocols used for the same type of organoid. For instance, the specific growth factors, signaling molecules, and cytokines added to the culture medium can vary between labs, affecting the differentiation and maturation of the organoids[32,42,43]. The duration and timing of various culture steps, as well as the physical and mechanical stimulation applied during the generation process, can also differ. These differences in protocols can result in variations in the structural organization, cell types present, cell-cell interactions, and functional properties of the generated skin organoids.

To address the issue of variability in skin organoid generation, efforts are being made to establish standardized protocols and quality control measures[42]. Collaborative initiatives among researchers and organizations are underway to develop guidelines and best practices for generating and characterizing skin organoids. Such standardization would enable more accurate comparisons of results between studies, facilitate the validation of findings, and promote advancements in the field of skin tissue engineering and regenerative medicine.

Two-dimensional cell culturing has served as a staple in skin biology studies for decades due to its simplicity, efficiency, and cost-effectiveness. The ease of maintaining and manipulating cells

in a 2D environment allows researchers to conduct experiments quickly, with high reproducibility. These cultures provide an invaluable system for studying individual cell types and for initial screens for potential drugs or cellular responses to different stimuli.

However, there are limitations to 2D cultures. They often fail to recapitulate the complex microenvironment of native skin accurately[44]. The skin is not merely a collection of individual cells but a three-dimensional structure of diverse cell types interacting in a specific architecture. These interactions and structural contexts play critical roles in many skin functions and pathologies, which get lost in 2D cultures. Furthermore, the absence of crucial skin components such as the extracellular matrix can limit the applicability of results obtained from 2D cultures to the in vivo setting[45].

On the other hand, skin organoids capture the three-dimensional structure of the skin and the interactions between different cell types, providing a more physiologically relevant model system[42,44]. They enable the study of multicellular dynamics, cell-matrix interactions, and cell-cell communication in a spatially organized environment, closely mimicking the in vivo context. This makes organoids an excellent tool for studying complex processes such as wound healing, aging, and disease progression, and for preclinical drug testing.

However, skin organoids come with their own set of challenges. They are generally more labor-intensive, time-consuming, and expensive to generate and maintain compared to 2D cultures[9]. Also, there's often variability in organoid formation, which can affect the reproducibility of experimental results. Lastly, while organoids capture many aspects of native skin, they still do not fully replicate it. For instance, they often lack certain cell types (like immune cells or nerves) or

structures (like hair follicles or sweat glands), and their diffusion-dependent nutrient supply doesn't reflect the in vivo vascularization.

Both 2D cell cultures and skin organoids have unique strengths and limitations[8,34,44]. Choosing the appropriate model depends on the specific research question at hand. For simple, high-throughput, or preliminary experiments, 2D cultures may be more suitable. In contrast, for studies requiring a more physiologically relevant context, especially those addressing multicellular or structural aspects of skin biology, organoids might be the better choice. A thoughtful combination of both models, complemented by in vivo studies, may provide the most comprehensive understanding of skin biology and pathology.

In comparison to mouse models, skin organoids have the advantage of being human-derived, thereby circumventing the species differences that can complicate the interpretation of animal studies[34]. However, they lack the systemic context of in vivo models, which can be crucial for studying certain aspects of skin biology and disease. Structural and functional similarities are evident in the skin of both humans and mice. Both species have skin composed of three primary layers: the epidermis, dermis, and subcutaneous tissue, housing similar cell types like keratinocytes, melanocytes, fibroblasts, and various immune cells. Both human and mouse skin execute vital functions such as protection against physical and chemical damage, regulation of body temperature, and sensation of touch, pain, and temperature. Another shared feature is the presence of hair follicles, which undergo cyclical phases of growth, regression, and rest.

A significant disparity is the skin's thickness, where human skin, specifically the epidermis, is generally thicker[34]. Additionally, the density and distribution of hair and melanocytes differ

considerably. Mice have a higher hair density covering their entire skin surface, while humans possess distinct hairless regions. Mouse melanocytes are primarily associated with hair follicles, whereas in humans, melanocytes permeate the basal layer of the epidermis[4,34]. Like hair follicles, another notable difference lies in the presence and distribution of sweat and sebaceous glands. Humans have eccrine sweat glands all over their body, crucial for thermoregulation, while mice possess them only on their footpads and do not regulate temperature via sweating. Sebaceous glands in humans usually associate with hair follicles, while in mice, these glands are larger and can exist independently of hair follicles.

A striking difference is the presence of the panniculus carnosus, a thin layer of striated muscle found in the subcutaneous tissue[34]. Well-developed in mice, this muscle enables skin twitching, beneficial in wound closure and parasite expulsion. Humans, however, have a rudimentary panniculus carnosus, predominantly located in the face and neck[46]. This has substantial implications for biomedical research, particularly in wound healing studies. Mouse wound closure primarily depends on wound contraction, facilitated by the panniculus carnosus. In contrast, human wound healing relies more on re-epithelialization and granulation tissue formation, involving cell proliferation and migration to repair the wound[26,47].

In humans, Rete ridges are well-developed and contribute to the mechanical strength of the skin and epidermal-dermal exchanges[4]. The increased surface area due to Rete ridges facilitates nutrient supply to the rapidly dividing cells in the epidermis, enhancing cell survival and function. However, in contrast, mice have an underdeveloped system of Rete ridges. Their skin is primarily smooth, lacking the undulating architecture characteristic of human skin. This difference potentially affects the resilience of the skin to mechanical stress and the epidermal-dermal

interaction, underlining another aspect in which mouse skin does not fully mimic human skin. The discrepancy in the structure of Rete ridges between the two species can impact the extrapolation of dermatological research findings from mice to humans–particularly in conditions like psoriasis and aging, where the structure of Rete ridges is significantly altered, or when studying the heterogeneous basal keratinocytes spatially organized around them[5,48].

Using Single-cell RNA Sequencing to Probe Cellular Heterogeneity

Single-cell RNA sequencing (scRNA-seq) has provided a transformative tool in skin biology, enabling the comprehensive exploration of cellular heterogeneity within native human skin at an unparalleled resolution[14,16,49]. This technology captures the transcriptomes of individual cells, revealing a spectrum of distinct cell populations within the skin[50]. These include diverse subsets of keratinocytes, melanocytes, fibroblasts, and immune cells–each with unique gene expression profiles and biological functions[14,16,27,49]. This level of detail has enriched our understanding of the complex cellular landscape in skin health, aging, and disease.

Extending the use of scRNA-seq to human skin equivalents holds significant promise. HSEs are utilized extensively in dermatological research as they offer a controlled and ethical alternative to native skin. However, their fidelity in replicating the cellular diversity and complexity of native skin is not entirely known. By employing scRNA-seq to analyze HSEs, we can precisely evaluate their cellular composition and the transcriptional states of these cells. This will allow us to determine the extent of heterogeneity in these models compared to native human skin and identify any existing transcriptional differences. The comparison of scRNA-seq data from HSEs with that from native skin can illuminate the strengths and limitations of these models, thereby refining their use in research and potentially leading to improvements in their design. Ultimately, such

comprehensive analysis has the potential to bridge the gap between in vitro studies and clinical application, accelerating the translation of research findings to therapeutic interventions.

Chapter 2

Single cell transcriptomics of human skin equivalent organoids

CONTRIBUTIONS

Adam Stabell and Scott Atwood conceived the project. Scott Atwood supervised research. Adam Stabell generated and analyzed scRNA-seq libraries. Shuxiong Wang performed SoptSC for lineage and entropy analysis. Adam Stabell, Sandrine Nguyen, Yunlong Jia, Kirsten Wong, and Grace Lee performed imaging experiments. J.L. and George Sen performed xenograft experiments. Yunlong Jia performed hypoxia experiments. Adam Stabell, Qing Nie, and Scott Atwood analyzed and interpreted data. Adam Stabell and Scott Atwood wrote the manuscript. All authors analyzed and discussed the results and commented on the manuscript. The work described in this chapter was published in *Cell Reports* (Stabell et al., 2023).

SUMMARY

Several methods for generating human skin equivalent (HSE) organoid cultures are in use to study skin biology, however, few studies thoroughly characterize these systems. To fill this gap, we use single cell transcriptomics to compare *in vitro* HSEs, xenograft HSEs, and *in vivo* epidermis. By combining differential gene expression, pseudotime analyses, and spatial localization, we reconstruct HSE keratinocyte differentiation trajectories that recapitulate known *in vivo* epidermal differentiation pathways and show that HSEs contain major *in vivo* cellular states. However, HSEs also develop unique keratinocyte states, an expanded basal stem cell program, and disrupted terminal differentiation. Cell-cell communication modeling shows aberrant EMT-associated signaling pathways that alter upon EGF supplementation. Lastly, xenograft HSEs at early timepoints post-transplantation significantly rescue many *in vitro* deficits, while undergoing a hypoxic response that drives an alternative differentiation lineage. This study highlights the strengths and limitations of organoid cultures and identifies areas for potential innovation.

INTRODUCTION

Skin is an essential organ with many roles including forming a water-tight barrier, aiding in thermoregulation, and acting as a sensory organ[4]. To fulfill these roles, the keratinocytes that constitute the epidermis must replenish themselves while withstanding a constant barrage of chemical, physical, pathological, and radiological insults from their environment[5,51]. The field of skin research has largely been driven by *in vivo* mouse models that show healthy skin is critical to an organism's wellbeing and the disruption of many of its functions can lead to a drastic decline in quality of life[47,52]. While mice are suitable to define the basic architecture and homeostatic signaling of skin, the anatomy, microstructure, and heterogeneity of mouse skin is inherently different from human[4,34]. For instance, mice have a distinct density of hair follicles and eccrine glands, a layer of striated muscle found beneath the hypodermis, a lack of melanocytes in the interfollicular epidermis, and the absence of rete ridges. These differences impact epidermal homeostasis, wound repair, and the severity of certain skin disorders, pointing to a need for a more human equivalent model system to study human-specific aspects of skin biology[47].

Three-Dimensional (3D) organoid cultures have long been a tool to investigate complex tissue interactions[30,38]. Typically composed of primary cells isolated from patient samples, the idea of building an organ from its basic components is an attractive premise that has profound scientific implications[9]. From gaining molecular insight by simplifying development and homeostasis to their essential parameters to the translational promise of a gold standard system to test drugs or a farm system to grow replacement tissues, 3D organoid cultures are gaining popularity as an elegant and relevant model system to study human biology. Current technologies include generating complex skin in spherical cell aggregates from human pluripotent stem cells[36,53], using conventional scaffolds - such as hydrogels[31,39,54] or bioprinting[36,55,56] - to assemble dermal and

keratinocyte layers with other relevant cells, and organ-on-a-chip that allows active perfusion and spatiotemporal control at the microscale level[41].

However, 3D cultures are not without their limitations. For instance, despite human skin equivalent (HSE) organoid cultures showing a high degree of morphological similarity to their *in vivo* counterparts, their composition and culturing conditions vary greatly from lab to lab which can affect interpretation of similar experiments[9,32,36,53,56,57]. Many components of the *in vivo* system are lacking, such as vasculature and immune cells, which limit the size of cultures and their response to experimental stimuli[9]. And many studies defining HSEs have shown marked molecular differences in basal and terminal gene expression that suggest epidermal differentiation is not quite analogous to their *in vivo* counterparts[58,59]. Given the variability that exists between culture systems and their limited characterization, it can be difficult to determine which conditions are best suited for a particular experiment (**Figure S1A-B**). Knowledge of the capacity and limitations of these systems is paramount to accurately interpret their results.

Recently, several labs have published single cell -omic studies examining the strengths and weaknesses of a variety of organotypic culture systems. These include organoids mimicking the central nervous system[60], gastric system[61], intestinal system[62], and gastrulation[63]. Human skin spheroids have recently been developed from human pluripotent stem cells that differentiate into spherical cell aggregates where cyst-like skin emerges composed of stratified epidermis, fat-rich dermis, pigmented hair follicles with sebaceous glands, and rudimentary neural circuitry[53]. Although these skin spheroids resemble fetal facial skin, their long incubation period and small size are not ideal for genetic manipulation of individual cell types or for grafting in the clinic. How HSEs built using conventional scaffolds like devitalized dermis compare to their *in vivo* counterparts is unclear, despite being ideally suited to address the deficiencies of spherical skin organoids.

Our lab, alongside others, have recently shown that human epidermis is more heterogeneous than previously thought[16,17,49,64]. Using single cell-RNA-sequencing (scRNA-seq) and subsequent *in vivo* validation, we spatially resolved four distinct basal stem cell populations within human interfollicular epidermis and delineated multiple spinous and granular cell populations that contributed to a hierarchical differentiation lineage supporting multi-stem cell epidermal homeostasis models[16]. Collectively, these studies have highlighted the complexity of the epidermis and their cell-cell interactions. The extent to which HSEs can recapitulate the cell type heterogeneity, cell-cell signaling, and differential gene expression of *in vivo* human skin remains unclear. To address this issue, we probed the transcriptomes of three HSE variants - two *in vitro* HSEs and the one xenografted HSE - and examined the differences in comparison to *in vivo* human skin at the single cell level. We found that all HSEs remarkably contained the relevant cellular states of their *in vivo* counterparts, but each HSE also possessed unique cell states not found during homeostasis. An expanded basal program, terminal differentiation defects, and ectopic EMT signatures predominate fibroblast- and Matrigel-derived HSEs, whereas xenografting HSEs onto immunodeficient mice largely rescued the various defects at the cost of inducing hypoxic conditions.

RESULTS

Histological characterization of HSEs

To compare commonly used *in vitro* HSEs to *in vivo* human epidermis, we chose to use devitalized human dermis as the scaffold for growing the HSEs because we reasoned that the extracellular matrix composition more accurately mimics the endogenous surface for keratinocyte stratification than a collagen-based hydrogel. We utilized the two most common HSE variants where primary human keratinocytes are seeded on top of devitalized dermis at the air-liquid interface and the

dermis is either treated with Matrigel (GelHSE)[65] or seeded with primary human dermal fibroblasts (FibHSE)[38] to supply necessary signals for keratinocyte stratification (**Figure 1A**). Keratinocyte stratification occurs under both conditions by day 7, where the HSEs show a tightly packed columnar basal cell layer, multiple irregular polyhedral squamous cell layers, several flattened granular cell layers, and a thin stratum corneum (**Figure 1B**). Histologically, the HSEs largely remain the same up through day 28 except for a thickening of the stratum corneum and a general spreading out of keratinocytes at all epidermal layers. Proliferation was reduced in the HSEs over time and day 28 tissue showed less proliferation compared to neonatal or adult epidermis, with no significant change in apoptosis (**Figure 1C-D, Figure S1A-B**). FibHSEs possess a significantly thicker living epidermal layer than the GelHSEs (**Figure 1E**). We chose to continue our analysis with day 28 HSEs due to the morphological similarity to *in vivo* tissue and to avoid active re-stratification or injury programs that may be operating at earlier timepoints.

Epidermal homoeostasis is disrupted in HSEs

To define the cellular states of keratinocytes derived from HSEs, we isolated viable, single cells from day 28 HSEs and subjected them to droplet-enabled scRNA-seq to resolve their individual transcriptomes (**Figure S1C**). We processed a total of 4,680 cells from two FibHSEs (including fibroblasts) and 4172 cells from two GelHSEs before performing quality control analysis on individual libraries using the R package Seurat (**Figure S1D**). The cells from each replicate FibHSE were clustered in an unsupervised manner, and tentatively annotated as keratinocytes or fibroblasts using the marker genes *KRT14* and *KRT10* to identify keratinocytes and *TWIST2* and *COL6A1* to identify fibroblasts (**Figure S2**). Keratinocytes were then subset from our HSE datasets and integrated with interfollicular keratinocytes from two *in vivo* human neonatal epidermal datasets that were previously generated by our lab[16] (**Figure S3A-B**). One cluster appeared to be low quality cells that passed our initial quality control thresholds, as their number of genes detected, unique molecular identifiers (UMIs), and the percent mitochondrial gene

expression for each cluster appeared far lower than the other clusters (**Figure S3C**). Although it is possible that this cluster represents a genuine cell state in our HSEs, we excluded them from our downstream analyses due to their metrics and the lack of gene expression markers to identify them. Cell types were then annotated based on known marker genes from the *in vivo* dataset, which differed from the marker genes of the HSE datasets (**Figure 1F-I, Figure S3D-F**). Remarkably, many of the major *in vivo* cellular states were found in the *in vitro* HSEs, including the full complement of *in vivo* basal cell states. Based on our previous characterization of basal (BAS) stem cell communities[16], BAS-I through IV represented approximately 27.3% of the *in vivo* cells, 55.6% of FibHSE, and 22.0% of GelHSE, and were enriched for known basal keratinocyte marker genes including *PTTG1*, *RRM2, KRT15*, and *PCNA*, respectively (**Figure 1J, Figure S3G-H**). The ratios of BAS-I and BAS-II cycling cells remained largely similar between the *in vivo* tissue and FibHSE, while the GelHSE had a reduction in cycling cells. BAS-III cells are enriched in both HSEs, with the FibHSE possessing over 3.5 times as many cells in this cluster than the *in vivo* tissue, whereas BAS-IV cells are depleted in the GelHSE compared to the *in vivo* environment (**Figure 1J**). Intriguingly, an HSE cell state clustered separately from the *in vivo* cells and was annotated HSE-1 (**Figure 1F**). HSE-specific keratinocytes constituted 0.6% of FibHSE and 9.3% of GelHSE (**Figure 1J**). 10 out of 12 cell type proportions were significantly changed in the GelHSE when compared to the *in vivo* datasets while only 6 out of 12 were significantly different in the FibHSE (**Figure 1K-L**). Both HSEs had a higher proportion of BAS-III and HSE-I cells and a lower proportion of the spinous (SPN) cell clusters, SPN-2, SPN-4, SPN-5, and the granular (GRN) cluster GRN-2, compared to the *in vivo* state.

Despite the relatively normal histological appearance of the HSEs, there is an expansion of KRT14+ cell layers and disrupted epidermal differentiation in both the GelHSE and FibHSE cultures (**Figure 2A, Figure S3I**). The expanded KRT14+ cell layers do not proliferate outside of

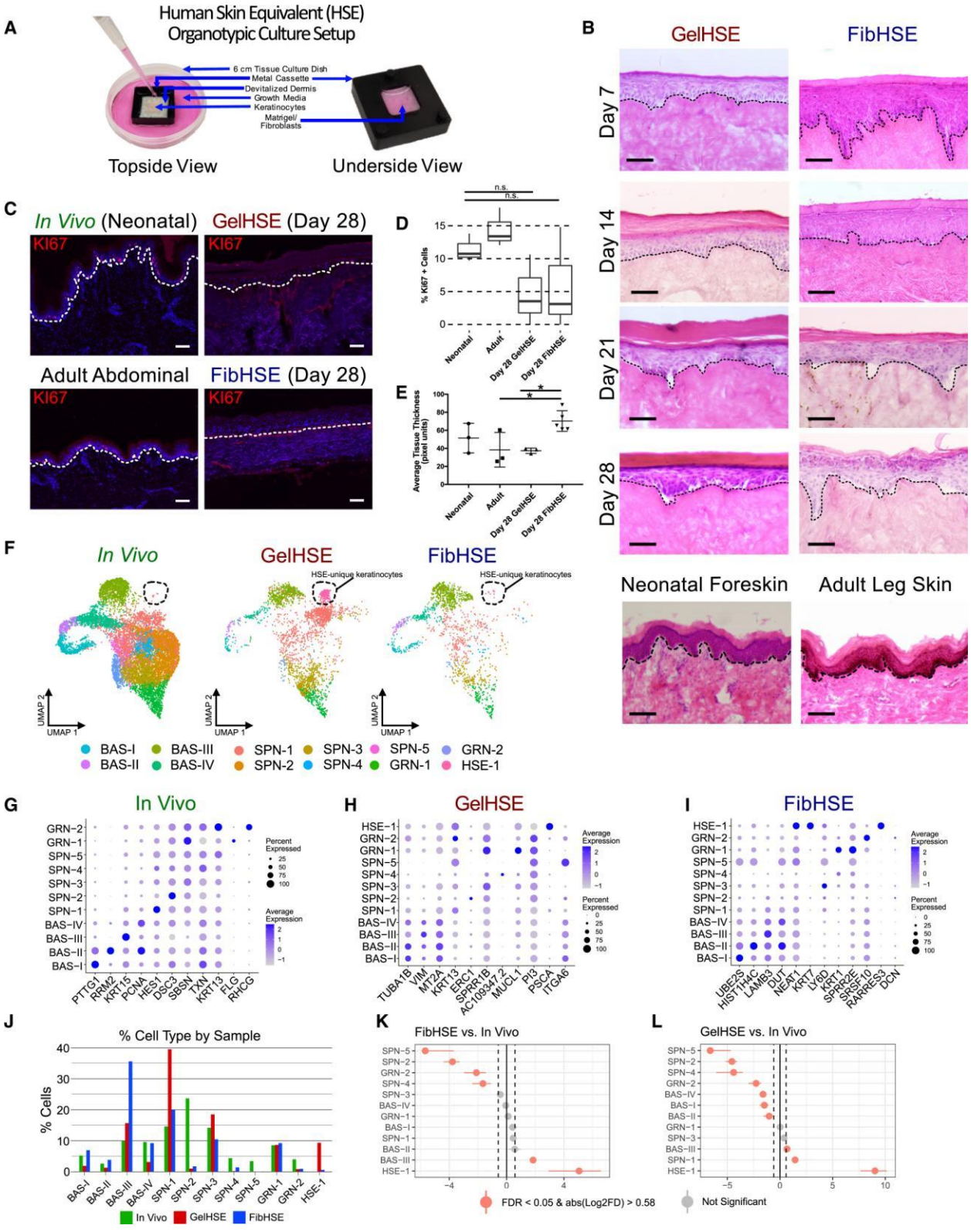

Figure 1. Defining human skin equivalent cell populations using scRNA-seq. A) Diagram of the human skin equivalent (HSE) organoid culture setup. **B)** Hematoxylin and eosin (H&E)

staining of Matrigel-grown HSEs (GelHSE) and fibroblast-seeded HSEs (FibHSE) after 7, 14, 21, and 28 days of growth on devitalized human dermis. Neonatal epidermis from foreskin and adult epidermis from the leg are shown for comparison. Scale bar 100 μm. Dashed lines denote the epidermal-dermal junction. **C)** Immunostaining of KI67 (red) and DAPI (blue) in human neonatal skin (top left), adult abdominal skin (bottom left), day 28 GelHSE (top right), and day 28 FibHSE (bottom right). Scale bar 100 μm. Dashed lines denote the epidermal-dermal junction. Quantification of **(D)** KI67+ cells and **(E)** average thickness of living epidermal cell layers in human neonatal skin, adult abdominal skin, day 28 GelHSE, and day 28 FibHSE. n = 3 each sample. Significance was determined by Tukey's HSD test. *p < 0.05. n.s., not significant. **F)** Seurat clustering of 15,573 single cells isolated from four HSE libraries (two GelHSE and two FibHSE) and two *in vivo* neonatal epidermis libraries using UMAP embedding. Libraries are split by sample type. Dashed lines encompass HSE-unique keratinocytes. Dot plots of the top differentially expressed marker genes for **(G)** *in vivo* clusters, **(H)** GelHSE clusters, and **(I)** FibHSE clusters. **J)** Percentage of total cells within each cluster split by sample type. Monte-Carlo permutation test showing the significance of the changes in proportion of each cell type for the FibHSE **(K)** and GelHSE **(L)** relative to the *in vivo* datasets.

the basal layer in contact with the basement membrane (**Figure 1C**) and differentiation markers such as DSG1, FLG, and LOR are still restricted from the basal-most layer (**Figure 2A-B**). Basal cell marker KRT15 does remain restricted to the basal-most layer of the HSEs, whereas KRT19 shows selective expansion in the GelHSE (**Figure 2C**), suggesting that suprabasal KRT14+ cells are not fully functioning basal cells and are likely to be differentiating without fully turning off the basal cell state. The mesenchymal marker VIM, which is normally restricted to fibroblasts, melanocytes, and Langerhans cells of *in vivo* skin, shows high RNA expression in GelHSE basal keratinocytes and VIM+ protein expression in both GelHSE and FibHSE basal keratinocytes (**Figure 2D, Figure S4**), suggesting a partial epithelial-to-mesenchymal transition (EMT) state. This partial EMT state is not entirely unexpected given the signals the keratinocytes are receiving from the Matrigel and culture media, with the GelHSE showing the greatest expression of *VIM*. Cell-cell contacts and terminal differentiation are also disrupted in HSEs with DSG1 protein no longer restricted to cell-cell contact sites, FLG protein expression turning on early in spinous (SPN) cell layers, and FLG and LOR no longer restricted to the granular (GRN) layers (**Figure 2A-B**). The HSE-specific cluster HSE-1 is readily identified by one of its marker genes, *PSCA* (**Figure 2D**). *PSCA* encodes for a GPI-anchored membrane glycoprotein typically found in basal cells of the prostate, the lining of the urinary tract, the mucosal epithelium of the gastrointestinal tract, and in the outermost layer of mouse fetal skin from E15 to E17[66]. Staining for PSCA demonstrated that these keratinocytes are exclusively localized to the outermost epidermal layers (**Figure 2D, Figure S4A**) and may indicate a remnant embryonic program that is reactivated as a result of growth factors in the culturing media.

Considering the apparent uncoupling of markers from their respective cell states, we averaged the RNA expression of every cell in each cluster and calculated a Pearson correlation between the HSE and *in vivo* clusters (**Figure S5A-E**). Both *in vivo* datasets were compared to each

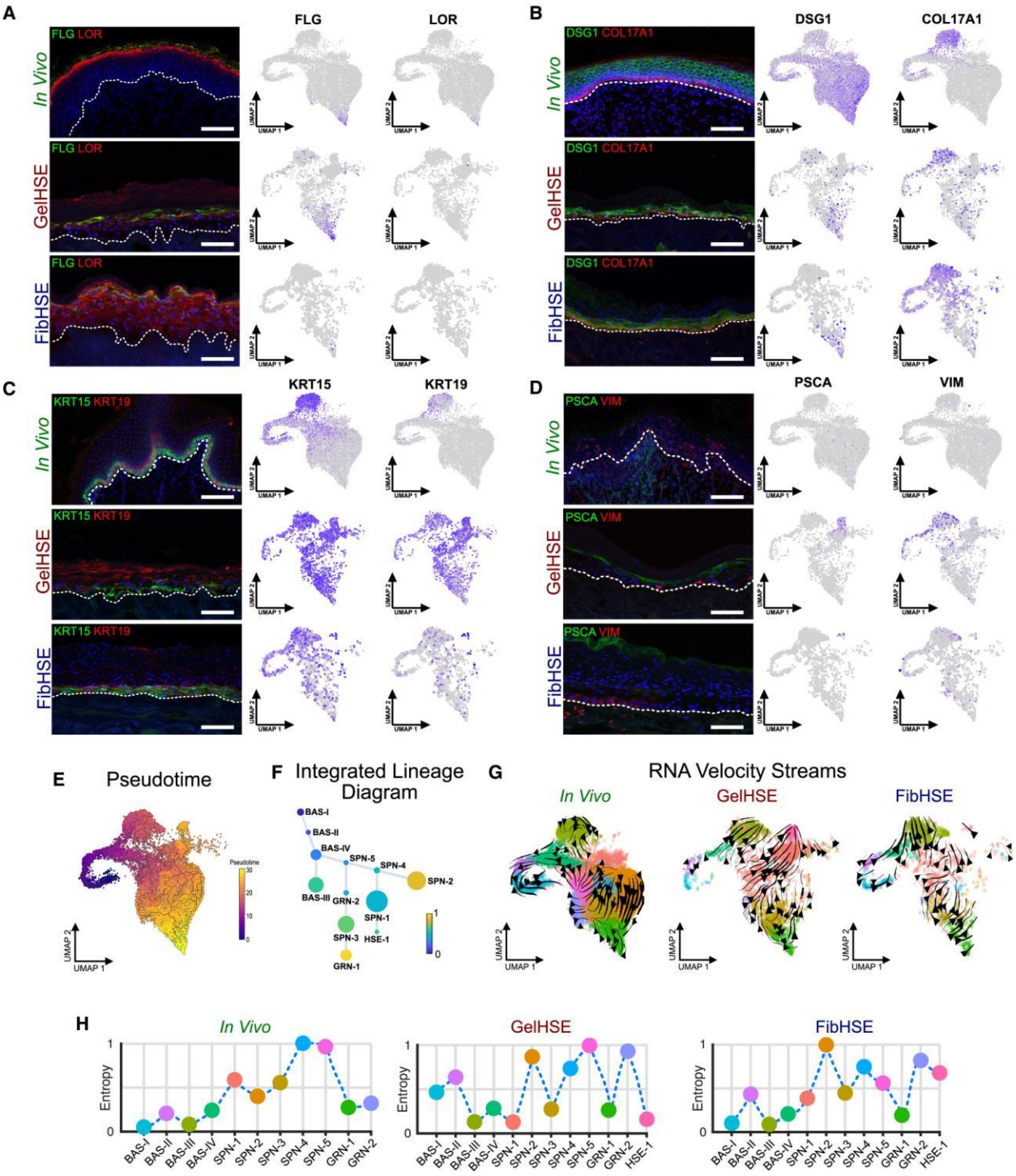

Figure 2. Human skin equivalents display altered expression patterns and lineage paths. Immunostaining of **(A)** terminal differentiation markers FLG and LOR, **(B)** structural proteins DSG1 and COL17A1, **(C)** basal stem cell markers KRT15 and KRT19, and **(D)** human skin equivalent (HSE) unique markers PSCA and VIM. Human neonatal skin (top), day 28 GelHSE

(middle), and day 28 FibHSE (bottom). Feature plots showing the RNA expression of indicated markers for each sample type are on the right. Scale bar 100 μm. Dashed lines denote the epidermal-dermal junction. **E)** Pseudotime inference of epidermal keratinocytes from the integrated datasets. **F)** Cell lineage diagram of keratinocytes from the integrated datasets. Edge weights denote probability of transition to each cluster. Dot size denotes number of cells. **G)** Splicing kinetics depicted as RNA velocity streams calculated using the python package scVelo. **H)** Quantification of Cellular Entropy (ξ) using the R package SoptSC.

other to establish the highest expected Pearson correlation between cell states. With respect to the HSEs, the most highly correlated clusters were the basal cell populations. Interestingly, the majority of HSE clusters showed the highest correlation with the *in vivo* BAS-III cluster, suggesting that the BAS-III transcriptional program is not shut off during HSE differentiation. Additionally, the Pearson correlation decreases as keratinocytes differentiate, reinforcing that terminal differentiation is disrupted in HSEs. The correlation between the *in vivo* tissue and FibHSE is higher overall than GelHSE, indicating that global RNA expression in FibHSE more accurately mimics *in vivo* human epidermis.

Human skin equivalents have altered lineage paths

Next, we examined how the HSE-specific clusters altered the inferred lineage trajectory of epidermal differentiation. We generated pseudotime and cell lineage inferences of the integrated keratinocytes using Monocle3[67] and SoptSC[68] and partially reconstructed the expected BAS-SPN-GRN keratinocyte differentiation trajectory (**Figure 2E-F**). Basal keratinocytes expressing *KRT15* were placed at the beginning of the trajectory and cells expressing the terminal differentiation gene *FLG* were placed towards one of the trajectory termini (**Figure 2F**). Intriguingly, HSE-1 was placed at a distinct trajectory terminus away from the GRN cell states, generating a BAS-SPN-HSE differentiation trajectory (**Figure 2F**).

To better define the BAS-SPN-HSE differentiation trajectory, we analyzed the splicing kinetics of every cell using scVelo's dynamical modeling, to infer the future state of each cluster[69]. We subset cells from each tissue from the integrated dataset and modelled them separately while keeping their spatial relationship within the integrated UMAP space intact (**Figure 2G**). The *in vivo* epidermal dataset showed the expected BAS-III and BAS-IV velocity vectors pointing towards the SPN clusters and SPN velocity vectors pointing towards the GRN clusters, reconstructing the BAS-SPN-GRN differentiation trajectory (**Figure 2G**). While the FibHSE trajectory largely followed

the aforementioned trend, many BAS and SPN velocity vectors for GelHSE point towards the HSE-1 cluster, with an undefined flow of vectors between the SPN and GRN clusters, suggesting that terminal differentiation may be disrupted and that HSE-1 may represent an alternative differentiation trajectory terminus in the GelHSE.

We next used SoptSC's cellular entropy estimator to infer the entropy of each cluster to determine the relative stability of each cellular state[16]. High entropy suggests a high probability that a cell will transition into another state and low entropy indicates a low probability that a cell will transition into another state. The *in vivo* epidermal dataset shows low entropy for the BAS and GRN clusters, indicating that these are stable states, whereas the SPN clusters have high probabilities of transitioning to a new state (**Figure 2H**). These *in vivo* entropy values reinforce the idea that once differentiation is initiated in the SPN state, there is momentum to reach terminal differentiation in the GRN state as an endpoint with high energy costs to stop at any intermediate stage. For the GelHSE and FibHSE datasets, BAS-III, BAS-IV, and GRN-1 remain stable states, suggesting that these states are robust to perturbations and remain a core lineage trajectory in the HSEs (**Figure 2H**).

HSEs exhibit abnormal signaling associated with EMT

We sought to infer how intercellular communication is altered in the HSEs using CellChat, a bioinformatic tool that predicts intercellular communication networks using ligands, receptors, and their cofactors to represent known heteromeric molecular complexes instead of the standard one ligand/one receptor gene pair[70]. CellChat detected 18 significant signaling pathways in the *in vivo* dataset and the HSEs recapitulated 16 of the 18 pathways (**Figure S5F-H, Table S1**). However, the HSEs also showed an extended network of significant signaling pathways, with 35 in GelHSE and 36 in FibHSE. A subset of these pathways, such as LAMININ, CD99, CDH1, EPHB, and MPZ, show similar signaling profiles across the *in vivo* and HSE tissues, whereas the other

pathways show marked differences (**Figure S5F-H**). Many of the outgoing and incoming signals in the *in vivo* dataset predominantly come from or go to the BAS-III and GRN-1 clusters, suggesting that these stable cell states have great influence over tissue function (**Figure S5F**). While BAS-III and GRN-1 are still signaling hubs in the GelHSE and FibHSE datasets, HSE-1-specific signaling exerts wide influence over GelHSE whereas all four BAS clusters actively signal in FibHSE with little contribution to or from HSE-specific cluster.

Given the abnormal VIM expression in the HSE basal keratinocytes that is normally found in mesenchymal cells, we decided to explore EMT signaling in the HSEs. We focused on EGF signaling, a well-documented inducer of EMT[71]. EGF signaling in *in vivo* epidermis mainly comes from the differentiated GRN or more differentiated SPN cell populations and signals to the BAS stem cell and early SPN populations (**Figure 3A**). However, sender EGF signaling is expanded to the BAS and early SPN populations in the HSEs, coinciding with the appearance of VIM+ basal cells (**Figure 2D and 3A**). The HSE-1 cluster is involved in both sending and receiving EGF pathway signals in GelHSE. Interestingly, the ligands and receptors facilitating EGF signaling are substantially altered in both HSEs compared to the *in vivo* state (**Figure 3B-C**). AREG-EGFR signaling is overrepresented in both HSEs and the *AREG* ligand is expressed in most HSE-cultured keratinocytes (**Figure 3B-C**). *EREG* and *TGFA* ligands also specifically contribute to EGF signaling in the HSEs, whereas HBEFG-EGFR signaling is reduced compared to the *in vivo* state (**Figure 3B-C**). These ligands have all been implicated in EMT induction by activation of the EGFR/ERK/NF-κB signaling pathway[72–77].

Several other genes associated with EMT, such as *LAMC2* and *LGALS1*, are also expressed in HSEs (**Figure 3D**). LAMC2 is a regulator of the EMT phenotype and silencing LAMC2 reverses EMT by inactivating EGF signaling[78,79], whereas *LGALS1* promotes EMT and may be a biomarker of this process[80,81]. Both HSE cultures have high levels of *LAMC2* and *LGALS1*

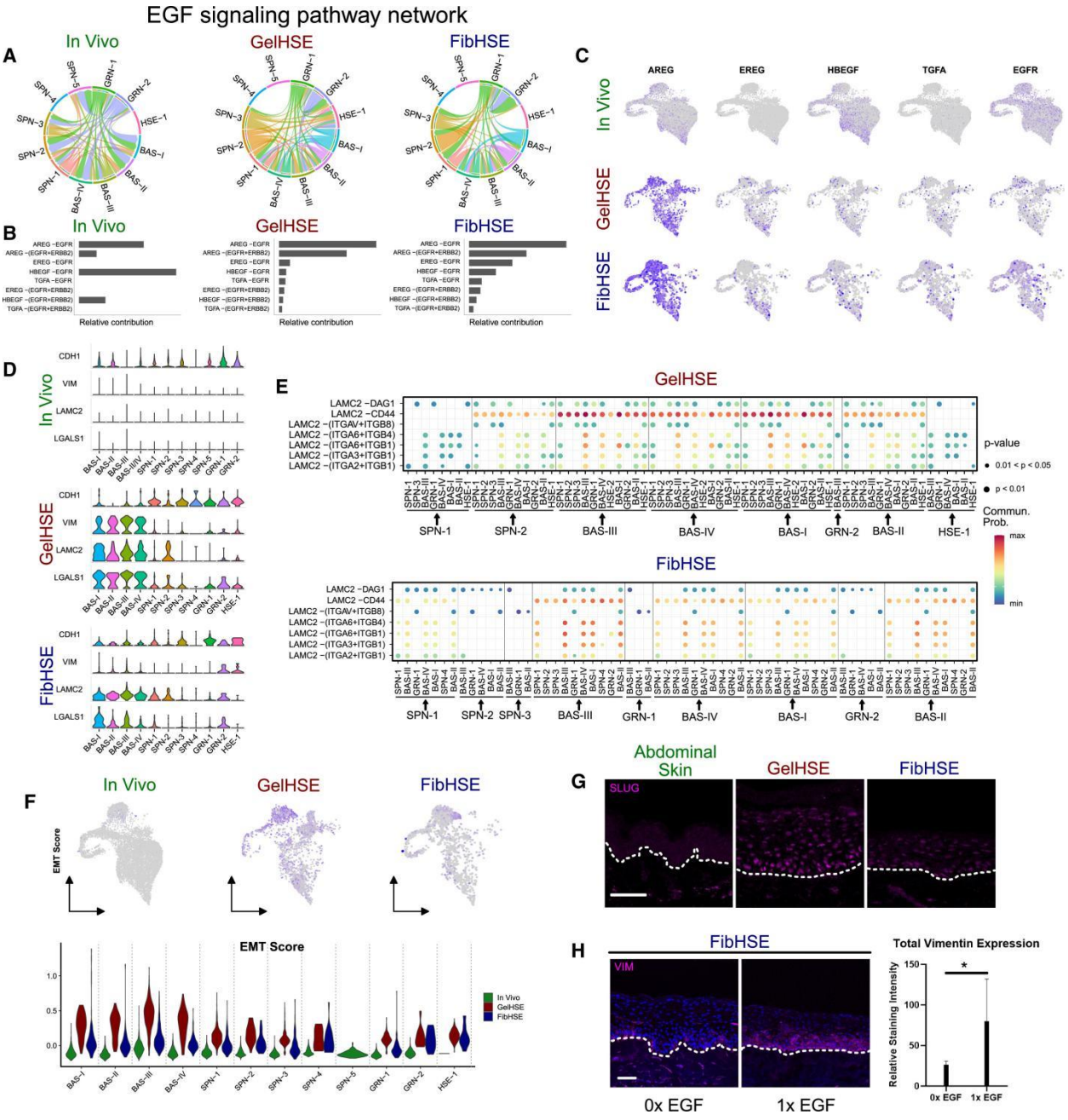

Figure 3. HSEs possess an EMT-like gene expression signature driven by EGF sigaling. A) Cell-cell communication networks predicted for the EGF signaling pathway inferred using the R package CellChat. Edge weights represent the probability of signaling between cell clusters. **B)** Relative contributions of each ligand, receptor, and cofactor group to the cell-cell communication predicted in panel A. **C)** Feature plots showing the expression patterns of EGFR and each of the ligands contributing to the EGF signaling network. **D)** Violin plots of relative gene expression for

positive markers (*VIM*, *LAMC2*, and *LGALS1*) and negative markers (*CDH1*) of EMT. **E)** Visualization of signaling probability scores of ligand-receptor/co-receptor pairs involving *LAMC2* for GelHSE and FibHSE datasets. *In vivo* datasets had no imputed signaling interactions involving LAMC2. Dot size represents p-value. **F)** Feature plots (top) and violin plots (bottom) showing the relative EMT gene score for each cell and cluster, separated by sample type. **G)** Immunostaining of SLUG in the FibHSE, GelHSE, and In Vivo samples. Scale bar = 100 μm. **H)** Immunostaining of VIM in FibHSEs supplemented with indicated concentrations of EGF. Quantification of VIM staining intensity is shown on the right. n = 3 each condition. One-tail student's t-test was used to determine significance. * denotes p-value < 0.1. Scale bar = 100 μm.

expression in all basal populations, and lower expression levels in more differentiated keratinocytes (**Figure 3D**), supporting the notion that many of the HSE basal cells may be undergoing EMT. *VIM*, *LAMC2*, and *LGALS1* expression are all higher in the Matrigel-supported GelHSE compared to the FibHSE cultures. Epithelial cell marker *CDH1* is negatively correlated with *VIM* and shows higher expression in *VIM*- HSE keratinocytes compared to the *in vivo* state (**Figure 3D**), suggesting that VIM+ keratinocytes may lose contact with the underlying basement membrane and potentially explaining the small gaps we observe between basal keratinocytes and the basement membrane in older HSE cultures (**Figure 1B**). Furthermore, *LAMC2* shows high probability interactions with several integrins expressed in basal keratinocytes, including *ITGA6*, *ITGB4*, *ITGB1*, and the cell-surface glycoprotein *CD44* (**Figure 3E**). *CD44* undergoes complex alternative splicing and at least one of these isoforms is implicated in EMT[82,83]. An EMT gene module consisting of 19 genes from multiple EMT studies was used to score the EMT signature in the different samples (**Table S2**). GelHSE had the highest EMT score, followed by FibHSE and the in vivo dataset (**Figure 3F**). SLUG (SNAI2), an EMT inducing transcription factor[84], was present in the nuclei of keratinocytes throughout all living layers of the HSEs, while human abdominal skin had little to no observable staining, further supporting the EMT signature (**Figure 3G**).

Primary human keratinocytes are regularly cultured with EGF to increase the number of viable passages[85]. To define the relationship between EGF signaling and VIM+ basal cells, FibHSEs were grown in normal growth media that includes EGF for one week to induce epidermal stratification and then the media was replaced with new growth media that was supplemented with either 0x, 1x, 2x, or 4x EGF for an additional week (**Figure 3H and Figure S4B**). The HSE growth media use 10ng/ml of EGF at 1X concentration. FibHSEs were used instead of GelHSEs despite the greater GelHSE EMT score because of the inability to remove EGF from Matrigel. Removal of EGF resulted in a significant decrease in VIM expression in FibHSE keratinocytes

(**Figure 3H**), whereas further EGF supplementation increased VIM expression (**Figure S4B**). These data suggest EGF supplementation may be a major driver of EMT in HSE cultures.

Given that EMT is associated with many transcriptional changes[86,87] that may result in unique cell states that we did not detect when examining all keratinocytes, we subclustered the BAS-specific keratinocytes and found 8 distinct cell states labeled BAS-1 through BAS-8 (**Figure S4C**). BAS-1 and BAS-8 were primarily composed of HSE-specific basal cells whereas BAS-4 was primarily found in the *in vivo* state (**Figure S4D-F**). The BAS-1 and BAS-8 clusters have a higher expression of VIM than the other clusters and have a higher EMT score, indicating that the keratinocytes expressing an EMT signature separate out from the other basal populations and are primarily composed of HSE-specific basal cells (**Figure S4G-H**)

Xenografting partially rescues HSE abnormalities

Despite using devitalized human dermis as a substrate, HSE organoid cultures have a simplified cellular composition that lack system-level aspects of normal skin, such as fully functioning vasculature, immune system, and innervation. One way to circumvent some of these issues is to xenograft HSE cultures onto mice to more accurately mimic endogenous conditions[30]. To explore how the cellular states and transcriptional profile of HSEs were altered when xenografted onto mice, we grew three GelHSE cultures for one week and subsequently grafted them onto a wound bed created within the dorsal back skin of NOD-SCID gamma (NSG) mice where they remained for 24 additional days before dissecting the tissue for scRNA-seq (**Figure 4A-B**). NSG mice were chosen due to their ability to engraft skin at very high levels and perivascular infiltration of immune cells[88]. Cell suspensions from the three xenografts were pooled prior to sequencing. The xenograft dataset was aligned and annotated twice, once using the human reference genome GRCh38 and again using the mouse genome mm10. Mitochondrial gene expression and RNA features were used to identify mouse and human cells

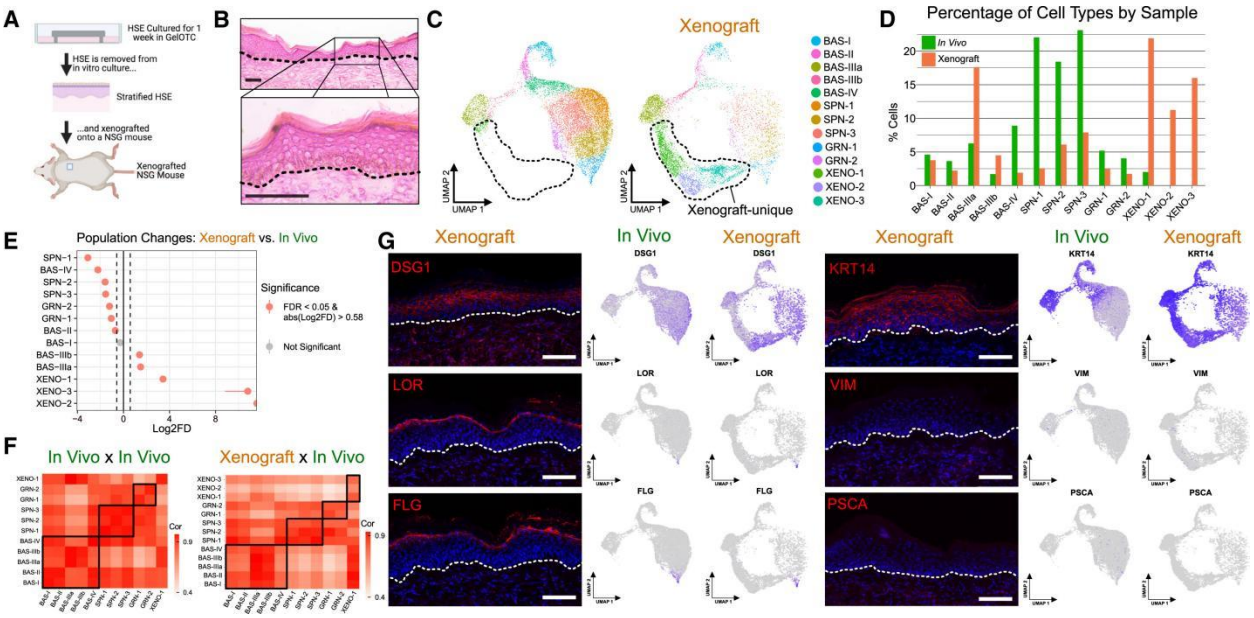

Figure 4. Xenografting rescues terminal differentiation, cell-cell adhesion, and organoid-specific programs. A) Schematic of strategy to xenograft human skin equivalent (HSE) tissue. **B)** H&E staining of xenograft tissue. Scale bar 100 µm. Dashed lines denote the epidermal-dermal junction. **C)** Seurat clustering of single cells isolated from pooled xenograft libraries (n = 3 samples pooled prior to sequencing) and two neonatal epidermal libraries and displayed using UMAP embedding. Libraries are split by sample type. Dashed lines encompass xenograft-unique clusters. **D)** Percentage of total cells within each cluster split by sample type. **E)** Monte-Carlo permutation test showing the significance of the changes in proportion of each cell type for the Xenograft relative to the in vivo datasets. **F)** Pearson correlation of average RNA expression of each cluster compared to all other clusters between the *in vivo* datasets (left) and between the xenograft dataset and both *in vivo* datasets (right)**. G)** Immunostaining of indicated markers in HSE xenografted tissue. Feature plots showing the RNA expression of indicated markers are to the right. Scale bar = 100 µm. Dashed lines denote the epidermal-dermal junction.

(**Figure S6A-B**). Human cells have more nuclear and mitochondrial RNA reads aligning to a human reference genome, and the same is true for mouse reads and a mouse reference genome (**Figure S6C-D**). After removing mouse cells, the dataset was compared to the *in vivo* epidermal datasets in the same manner as our HSE analyses. We excluded one cluster from our downstream analysis that appeared to be low quality cells that passed our initial quality control thresholds, as their number of genes detected and unique molecular identifiers (UMIs) appeared far lower than the other clusters, and the percent mitochondrial gene expression appeared higher, suggesting these were likely apoptotic cells (**Figure S6E-F**). Surprisingly, we observe three xenograft-unique clusters in the xenograft, alongside the expected BAS, SPN, and GRN keratinocyte clusters (**Figure 4C**).

The xenograft-unique clusters were designated XENO-1 through XENO-3 and collectively comprise ~49.2% of the total xenograft cells (**Figure 4D**). To better define the difference between the HSE and XENO cellular states, we subset and integrated the HSE-unique cells (HSE-1) with the xenograft-unique cells (XENO-1 through XENO-3). The xenograft-unique keratinocytes cluster separately from the HSE-unique cells (**Figure S6G)**, suggesting that the HSE-specific keratinocytes are unique to organoid culturing and that the xenograft-unique keratinocytes are new cellular states induced after engraftment.

All of the *in vivo* cellular states are present in the xenograft HSEs (**Figure 4C-D**). However, the proportion of BAS-III and BAS-IV keratinocytes are not similar to each other, with BAS-III proportions being much higher and BAS-IV being lower in the xenograft than the *in vivo* setting (**Figure 4D and 4G**), a relationship found in the GelHSE and FibHSE cultures (**Figure 1H**) and suggesting that the abnormal basal cell proportions are not rescued by engraftment. The correlation between *in vivo* cell states improves in the xenograft cultures compared to the HSE cultures and the BAS-III state is no longer expanded into the SPN and GRN states (**Figure 4F vs**

Figure S5). Histologically, the xenografts appear relatively normal, with some basal keratinocytes adopting a cuboidal morphology (**Figure 4B**). Terminal differentiation appears to be rescued as RNA expression and immunofluorescence staining of FLG and LOR are now restricted to the granular layer and cell-cell contacts appear more normal with DSG1 now localizing to cell-cell contact sites (**Figure 4I**), suggesting that barrier formation, which is disrupted in HSE cultures, may be rescued upon engraftment. The basal cell states still appear to be partly disrupted, where total RNA expression for all four BAS clusters in the xenograft have the highest correlation with *in vivo* BAS-III rather than their respective cluster (**Figure 4F**), and KRT14 protein and RNA are still expanded into suprabasal layers (**Figure 4I**). Several basal cell markers are now appropriately expressed in their corresponding cell states compared to the HSE cultures (*PTTG1* with BAS-I, *RRM2* with BAS-II, and *ASS1* and *KRT19* with BAS-III), with *COL17A1* still showing abnormal expression (**Figure S6H**). The two abnormal features of the HSE cultures, the partial VIM+ EMT-like state and remnant PSCA+ embryonic program, are no longer detected in the xenograft tissue (**Figure 4I**), suggesting that the two abnormal programs seen in the HSEs are rescued. All three XENO clusters had higher GLUT1 RNA and protein expression **(Figure S7A)**, while XENO-3 showed an enrichment for KRT16 expression at the RNA and protein level **(Figure S7B)**. KRT16 is expressed in the spinous layer of human epidermis, however its localization has shifted to the granular layer demonstrating another change in cell state. The xenograft-unique clusters notwithstanding, the xenograft tissue more closely reflects the *in vivo* state compared to the HSE cultures with restored terminal differentiation, cell-cell adhesion, and partially restricted basal programs.

Xenograft HSEs contain two distinct transcriptional trajectories

To characterize how the XENO clusters influence the keratinocyte's differentiation trajectory, we employed pseudotime analysis overlayed onto the UMAP of the integrated *in vivo* and xenograft epithelial cells and found that xenografted keratinocytes likely follow two distinct transcriptional

trajectories from basal to granular cells (**Figure 5A-B**). The XENO states are highly stable, along with the BAS-III state, whereas the other BAS, SPN, and GRN states are more unstable in the xenograft compared to their *in vivo* counterpart (**Figure 5C**). The inferred trajectory showed a progression from least differentiated to most differentiated for the xenograft-unique cell clusters, with progression from the highest *COL17A1*+ state (XENO-1) to increasing *SBSN*+ expression (XENO-3) (**Figure 5D**). The splicing kinetics further supports two distinct differentiation trajectories, a BAS-SPN-GRN and a BAS-XENO-GRN trajectory possessing uniform velocity streams flowing from one state to the next (**Figure 5E**). The abundance of the XENO cluster cells (**Figure 4D**) suggests that the BAS-XENO-GRN differentiation trajectory is more favored in the xenograft.

When we compare the relative information flow for the xenograft and *in vivo* datasets for each significant imputed pathway, several pathways show exclusive enrichment in the xenograft (OCLN, MIF, GRN, ANGPTL, NECTIN, and THBS) as well as the *in vivo* (PTN, NRG, CADM, IGF, PROS) datasets (**Figure 5F, Table S1**). All of the pathways that are unique to xenograft are also present in at least one of the HSE cultures (**Table S1**). Although their functional roles within the HSE cultures are unclear, their known roles in skin biology suggest significant remodeling of the tissue and the extracellular environment. THBS signaling mainly originates in the BAS-III and XENO-1, whereas ANGPTL signaling mainly originates in XENO-2 and XENO-3 clusters (**Figure 5G**), and both are known to promote angiogenesis[89,90], suggesting that the XENO clusters within the xenograft tissue may be hypoxic due to a lack of vasculature and the wound healing process from the xenograft technique. NECTIN signaling shows promiscuous signaling throughout each cluster (**Figure 5G**), which is to be expected given its role in cell adhesion and skin morphogenesis[91]. The MIF signaling pathway largely signals to XENO-1 and XENO-2 clusters (**Figure 5G**) and has been shown to be upregulated during wound healing in mice[92].

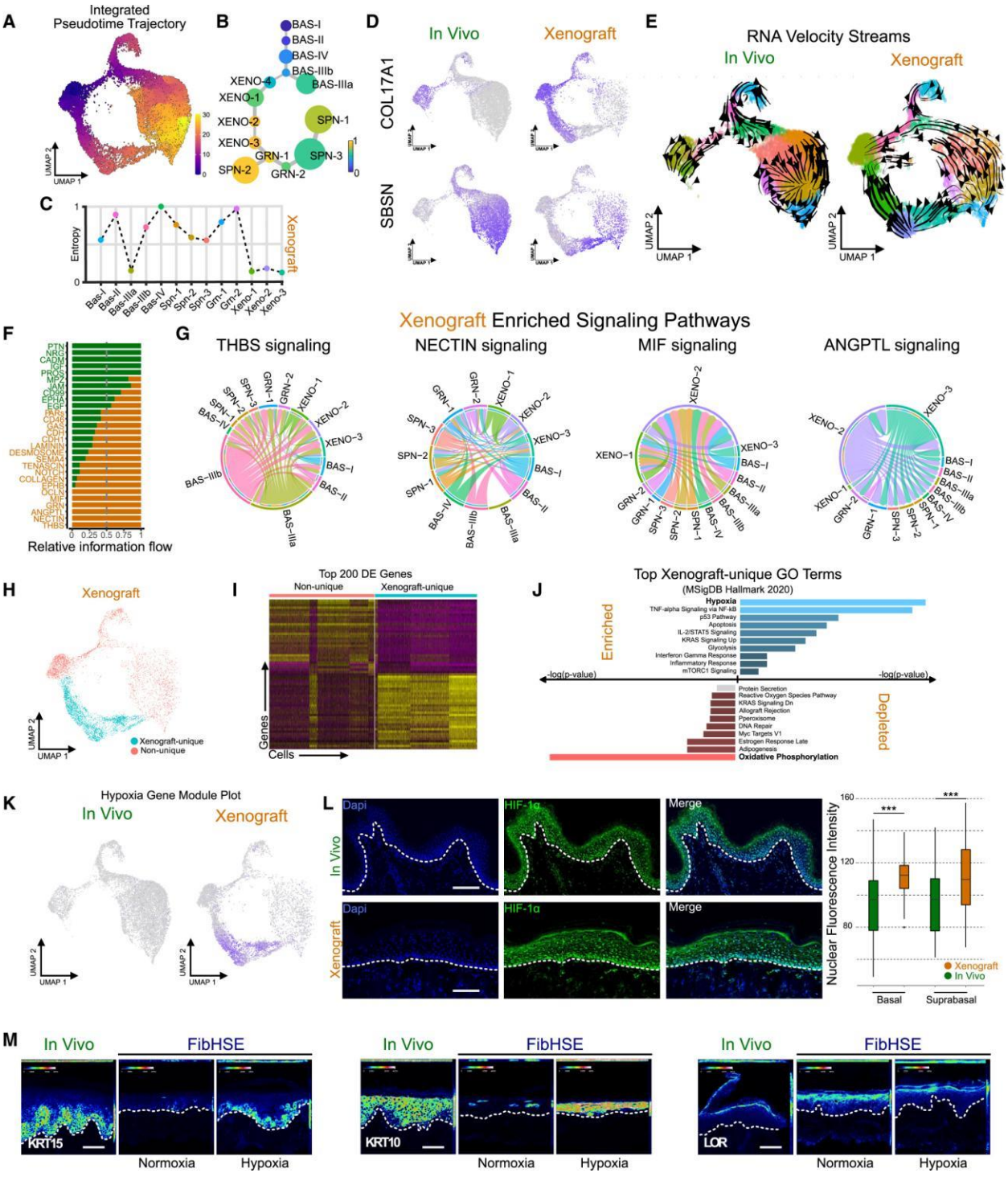

Figure 5. Hypoxia-driven transcriptional changes are observed in xenografts. A) Pseudotime inference and **B)** cell lineage diagram of epidermal keratinocytes from the integrated *in vivo* and xenograft datasets. Edge weights denote probability of transition to each cluster. Dot size denotes number of cells. **C)** Quantification of Cellular Entropy (*ξ*) using the R

package SoptSC. **D)** Feature plots showing *SBSN* and *COL17A1*, marking differentiated and undifferentiated keratinocytes, respectively. **E)** Splicing kinetics depicted as RNA velocity streams calculated using the python package scVelo. **F-G)** Significant cell-cell communication networks inferred using the R package, CellChat. **H)** Metaclustering of xenograft cells into xenograft-unique and non-unique cohorts. **I)** Heatmap showing the top 200 differentially expressed (DE) genes between the two metaclusters. X-axis represent cells from the xenograft dataset and y-axis are DE genes. Yellow represents a relatively higher expression while purple represents relatively low expression. **J)** GO analysis of the top DE genes shown in panel I. Blue bars indicate biological processes upregulated in xenograft-unique cells; red bars indicate biological process downregulated in xenograft-unique cells. **K)** Feature plots showing expression of a hypoxia gene module consisting of 34 hypoxia-related genes. **L)** Immunostaining of HIF1-α in human neonatal epidermis and xenograft tissue. Quantification of nuclear HIF1-α stain is shown to the right. Significance was determined by unpaired two-tailed *t* test. *$p < 0.001$. **M)** Immunostaining for KRT15 (Left), KRT10 (Middle), and LOR (Right) Pseudocoloring represents fluorescence intensity. Scale bar = 100 μm.

Hypoxia partially drives transcriptome-wide changes in xenograft-unique cells

As xenograft-unique signaling pathways indicate significant tissue remodeling, likely from the wounding process for engraftment, including enrichment for pathways that promote angiogenesis, we hypothesized that hypoxia may be a driving force behind the alternative transcriptional trajectory in the XENO clusters. This would align with the increased GLUT1 expression, a downstream target gene of the hypoxia transcription factor HIF1A, throughout all epidermal layers of the xenograft (**Figure S7A**). To explore this possibility, xenograft cells were metaclustered into two groups, xenograft-unique (XENO-1 through XENO-3) and non-unique clusters (BAS, SPN, and GRN) (**Figure 5H**). The xenograft-unique and non-unique metaclusters showed unique gene expression signatures (**Figure 5I**) and gene ontology analysis was performed on the top 100 marker genes for each metacluster using the MSigDB Hallmark 2020 database (**Figure 5J**). The most significantly enriched term for the xenograft-unique metacluster identified hypoxia, whereas the most significantly depleted pathway was oxidative phosphorylation (**Figure 5J**), which been shown to be down-regulated in response to hypoxia[93]. To explore this relationship further, we created a hypoxia gene module using Seurat's gene module function that included a manually curated list of 34 genes that have been experimentally shown to be upregulated in response to hypoxia and/or possess a hypoxia response element in the promoter region[94–97] (**Table S2**). The hypoxia gene module showed enhanced gene expression in the xenograft-unique metacluster with enrichment in all XENO clusters (**Figure 5K**), suggesting that the xenograft tissue is under hypoxic conditions. To validate the gene expression module, we immunostained the xenografted HSE for the transcription factor HIF1A and found nuclear HIF1A expression is significantly higher in the xenografts than the *in vivo* tissues (**Figure 5L**), suggesting that hypoxia is contributing to widespread transcriptional changes in the xenografted keratinocytes. To define the relationship between hypoxia and the HSE tissue architecture, we cultured FibHSEs for 14 days at 3% O_2 to mimic endogenous oxygen conditions[98,99]. Hypoxic FibHSEs expressed higher GLUT1 (**Figure S7C**), a downstream target gene of hypoxia and HIF1A[100], indicating these tissues were hypoxic

under the new culture conditions. The hypoxic HSEs showed a partially repaired basal program with KRT15 showing more uniform basal enrichment compared to normoxic conditions (**Figure 5M**). The differentiation program also appeared to be partially rescued with KRT10 expression in the spinous and granular compartments, compared to the sporadic staining under normoxic conditions, and LOR showing more restriction to the granular layer. These data suggests that culturing HSEs under hypoxic conditions mimicking physiological levels instead of atmospheric oxygen levels likely improves the basal and terminal differentiation programs of HSEs.

DISCUSSION

Human skin equivalents have long served as models of human IFE in place of murine skin[30,57,101,102]. We have shown that basal cell heterogeneity in our organoids fully mimics *in vivo* basal cell heterogeneity during homeostasis, with most of the differentiated states also present. However, HSE cultures exhibited signaling patterns characteristic of EMT events, contained organoid-unique cell states not found in *in vivo* neonatal epidermis where the cells were initially isolated, and showed differentiation abnormalities. Xenografting GelHSE cultures onto NSG mice rescued many of the defects in HSE cultures, but harbored xenograft-unique cell states likely driven by hypoxic conditions. These hypoxic conditions would likely last until the transplanted tissues reach homeostasis and wound repair pathways cease. For instance, wounding keratins KRT6/KRT16 were expressed in the grafted region at both days 16 and 37 in HSEs transplanted onto humans, with their expression disappearing a year after transplantation[103]. Similarly, KRT14 was expressed in all layers of the epidermis until a year post-grafting where it resumed a normal basal layer expression, suggesting that the tissue did not reach homeostasis until a year post-grafting[103]. However, transplantation of HSEs onto burn patients or recent transplantation of HSEs to cure junctional epidermolysis bullosa demonstrate their clinical importance and remains the gold standard[104].

Although basal cell heterogeneity was intact in the HSE and xenograft tissues, the proportions of BAS-III cells were enriched and BAS-IV cells were depleted compared to the *in vivo* state. BAS-III cells typically sit atop the rete ridges *in vivo*, whereas BAS-IV cells lie at the bottom of rete ridges[16]. However, this spatial environment is lost in the HSEs as the devitalized human dermis tends to flatten out during processing (**Figure 1B**), suggesting that spatial positioning may be important to specify the correct proportion of BAS-III-to-BAS-IV cells. The BAS-III state also shows more stability than BAS-IV, and BAS-III transcripts are retained throughout most of the other cellular states, suggesting the BAS-III program is not sufficiently shut down and may be the underlying cause of the differentiation defects seen in the SPN and GRN layers. Inappropriate signals from the dermis may also be the cause of the BAS defects. Although basal cells in both HSEs expressed canonical basal layer markers, they also expressed EMT-specific genes such as *VIM*, *LAMC2*, and *LGALS1*. The expression of these genes was higher in the GelHSE but still present in FibHSE, suggesting that while Matrigel may be enhancing EMT-like programs, replacing Matrigel with primary human dermal cells is not sufficient to induce the appropriate *in vivo* expression programs and may be due to the culture media. Our results also suggest that HSEs may represent a wound regeneration or development model due to their EMT features and inappropriate expression of KRT14[86]**.**

We identified a PSCA+ keratinocyte population, which we denoted HSE-1, unique to HSEs. Curiously, Psca expression occurs in the outermost layers of murine skin epithelium during E15-E17[66]. During this time, the outermost epithelial layer of the murine epidermis is periderm, which forms during stratification at E11.5 and disaggregates between E16-E17 when barrier formation occurs[105]. The periderm temporally expresses different marker genes as the epidermis differentiates, such as Krt17 during early stages and Krt6 during later stages[105]. *Psca* is upregulated in E18.5 murine epidermis of *Cyp26b1 -/-* mice which retains the periderm,

suggesting *Psca* may be a marker gene of periderm at later stages. Taken together, this data suggests that primary keratinocytes from newborn epidermal tissue may retain enough plasticity to differentiate into prenatal cell types that are no longer found postnatally. Staining for KRT4, a reported periderm marker[106], is found to be expressed in the GelHSE and FibHSE in all layers, but it is also detected lightly in adult abdominal skin and therefore it is unclear if this supports our hypothesis (**Figure S8**).

The presence of abnormal cell states and altered differentiation patterns in organoid cultures have been observed in a variety of tissues[52], including skin[9], using more conventional methods. Matrigel is used in the majority of organoid systems[52] and more than likely induces similar effects to those observed here. Recent papers using scRNA-seq to characterize organoid cultures of other tissue types have also identified abnormal cell populations present in their organoid cultures. For instance, melanoma-like, neuronal-like, and muscle-like cells were found using scRNA-seq of kidney organoids[107], which were consistent with previous observations using conventional methods in this system. scRNA-seq analysis of human intestinal and brain organoids used random forest classifiers to identify the cell types in their organoid cultures[108,109], however, doing so precludes the possibility of classifying cells as anything other than predefined types. This is true of any supervised machine learning algorithm and can be misleading when examining cellular heterogeneity.

Despite the transcriptional and molecular differences we see in HSE organoid cultures, they still are attractive systems for investigative dermatology and are superior to two-dimensional tissue culture of primary keratinocytes. Both HSE culture conditions form fully stratified tissues, generate the majority of *in vivo* cellular states, and largely reach homeostatic conditions after transplantation. Although xenografted HSEs are still utilizing wound repair programs 24 days post engraftment, allowing more time for the graft to heal would presumably return it to a fully

homeostatic state. Potential ways to improve HSEs to more faithfully mimic *in vivo* skin could include the addition of cell types such as Langerhans cells, melanocytes, endothelial cells, and other immune cells. Altering culturing conditions or bioengineering 3D scaffolds may also help restrict basal and terminal differentiating programs to their proper cellular states.

Limitations of the study

Limitations of the study include how we culture the HSE organoids. Contrary to our results, other studies do not observe any FLG and LOR expression defects when generating fibroblast-seeded HSEs. This difference may be due to the variations in culturing methods. For instance, HSEs can be completely submerged in media for multiple days prior to raising to an air-liquid interface to promote stratification[110], generated with immortalized keratinocyte cell lines[111], or seeded onto collagen layers[112]. The extent to which these changes resolve the underlying differentiation defects or give rise to new issues remains unclear. More pertinent to our study, hypoxia and angiogenesis are causally linked to wound repair which collectively induces substantial molecular and morphological changes to tissues during repair[113,114]. While we cannot rule out wound repair as the major cause of transcriptional changes in our xenograft HSEs, hypoxia was among the most prominent differences between the xenograft HSE and the *in vivo* cell states. As the epidermis is not directly supplied with blood, *in vivo* oxygen levels range between 0.5% and 8%[98,99]. Culturing FibHSEs under hypoxic conditions at 3% O_2 versus normoxic atmospheric conditions at 18-20% O_2 induced molecular changes that partially resembled the xenograft HSE, suggesting that culturing HSEs under hypoxia may be advantageous and in agreement with other findings[95].

Chapter 3

Conclusions

Summary

The future potential for skin organoids is immense. As this technology continues to evolve, it is anticipated that skin organoids will play an increasingly pivotal role in dermatological research and therapy. They could be harnessed to develop personalized treatments for skin diseases, to test the safety and efficacy of new skincare products, to study the effects of environmental factors on skin health, or to engineer skin grafts for burn victims. However, to fully harness their potential, ongoing research is required to improve their fidelity and reproducibility, and to incorporate additional components that mimic the in vivo environment more accurately. With continued advancements in this field, skin organoids are poised to become an integral component of dermatological research and therapy, potentially revolutionizing our understanding and treatment of skin diseases.

Revisiting HSE Keratinocyte Transcriptional States

In our research, we undertook a comprehensive analysis of the heterogeneity within in vitro and xenografted HSEs. This analysis was pivotal in understanding the cellular dynamics and differentiation pathways within these in vitro models. Our findings revealed a number of notable differences in keratinocyte composition and transcriptional state. While the basal cell heterogeneity in our organoids does not perfectly mirror in vivo basal cell heterogeneity during homeostasis, it does capture many key aspects of it. Our research also highlights several unique characteristics and abnormalities in HSEs. We observed signaling patterns characteristic of EMT, abnormal differentiation trajectories, and cell states that were not observed in native human skin.

Discussion on the BAS cell heterogeneity in HSEs and xenograft tissues

All subpopulations of basal cells were present in the HSEs, albeit with skewed proportions. Notably, the BAS-III subtype was overrepresented, especially in FibHSE organoids, while BAS-I, II, and IV were underrepresented. What this means functionally is an area that remains to be explored. The roles that different basal keratinocyte subtypes play in homeostasis, wound repair, and disease is unknown, due largely to two main reasons: this heterogeneity wasn't well characterized prior to recent single cell sequencing technologies; and a convenient model system for studying epidermal stem cell heterogeneity hasn't been identified. There are several hypotheses that could explain the reduction in specific basal cell subpopulations. It's possible that the BAS-III subtype is primarily responsible for re-epithelializing the devitalized dermis and these cells don't readily transition to other basal cell states. An argument against this would be that the xenograft has a more appropriate balance of cell types, but we do still see an overall increase in BAS-III cells there as well. Considering that two of the populations are cycling cells, another explanation is that because the cells are not proliferating as much at the week four time point

when samples were collected for sequencing, the basal cells in our HSEs don't resemble these specific basal subtypes. As a direct consequence of this, BAS-IV cells, which appear to be further along in the keratinocyte lineage, would decrease as the number of new cells to replace them diminishes. Alternatively, the organoid cultures may not fully recapitulate the spatiotemporal signaling cues present in the epidermis needed to specify these subpopulations. Future experimentation is necessary to address these questions.

Examination of the signaling patterns characteristic of EMT events and differentiation abnormalities

EMT is a crucial process in various physiological and pathological contexts, including wound healing[86,114], fibrosis[115], and cancer progression[74]. However, EMT events are not typically observed in *in vivo* epidermis under homeostatic conditions. The EMT-like phenotype we observed in the HSEs persisted throughout every time point examined which suggested that wound healing programs activated during re-epithelialization of the devitalized dermis are not solely responsible for the EMT-associated expression patterns. These observations, alongside the cell-cell communication inference which showed a substantial increase in EGF signaling, prompted us to check whether our culture conditions were at all contributing to the EMT-like phenotype. Considering that the media is supplemented with EGF ligand, we reasoned that this would be the best place to start when making alterations to the media formulation. We saw a significant decrease in the amount of Vimentin expression in the FibHSEs when EGF was removed after the 1st week of culturing. Furthermore, the amount of Vimentin being detected was far more consistent across samples. While Vimentin protein levels were decreased, they were not completely gone, indicating that there is something else contributing to the EMT-like state or that the initial culturing with EGF causes a persistent effect even after removing EGF. It is unclear if the Vimentin expression persists throughout all time points when EGF is removed.

In addition to the EMT-like phenotype, HSE cultures also contained organoid-unique cell states and showed differentiation abnormalities. Prostate stem cell antigen (PSCA) is ectopically expressed in the GelHSEs and serves as an excellent marker for the HSE-1 population. Very few studies have ever described PSCA expression in the epidermis. A 2001 paper by Ross et al., published in the American Journal of Pathology, described the expression of PSCA in murine epithelial tissues during development. In this study, the researchers noted that PSCA was only expressed from embryonic day 15 to 17 in mouse epidermis, specifically in the outermost living layer[66]. This localization is consistent with our findings and may suggest that the neonatal epidermal stem cells used to generate the HSEs possess enough plasticity to reactivate embryonic programs, provided that the proper signals are given. It is unclear if adult keratinocytes can differentiate into the HSE-1 population since only keratinocytes from neonatal tissue were used. Further studies looking at expression in human embryonic tissue could help address this hypothesis.

Skin organoids are not the only type of organoid that possess molecular and histological differences. A study that used RNA-seq on intestinal organoids found that those organoids had many unique expression patterns that were not present in the in vivo tissue[116]. These unique patterns were attributed to the artificial environment of the organoid culture, which lacked the complex mix of signals present in the in vivo intestinal tissue. Similarly, a study on brain organoids reported that the organoids had variable shapes and sizes depending upon the conditions in the organoid cultures[109]. The in vitro environment can be vastly different from the in vivo conditions that cells naturally experience. Factors such as the composition of the culture medium, the physical properties of the extracellular matrix, the absence of systemic signals, and the lack of interaction with other cell types can all influence cell behavior and differentiation.

Analysis of the GelHSE lineage: Basal to Spinous to HSE-unique

Our pseudotime and RNA velocity analyses of the GelHSE lineage revealed a differentiation progression from Basal to Spinous to HSE-unique cells. This is further supported by the position of the HSE-1 keratinocytes in the epidermis. Since keratinocytes migrate outward as they terminally differentiate and ultimately sloth off, we would expect these cells to be positioned just above the spinous cells they are differentiating from. This unique trajectory, not observed in in vivo epidermis, further emphasizes the distinct cellular dynamics within HSE organoids.

In addition to the abnormal differentiation trajectory, the normal trajectory also possessed some differences. The differentiated keratinocytes in the two in vitro HSEs were more homogenous than native human skin, specifically in the spinous and granular cells, which were missing entire subpopulations. A recent 2023 paper, by Wiedemann et al., characterized the heterogeneity that exists amongst spinous cells across multiple anatomical sites in humans[117]. They consistently found heterogeneous spinous populations in the palms, hips, and soles, highlighting the importance of these populations in various biological contexts. The absence of spinous and granular subpopulations in the HSEs suggest that these models may not fully replicate the complex process of keratinocyte differentiation and maturation that occurs in vivo and even deviate from it given the right (wrong) conditions. This could impact the HSE's ability to accurately model certain aspects of skin biology including the skin's barrier function, response to environmental stressors, or the pathogenesis of skin diseases that involve abnormalities in keratinocyte differentiation.

Implications of these findings for skin biology studies

These observations have significant implications for the use of HSEs as models for studying skin biology. On one hand, the presence of EMT-like signaling patterns and unique cell states could provide novel insights into the plasticity of skin cells and their response to different environmental conditions. On the other hand, these abnormalities could limit the physiological relevance of HSEs and affect their ability to accurately model in vivo skin biology. Therefore, these findings underscore the need for further research to understand the factors driving these changes in the HSEs and to develop strategies for mitigating these effects.

Addressing Limitations and Identifying Areas for Innovation in Organoid Cultures

Summary of key limitations identified related to the use of skin organoid cultures

Our research has identified several key limitations that could potentially impact the physiological relevance and utility of HSEs as a model. One of the primary limitations observed is impaired differentiation. Differentiating keratinocytes in the HSE cultures fail to fully adopt the characteristics of their in vivo counterparts, which could limit the ability of these models to accurately recapitulate in vivo skin biology. This issue is further compounded by the presence of cells with abnormally large and misshapen nuclei, possibly indicating genomic instability[118] or altered cell cycle regulation[119]. In addition to these issues, HSEs exhibit an EMT-like phenotype, poorly defined cell borders, and gaps in the intercellular space. This could disrupt the integrity and function of the tissue, further limiting the physiological relevance of these models. Addressing these issues will likely require a multifaceted approach. This could include optimizing the composition of the culture media, introducing additional cell types to better mimic the in vivo environment, and potentially using bioengineering techniques to create more physiologically relevant 3D structures.

Impaired differentiation in the HSE cultures could stem from factors like inappropriate signaling cues from the culture media or missing critical cell-cell or cell-matrix interactions. This impaired differentiation could confound the organoid models' accuracy in replicating aspects of skin biology that depend on proper keratinocyte differentiation. In skin organoid studies aiming to model specific diseases or investigate skin development, this impairment could lead to misleading outcomes due to the absence or improper representation of cell states throughout the keratinocyte lineage. For instance, some studies have proposed anticancer mechanisms that rely on inducing terminal differentiation. Researchers following up on these studies would be presented with issues when attempting to model this process in HSEs. The importance of further investigation and optimization of organoid cultures to ensure the faithful recapitulation of differentiation cannot be overstated.

Abnormally large and misshapen nuclei in the HSE organoid cultures might be symptomatic of genomic instability[118] or modified cell cycle regulation[119]. Intricate biological processes govern nuclear size and shape, and any alterations can signify issues with DNA replication, chromosome segregation, or other facets of cell division, potentially precipitating an accumulation of genetic errors. Such errors can perturb normal cell function. Apart from genomic instability or modified cell cycle regulation, these nuclear aberrations could also be suggestive of laminopathies, a group of disorders caused by defects in the lamin proteins that maintain nuclear structure[120,121]. Certain culture conditions may be contributing to this phenotype, but the exact impact of individual media components on nuclear lamina and the potential onset of laminopathies in organoid cultures is not well-understood. Regardless of the exact underlying cause behind the large and misshapen nuclei, a distorted nucleus doesn't merely indicate a size increase but implies potential changes to the chromatin arrangement within the nucleus, profoundly impacting transcription[122].

Experimental evidence has corroborated this notion, highlighting that any alteration in nuclear structure can have significant repercussions on gene expression and cellular behavior. Nuclear abnormalities in organoid cultures warrant further investigation and remedial strategies due to their potential far-reaching effects on cell function and health.

While the EMT process is crucial in certain physiological contexts, such as wound healing[86,114] and development[123], it is not typically observed in normal, healthy skin. The presence of an EMT-like phenotype in organoid cultures could be indicative of abnormal signaling cues or stress conditions in the culture environment. Numerous studies have shown that EMT leads to alterations in keratinocyte behavior that diverges from those of homeostatic skin[86,87,115,123,124]. Such alterations could profoundly affect organoid studies, including those aiming to model specific diseases. If a disease state under investigation is accompanied by an EMT-like phenotype, this could change the organoid's response to therapeutic interventions or potentially alter our understanding of the disease's underlying mechanisms. In some circumstances, it might impede our ability to model the disease at all. Hence, recognizing and addressing the influence of EMT-like phenotypes in organoid cultures is crucial for the accurate modelling of diseases and the development of effective therapeutic strategies.

The presence of larger cells and decreased cell density observed in organoid cultures, compared to in vivo skin, may reflect modified cell proliferation and differentiation dynamics. The increase in cell size could be a consequence of diminished proliferation, as the existing cells may expand to occupy the available space. This could occur due to extended time in the growth phase of the cell cycle (interphase) or lack of contact inhibition typically experienced when cells are in close proximity. Alternatively, the larger size may suggest augmented protein synthesis and growth,

possibly stimulated by high concentrations of growth-promoting signals in the culture media. The reduced cell density, in turn, could be a direct outcome of the larger cell size. Both these phenomena - enlarged cell size and decreased cell density - are interconnected in this context and could collectively affect the organoid's structural and functional attributes, thereby limiting their physiological relevance.

The occurrence of poorly defined cell borders and intercellular gaps within human skin equivalents might signify a disruption in cell-cell adhesion. Cell-cell adhesion is pivotal for maintaining the integrity and function of all epithelial tissues, including the skin, and its disruption could stem from irregular expression or function of adhesion molecules[125], potentially incited by inappropriate signaling cues from the culture media. This disruption could foster the creation of intercellular gaps, compromising tissue integrity and function. Notably, this phenotype is more pronounced at later stages, around weeks 3 and 4 of culture, suggesting a progressive deterioration of tissue health over time. The EMT phenotype, previously discussed, could contribute to this poor adhesion, but it likely wouldn’t be the only driver since these symptoms don’t manifest themselves until after a few weeks of culturing.

Proposal of potential strategies for overcoming these limitations, such as adding other cell types or altering culture conditions

While Epidermal Growth Factor (EGF), a potent mitogen[126,127], and calcium, known for its key role in keratinocyte differentiation[128], are both crucial components in the media, their balance can significantly impact the differentiation dynamics within the HSEs. EGF is regularly used in culturing to shift the equilibrium towards proliferation, potentially impairing differentiation due to the often inverse relationship between these two processes. Concurrently, suboptimal calcium

levels might impair differentiation, as higher calcium concentrations are necessary to induce keratinocyte differentiation. However, these deductions warrant careful consideration, particularly in light of observed reduced proliferation in the HSEs at later stages. Proposing modifications to the HSE organoid cultures, such as adjusting EGF and calcium concentrations, should account for potential tradeoffs. For instance, while reducing EGF levels could improve differentiation, it might also affect necessary proliferation at earlier stages. A holistic understanding and approach are required to optimize these cultures without adversely affecting other crucial parameters.

While adenine (a component of DNA that is involved in diverse cellular processes like cell growth and division) and insulin (a known growth factor that promotes cell proliferation[129]) are both vital for cellular functioning, their concentration balance within the HSE culture media may significantly influence cellular dynamics. The presence of adenine in abnormal amounts could hypothetically disrupt these processes, potentially inducing genomic instability or altered cell cycle regulation, although this requires further validation given the limited existing evidence on this aspect. Similarly, excess insulin might potentially trigger abnormal cell growth, alterations in nuclear size, and shape[130]. An understanding of how the reagents are modulating the HSE cultures might help in resolving the observed issues and follow up experiments on them are warranted.

EGF and cholera toxin significantly impact key aspects of cellular processes such as cell migration and cell-cell adhesion, and each has been shown to induce EMT in keratinocytes[71,131]. EGF, a recognized growth factor, can stimulate cell migration and invasion, facilitating tissue development and wound healing. Cholera toxin is often incorporated in cultures due to its ability to increase the production of cyclic AMP (cAMP) within cells[132]. This rise in cAMP levels increases cell proliferation which is crucial for maintaining robust organoid cultures. However, cholera toxin

may also disrupt cell-cell adhesion by modifying the functionality of adhesion molecules, presumably via its EMT inducing activity. In chapter 2, it was demonstrated that EGF contributes to the EMT phenotype, but it is not solely responsible for it. Cholera toxin could potentially contribute to the EMT-like phenotype in the cultures, and follow-up experiments adjusting its concentration would shed light on this.

Insulin, a critical component in cell culture media, triggers a cascade of events facilitating protein synthesis and cell growth[133], while simultaneously suppressing apoptosis[134]–processes fundamental to maintaining the vitality of the organoid cultures. Studies have demonstrated that a surplus of insulin can result in increased cell size. However, it's important to consider the potential ramifications of drastically altering insulin levels in the culture media. Although reducing insulin might mitigate issues related to abnormal cell growth, it could also compromise cell survival and induce unnecessary stress within the cultures.

Improving the fidelity of human skin equivalents (HSEs) can be achieved through the incorporation of additional cell types. Among these, melanocytes present an ideal starting point for several reasons. Firstly, melanocytes are known to have direct interactions with keratinocytes, the predominant cell type in the epidermis[135]. This interaction is crucial for the maintenance of skin homeostasis and the regulation of various skin functions. By including melanocytes in HSEs, we can better model these interactions and gain a deeper understanding of their role in skin biology. Secondly, melanocytes produce melanin, a pigment that plays a significant role as an antioxidant. Melanin protects the skin from harmful ultraviolet radiation, reducing the risk of DNA damage that can lead to skin cancer. The inclusion of melanocytes in HSEs would allow for the modeling of melanin production and its protective effects, providing a more accurate

representation of skin's response to environmental stressors. Lastly, the presence of melanocytes in HSEs would enable the modeling of skin pigmentation in vitro. This could be particularly useful for studying pigmentation disorders and testing treatments for these conditions.

Several studies focusing on vitiligo, an autoimmune disease characterized by the immune system attacking melanocytes, have provided further evidence of the importance of melanocytes in skin health[136]. These studies have found that in patches of vitiligo skin that lack melanocytes there is an increased rate of keratinocyte apoptosis compared to the surrounding tissue[137]. While the exact mechanism behind this observation remains unknown, it suggests a potential pro-survival interaction between melanocytes and keratinocytes in healthy skin. This interaction could be crucial for maintaining skin integrity and function, and its disruption could contribute to skin disorders. It is worth noting that it was never determined if the increased apoptosis was simply due to increased UV damage. Nevertheless, by including melanocytes in HSEs, we could potentially model and study this interaction, shedding light on its role in skin health and disease.

Discussion on the existing variations in culturing methods and their potential impact

Full-thickness human skin equivalents like those described in chapter 2 are advantageous for studying basic skin biology and specific diseases since they incorporate both epidermal and dermal components, but they may not fully replicate the complex skin interactions involved in certain disorders due to a lack of additional cellular components like immune cells. When used for pharmaceutical testing, these models can give a preliminary idea of how a drug might interact with skin cells, but the lack of immune cells or vascular elements may limit their predictive capacity for possible systemic effects or complex inflammatory reactions. Their potential for grafting onto patients is largely limited if collagen matrix is used as it doesn't fully mimic the properties of human

dermal tissue. The use of devitalized dermis as the substrate can help resolve this, but it requires a donor whereas engineered substrates do not. A highly reproducible, donor-free method for engineering full-thickness skin human skin equivalents can be a substantial boon for high-throughput drug screening. The use of immortalized, but otherwise normal, keratinocytes and fibroblasts would allow for prolonged use of genetically modified cells capable of modeling a variety of skin diseases.

Organ-on-a-chip Technology can provide a more detailed understanding of skin and its interactions with other tissues, which can be particularly useful in disease modeling. With this method, diseases that involve multiple organs can be studied more effectively[40]. For pharmaceutical testing, the technology's high-throughput nature allows for rapid, simultaneous testing of multiple compounds, possibly outperforming a simpler full-thickness HSE. However, the complexity and high cost of the technology may hinder its widespread application in these areas. When it comes to grafting, the technology is not directly applicable, but insights gained from the chip model could aid in developing more effective grafts.

Spheroid Cultures provide a 3D environment that more closely mimics the in vivo conditions of the skin than 2D cultures, thus improving the accuracy of disease models[36]. However, the nutrient, oxygen, and drug gradients in larger spheroids can influence cell behavior, potentially impacting the results of disease models and drug tests, making it a less desirable choice compared to other organoid systems. Additionally, spheroids are ill-suited for use as grafts due to their irregular morphology. In a spheroid culture, the cells self-assemble into a three-dimensional ball-like structure. This simple structure can represent some aspects of the in vivo environment better than a two-dimensional culture. For instance, it enables cell-cell and cell-matrix interactions that are

critical for many cellular processes. However, this spherical arrangement does not truly reflect the more complex architecture of actual human skin. This lack of structural fidelity can also affect the penetration of drugs, limiting the model's usefulness for pharmaceutical testing.

Bioprinting offers a high degree of control over the structure of the skin equivalent, potentially leading to more accurate disease models and more relevant drug testing results[36]. However, the high cost and technical complexity of the method could limit its use, especially in the production of grafts. The challenge of recreating the mechanical properties of skin also hinders the use of bioprinted skin as grafts. This technology holds great promise that is unfortunately far from being realized.

Induced pluripotent stem cells (iPSCs) can be used to create patient-specific skin equivalents, potentially revolutionizing personalized medicine[53]. For disease modeling, they can be used to create skin equivalents that closely match the patient's own diseased skin. However, the complex, time-consuming, and costly process of reprogramming and differentiating the cells can be a deterrent. There's also a risk of teratoma formation from undifferentiated cells when grafting these models onto patients. iPSCs would likely need to be combined with one of the other existing methods of HSE generation as it would be impractical to provide all the necessary signals and cues for them to fully self-assemble, including the production of ECM.

Understanding the Role of Xenografting and Hypoxia in HSEs

Discussion on the role of xenografting in rescuing defects in HSE cultures

Xenografting, a technique wherein tissues or cells from one species are transplanted into a different species, serves as an alternative approach to simulate endogenous conditions more accurately than in vitro HSEs. In the context of this study, HSEs are xenografted onto mice. Despite the structural similarities of HSEs to native human skin, they inherently lack several crucial features of the skin, such as a fully functioning vasculature, immune system, and innervation. By xenografting HSEs onto mice, these deficiencies can be partially overcome. The in vivo environment of a mouse host provides a more intricate interplay of cellular signaling, closely mimicking the dynamics of human skin. Immunocompromised mice lacking an adaptive immune system are often used to prevent graft vs host disease. This does remove the immune component, but it preserves all other interactions. This advanced model aims to replicate the diverse microenvironment and functionality of human skin more effectively at the expense of lower throughput.

While xenografted HSEs are often thought of as the gold standard for modeling human skin, prior to the work described in chapter 2, this claim had never been evaluated at the transcriptome level. We found that xenografting HSEs onto mice altered the cellular states and transcriptional profile of HSEs. The xenografted HSEs were found to have three unique clusters of cells, designated XENO-1 through XENO-3, which were not present in the original HSE cultures. These clusters represented new cellular states induced after engraftment, suggesting that the HSE-specific keratinocytes are unique to organoid culturing and that the xenograft-unique keratinocytes are new cellular states induced after engraftment.

The xenograft HSEs contained all the in vivo cellular states, but the proportions of certain keratinocyte subtypes (BAS-III and BAS-IV) were not similar to native skin. BAS-III proportions

were much higher, and BAS-IV were lower in the xenograft than the in vivo setting. This suggests that the abnormal basal cell proportions are not rescued by engraftment. In the context of mouse skin, this might make sense. The proportions of certain keratinocytes are normally different in mice relative to humans. The epidermis of mice is much thinner and has far fewer differentiated keratinocytes relative to the basal ones[34]. And perhaps the BAS-IV population is underrepresented in mice because this population is far more transient in this species. A large comparison of the differences that exist between human and mouse transcriptomes in epidermal keratinocytes needs to be performed to answer these questions, but cross species comparisons like this can be quite challenging.

Despite these differences in proportions, the xenograft HSEs did show some improvements over the original HSE cultures. Terminal differentiation appeared to be rescued, with RNA expression and immunofluorescence staining of certain proteins now restricted to the granular layer. This suggests that barrier formation, which is disrupted in HSE cultures, may be rescued upon engraftment. Additionally, the two abnormal features of the HSE cultures, the partial VIM+ EMT-like state and remnant PSCA+ embryonic program, were no longer detected in the xenograft tissue, suggesting that these abnormal programs were rescued by xenografting. It remains to be seen if the reason for these changes is due to additional signaling provided by the mouse or the removal of ectopic signaling from the culture.

Examination of the impact of hypoxic conditions on xenograft-unique cell states

Additionally, our investigation of the xenograft data revealed an abnormal differentiation trajectory, likely driven by the hypoxic conditions in the xenografts. Pseudotime analysis of the xenograft HSEs suggested that the xenografted keratinocytes likely follow two distinct transcriptional

trajectories through gene space as they progess from basal to granular cells. The xenograft-unique cell cluster trajectory mirrored the normal trajectory in its expression of many canonical markers. Pseudotime and RNA velocity analysis showed a progression from least differentiated to most differentiated as keratinocytes transitioned along the two different paths, initially diverging at the BAS-III population and converging at the GRN population. While this separate path does represent unique transcriptional states that these keratinocytes are passing through as they differentiate, it does not necessarily imply that the keratinocytes are undergoing differentiation via some abnormal mechanism. All of the same signaling cascades responsible for normal differentiation can be occurring while the global transcriptional state appears different.

Our study also found that several signaling pathways that showed exclusive enrichment in the xenograft indicated significant remodeling of the tissue and the extracellular environment. The xenograft-unique signaling included many pathways known to be involved in the wounding process, including enrichment for pathways that promote angiogenesis and hypoxia. This led to the hypothesis that hypoxia may be a driving force behind the alternative transcriptional trajectory in the XENO clusters. When in vitro HSEs were grown under hypoxic conditions to emulate the hypoxia present in the xenograft, curiously, many of the markers for differentiated keratinocytes that were inappropriately expressed appeared to be restricted to the regions of the epidermis that they were supposed to be in. The “hypoxic” oxygen levels that the HSEs were grown in were the levels that would normally be present in in vivo human epidermis and likely represented a more physiologically relevant amount. The transcriptomes of the hypoxic HSEs were not examined and future studies exploring this would be better suited to explain how closely the in vitro hypoxic HSE states resemble the xenograft states.

Implications of these findings for the future use of HSEs and skin grafts

These findings highlight the need for careful interpretation of data from organoid cultures and for the development of more physiologically relevant culture conditions. This could involve the use of co-culture systems to incorporate other cell types, the use of bioengineered scaffolds to provide more accurate spatial cues, or the optimization of culture medium composition to better mimic the in vivo conditions. Despite these challenges, organoids remain a powerful tool for studying human biology due to their ability to recapitulate key aspects of organ structure and function in vitro.

Future Directions for Omics Studies in Skin Biology

Potential of Omics Studies in Skin Biology

The advent of omics technologies, including single-cell RNA sequencing (scRNA-seq), spatial transcriptomics, proteomics, and metabolomics, has spurred a paradigm shift in the realm of skin biology. These cutting-edge techniques provide granular insights into the molecular intricacies underlying various biological processes, extending from gene expression profiles to the functional dynamics of proteins and metabolic pathways within skin cells. More specifically, scRNA-seq facilitates the exploration of cellular heterogeneity[16], spatial transcriptomics adds a spatial dimension to transcriptomic data enhancing our understanding of tissue organization[63], and proteomics along with metabolomics, complement this information by deciphering the post-transcriptional modifications and metabolomic responses, respectively[138]. These technologies, individually and synergistically, have the potential to revolutionize the understanding of skin physiology and pathology, enhance the physiological relevance of Human Skin Equivalent (HSE) organoid models, and provide unprecedented insights into the molecular underpinnings of skin diseases.

The work in chapter 2, along with other groundbreaking publications, have underscored the power of scRNA-seq technology to distinguish cell types at an unprecedented level of detail. This approach has revolutionized gene expression analysis by enabling the exploration of individual cells, facilitating the identification of distinct cell types and states within the skin. Utilizing scRNA-seq, we have illuminated the diversity of cell populations in the skin, enriching our understanding of similarities and differences between HSEs and native skin on a molecular level. Furthermore, numerous studies have leveraged this technique on samples from both healthy and diseased tissues, offering profound insights into underlying biological mechanisms. As the costs associated with library preparation and sequencing technologies continue to decrease, a key challenge - affordability - is being addressed. This will eventually allow for larger sample sizes and increased biological replicates as sequencing becomes more cost-effective, leading to enhanced statistical power and ultimately bolstering confidence in the findings.

Spatial transcriptomics offers a remarkable advantage over other techniques by adding a spatial dimension to gene expression data. This methodology enables researchers to perceive the intricate interactions between varying cell types within their natural tissue context, which is particularly beneficial for the study of well-organized and layered organs such as skin. This cutting-edge technology fosters a more precise representation of cell-cell interactions by offering immediate information about the location of target cell populations. This not only allows for more accurate quantification of cell proportions but also facilitates the correlation of these data with splicing kinetics and pseudotime analysis, thereby generating a more comprehensive understanding of cellular dynamics. The potential applications of spatial transcriptomics extend beyond current usage, opening the door to numerous yet unimagined research opportunities. Further, combining spatial transcriptomics with single-cell RNA sequencing could provide a

holistic view of the cellular landscape, marrying the benefits of high-resolution cellular characterization with contextual insights from the native tissue architecture.

Proteomics and metabolomics are powerful analytical techniques that provide unique insights extending beyond those offered by transcriptomics. Proteomics reveals the dynamic protein landscape of skin, uncovering the functional proteins expressed and providing insights into post-translational modifications that cannot be inferred from gene transcripts alone. Metabolomics, on the other hand, unravels the metabolic state of skin cells, elucidating the complex interplay of small molecules that reflect immediate cellular responses to stimuli, which are not directly evident from transcript or protein data.

While each omics technology independently offers valuable data, a synergistic approach can result in a more comprehensive understanding of skin biology. Integrating data from transcriptomics, proteomics, and metabolomics can provide a comprehensive view of skin biology at multiple molecular levels. This integrative approach can help decipher complex regulatory networks and reveal how changes at one level may propagate and affect other levels, thereby creating a more accurate picture of the underlying biological phenomena.

As of now, proteomics and metabolomics face challenges in terms of sensitivity, quantification, and coverage compared to transcriptomics. Proteomics often struggles with the detection of low-abundance and transient proteins, while metabolomics faces difficulties in annotating and quantifying all detected metabolites. However, ongoing advancements in analytical methods, data acquisition techniques, and bioinformatic tools are continually enhancing these technologies. In

the foreseeable future, these hurdles are likely to be overcome, making proteomics and metabolomics even more effective and indispensable in the multi-omics landscape.

Advancing HSE Organoid Cultures and Unveiling New Aspects of Skin Diseases

Omics technologies can play a pivotal role in enhancing the physiological relevance of HSE organoid cultures. Utilizing scRNA-seq, we have been able to analyze and compare the cellular composition of HSEs and in vivo skin, enabling the identification of potential areas for improvement within the organoid models. Spatial transcriptomics, on the other hand, offers insights into the spatial organization of cells in organoids, thereby guiding improvements in the structural composition of these cultures. Proteomics and metabolomics provide a deeper understanding of the functional status and metabolic responses of organoids. Moreover, the implementation of omics technologies in skin biology can shed light on previously unexplored facets of skin diseases. By comparing the omics profiles of healthy and disease-afflicted skin, molecular changes linked with specific diseases can be pinpointed.

Challenges and Solutions

The employment of omics technologies in skin biology research, while promising, is clearly not devoid of challenges. The financial investment and technical expertise required for these advanced technologies can prove to be prohibitive for some researchers. Yet, with the continuous progress in sequencing technologies, the cost is rapidly decreasing and new bioinformatics tools tailored for the analysis of complex omics datasets are streamlining the extraction of meaningful and impactful insights. Everyday the accessibility of these technologies for all researchers is increasing.

Summary

Omics technologies are unlocking new frontiers in the understanding of skin biology, shaping the way we perceive cellular and molecular complexity, refining the physiological relevance of HSE organoid cultures, and revealing fresh perspectives on skin diseases. These technologies, be it single-cell RNA sequencing, spatial transcriptomics, proteomics, or metabolomics, have the potential to revolutionize our approach to skin biology research by enabling detailed cellular and molecular characterizations. They offer not only individual insights into gene expression, cellular organization, protein dynamics, and metabolic responses but, when integrated, provide a comprehensive and holistic view of the skin biology at multiple molecular levels. This integrative approach is particularly advantageous, helping to decipher complex regulatory networks, and revealing how changes at one level may propagate and affect others, thereby creating a more accurate picture of the underlying biological phenomena.

Despite the challenges that currently exist, such as the high financial investment, technical expertise requirements, and the complexity of skin tissues, the rapid pace of technology and bioinformatics advancements is progressively mitigating these barriers. The future of omics in skin biology research appears promising, with an increasing shift towards a more affordable, accessible, and efficient extraction of meaningful insights from complex omics datasets. Omics technologies marks the dawning of a new era in skin biology research, paving the way for unprecedented advancements in our understanding of skin physiology and pathology.

REFERENCES

1. Proksch, E., Brandner, J.M., and Jensen, J.-M. (2008). The skin: an indispensable barrier. Exp. Dermatol. *17*, 1063–1072. 10.1111/j.1600-0625.2008.00786.x.

2. Slominski, A.T., Zmijewski, M.A., Skobowiat, C., Zbytek, B., Slominski, R.M., and Steketee, J.D. (2012). Sensing the environment: Regulation of local and global homeostasis by the skin neuroendocrine system. Adv. Anat. Embryol. Cell Biol. *212*, v–115.

3. Fuchs, E., and Horsley, V. (2008). More than one way to skin . . . Genes Dev. *22*, 976–985. 10.1101/gad.1645908.

4. Kolarsick, P.A.J., Kolarsick, M.A., and Goodwin, C. (2011). Anatomy and Physiology of the Skin. J. Dermatol. Nurses Assoc. *3*, 203–213. 10.1097/JDN.0b013e3182274a98.

5. Khavkin, J., and Ellis, D.A.F. (2011). Aging skin: histology, physiology, and pathology. Facial Plast. Surg. Clin. N. Am. *19*, 229–234. 10.1016/j.fsc.2011.04.003.

6. Gilchrest, B.A., and Krutmann, J. eds. (2006). Skin Aging (Springer-Verlag) 10.1007/3-540-32953-6.

7. Rosen, E.D., and Spiegelman, B.M. (2014). What we talk about when we talk about fat. Cell *156*, 20–44. 10.1016/j.cell.2013.12.012.

8. Fang, Y., and Eglen, R.M. (2017). Three-Dimensional Cell Cultures in Drug Discovery and Development. Slas Discov. *22*, 456–472. 10.1177/1087057117696795.

9. Atwood, S.X., and Plikus, M.V. (2021). Fostering a healthy culture: Biological relevance of in vitro and ex vivo skin models. Exp. Dermatol. *30*, 298–303. 10.1111/exd.14296.

10. Abhishek, S., and Palamadai Krishnan, S. (2016). Epidermal Differentiation Complex: A Review on Its Epigenetic Regulation and Potential Drug Targets. Cell J. Yakhteh *18*, 1–6.

11. Brenner, M., and Hearing, V.J. (2008). The Protective Role of Melanin Against UV Damage in Human Skin. Photochem. Photobiol. *84*, 539–549. 10.1111/j.1751-1097.2007.00226.x.

12. Clayton, K., Vallejo, A.F., Davies, J., Sirvent, S., and Polak, M.E. (2017). Langerhans Cells—Programmed by the Epidermis. Front. Immunol. *8*.

13. Clausen, O.P.F., and Potten, C.S. (1990). Heterogeneity of keratinocytes in the epidermal basal cell layer. J. Cutan. Pathol. *17*, 129–143. 10.1111/j.1600-0560.1990.tb00072.x.

14. Joost, S., Zeisel, A., Jacob, T., Sun, X., La Manno, G., Lönnerberg, P., Linnarsson, S., and Kasper, M. (2016). Single-Cell Transcriptomics Reveals that Differentiation and Spatial Signatures Shape Epidermal and Hair Follicle Heterogeneity. Cell Syst. *3*, 221-237.e9. 10.1016/j.cels.2016.08.010.

15. Lavker, R.M., and Sun, T.T. (1982). Heterogeneity in epidermal basal keratinocytes: morphological and functional correlations. Science *215*, 1239–1241. 10.1126/science.7058342.

16. Wang, S., Drummond, M.L., Guerrero-Juarez, C.F., Tarapore, E., MacLean, A.L., Stabell, A.R., Wu, S.C., Gutierrez, G., That, B.T., Benavente, C.A., et al. (2020). Single cell transcriptomics of human

epidermis identifies basal stem cell transition states. Nat. Commun. *11*, 4239. 10.1038/s41467-020-18075-7.

17. Reynolds, G., Vegh, P., Fletcher, J., Poyner, E.F.M., Stephenson, E., Goh, I., Botting, R.A., Huang, N., Olabi, B., Dubois, A., et al. (2021). Developmental cell programs are co-opted in inflammatory skin disease. Science *371*. 10.1126/science.aba6500.

18. Lin, C.-H., Chiu, P.-Y., Hsueh, Y.-Y., Shieh, S.-J., Wu, C.-C., Wong, T.-W., Chuong, C.-M., and Hughes, M.W. (2019). Regeneration of rete ridges in Lanyu pig (Sus scrofa): Insights for human skin wound healing. Exp. Dermatol. *0*. 10.1111/exd.13875.

19. Botchkarev, V.A., and Sharov, A.A. (2004). BMP signaling in the control of skin development and hair follicle growth. Differentiation *72*, 512–526. 10.1111/j.1432-0436.2004.07209005.x.

20. Inamatsu, M., Tochio, T., Makabe, A., Endo, T., Oomizu, S., Kobayashi, E., and Yoshizato, K. (2006). Embryonic dermal condensation and adult dermal papilla induce hair follicles in adult glabrous epidermis through different mechanisms. Dev. Growth Differ. *48*, 73–86. 10.1111/j.1440-169X.2006.00848.x.

21. Dong, B., Vold, S., Olvera-Jaramillo, C., and Chang, H. (2018). Functional redundancy of frizzled 3 and frizzled 6 in planar cell polarity control of mouse hair follicles. Development *145*, dev168468. 10.1242/dev.168468.

22. Duverger, O., and Morasso, M.I. (2009). Epidermal Patterning and Induction of Different Hair Types during Mouse Embryonic Development. Birth Defects Res. Part C Embryo Today Rev. *87*, 263–272. 10.1002/bdrc.20158.

23. Collu, G.M., Hidalgo-Sastre, A., and Brennan, K. (2014). Wnt–Notch signalling crosstalk in development and disease. Cell. Mol. Life Sci. *71*, 3553–3567. 10.1007/s00018-014-1644-x.

24. Lu, C., and Fuchs, E. (2014). Sweat Gland Progenitors in Development, Homeostasis, and Wound Repair. Cold Spring Harb. Perspect. Med. *4*, a015222. 10.1101/cshperspect.a015222.

25. Breitkreutz, D., Koxholt, I., Thiemann, K., and Nischt, R. (2013). Skin Basement Membrane: The Foundation of Epidermal Integrity—BM Functions and Diverse Roles of Bridging Molecules Nidogen and Perlecan. BioMed Res. Int. *2013*. 10.1155/2013/179784.

26. Amiri, N., Golin, A.P., Jalili, R.B., and Ghahary, A. (2022). Roles of cutaneous cell-cell communication in wound healing outcome: An emphasis on keratinocyte-fibroblast crosstalk. Exp. Dermatol. *31*, 475–484. 10.1111/exd.14516.

27. Lynch, M.D., and Watt, F.M. (2020). Fibroblast heterogeneity: implications for human disease. J. Clin. Invest. *128*, 26–35. 10.1172/JCI93555.

28. Townsend, K., and Tseng, Y.-H. (2012). Brown adipose tissue. Adipocyte *1*, 13–24. 10.4161/adip.18951.

29. Tsuji, W., Rubin, J.P., and Marra, K.G. (2014). Adipose-derived stem cells: Implications in tissue regeneration. World J. Stem Cells *6*, 312–321. 10.4252/wjsc.v6.i3.312.

30. Bell, E., Sher, S., Hull, B., Merrill, C., Rosen, S., Chamson, A., Asselineau, D., Dubertret, L., Coulomb, B., Lapiere, C., et al. (1983). The reconstitution of living skin. J. Invest. Dermatol. *81*, 2s–10s. 10.1111/1523-1747.ep12539993.

31. Stark, H.J., Baur, M., Breitkreutz, D., Mirancea, N., and Fusenig, N.E. (1999). Organotypic keratinocyte cocultures in defined medium with regular epidermal morphogenesis and differentiation. J. Invest. Dermatol. *112*, 681–691. 10.1046/j.1523-1747.1999.00573.x.

32. Li, J., and Sen, G.L. (2015). Generation of Genetically Modified Organotypic Skin Cultures Using Devitalized Human Dermis. JoVE J. Vis. Exp., e53280. 10.3791/53280.

33. Lee, J., Boescke, R., Tang, P.-C., Hartman, B.H., Heller, S., and Koehler, K.R. (2018). Hair follicle development in mouse pluripotent stem cell-derived skin organoids. Cell Rep. *22*, 242–254. 10.1016/j.celrep.2017.12.007.

34. Schmook, F.P., Meingassner, J.G., and Billich, A. (2001). Comparison of human skin or epidermis models with human and animal skin in in-vitro percutaneous absorption. Int. J. Pharm. *215*, 51–56. 10.1016/s0378-5173(00)00665-7.

35. Viswanathan, P., Guvendiren, M., Chua, W., B. Telerman, S., Liakath-Ali, K., A. Burdick, J., and M. Watt, F. (2016). Mimicking the topography of the epidermal–dermal interface with elastomer substrates. Integr. Biol. *8*, 21–29. 10.1039/C5IB00238A.

36. Zhang, Y., Enhejirigala, null, Yao, B., Li, Z., Song, W., Li, J., Zhu, D., Wang, Y., Duan, X., Yuan, X., et al. (2021). Using bioprinting and spheroid culture to create a skin model with sweat glands and hair follicles. Burns Trauma *9*, tkab013. 10.1093/burnst/tkab013.

37. Mobasseri, S.A., Zijl, S., Salameti, V., Walko, G., Stannard, A., Garcia-Manyes, S., and Watt, F.M. (2019). Patterning of human epidermal stem cells on undulating elastomer substrates reflects differences in cell stiffness. Acta Biomater. *87*, 256–264. 10.1016/j.actbio.2019.01.063.

38. Bell, E., Ehrlich, H.P., Buttle, D.J., and Nakatsuji, T. (1981). Living tissue formed in vitro and accepted as skin-equivalent tissue of full thickness. Science *211*, 1052–1054. 10.1126/science.7008197.

39. Fauzi, M.B., Rashidbenam, Z., Bin Saim, A., and Binti Hj Idrus, R. (2020). Preliminary Study of In Vitro Three-Dimensional Skin Model Using an Ovine Collagen Type I Sponge Seeded with Co-Culture Skin Cells: Submerged versus Air-Liquid Interface Conditions. Polymers *12*, E2784. 10.3390/polym12122784.

40. Risueño, I., Valencia, L., Jorcano, J.L., and Velasco, D. (2021). Skin-on-a-chip models: General overview and future perspectives. APL Bioeng. *5*, 030901. 10.1063/5.0046376.

41. Zhang, Q., Sito, L., Mao, M., He, J., Zhang, Y.S., and Zhao, X. (2018). Current advances in skin-on-a-chip models for drug testing. Microphysiological Syst. *2*, 4. 10.21037/mps.2018.08.01.

42. Sun, H., Zhang, Y.-X., and Li, Y.-M. (2021). Generation of Skin Organoids: Potential Opportunities and Challenges. Front. Cell Dev. Biol. *9*, 709824. 10.3389/fcell.2021.709824.

43. Generation of a Three-dimensional Full Thickness Skin Equivalent and Automated Wounding | Protocol (2021). https://www.jove.com/t/52576/generation-three-dimensional-full-thickness-skin-equivalent-automated.

44. Kapałczyńska, M., Kolenda, T., Przybyła, W., Zajączkowska, M., Teresiak, A., Filas, V., Ibbs, M., Bliźniak, R., Łuczewski, Ł., and Lamperska, K. (2018). 2D and 3D cell cultures – a comparison of different types of cancer cell cultures. Arch. Med. Sci. AMS *14*, 910–919. 10.5114/aoms.2016.63743.

45. Watt, F.M., and Fujiwara, H. (2011). Cell-Extracellular Matrix Interactions in Normal and Diseased Skin. Cold Spring Harb. Perspect. Biol. *3*, a005124. 10.1101/cshperspect.a005124.

46. Naldaiz-Gastesi, N., Bahri, O.A., López de Munain, A., McCullagh, K.J.A., and Izeta, A. (2018). The panniculus carnosus muscle: an evolutionary enigma at the intersection of distinct research fields. J. Anat. *233*, 275–288. 10.1111/joa.12840.

47. Zomer, H.D., and Trentin, A.G. (2018). Skin wound healing in humans and mice: Challenges in translational research. J. Dermatol. Sci. *90*, 3–12. 10.1016/j.jdermsci.2017.12.009.

48. Tirumalae, R. (2013). Psoriasiform Dermatoses: Microscopic Approach. Indian J. Dermatol. *58*, 290–293. 10.4103/0019-5154.113945.

49. Solé-Boldo, L., Raddatz, G., Schütz, S., Mallm, J.-P., Rippe, K., Lonsdorf, A.S., Rodríguez-Paredes, M., and Lyko, F. (2020). Single-cell transcriptomes of the human skin reveal age-related loss of fibroblast priming. Commun. Biol. *3*, 1–12. 10.1038/s42003-020-0922-4.

50. Macosko, E.Z., Basu, A., Satija, R., Nemesh, J., Shekhar, K., Goldman, M., Tirosh, I., Bialas, A.R., Kamitaki, N., Martersteck, E.M., et al. (2015). Highly parallel genome-wide expression profiling of individual cells using nanoliter droplets. Cell *161*, 1202–1214. 10.1016/j.cell.2015.05.002.

51. Ghazizadeh, S., and Taichman, L.B. (2005). Organization of Stem Cells and Their Progeny in Human Epidermis. J. Invest. Dermatol. *124*, 367–372. 10.1111/j.0022-202X.2004.23599.x.

52. Corrò, C., Novellasdemunt, L., and Li, V.S.W. (2020). A brief history of organoids. Am. J. Physiol. Cell Physiol. *319*, C151–C165. 10.1152/ajpcell.00120.2020.

53. Lee, J., Rabbani, C.C., Gao, H., Steinhart, M.R., Woodruff, B.M., Pflum, Z.E., Kim, A., Heller, S., Liu, Y., Shipchandler, T.Z., et al. (2020). Hair-bearing human skin generated entirely from pluripotent stem cells. Nature *582*, 399–404. 10.1038/s41586-020-2352-3.

54. Morrison, K.A., Weinreb, R.H., Dong, X., Toyoda, Y., Jin, J.L., Bender, R., Mukherjee, S., and Spector, J.A. (2020). Facilitated self-assembly of a prevascularized dermal/epidermal collagen scaffold. Regen. Med. *15*, 2273–2283. 10.2217/rme-2020-0070.

55. Patra, S., and Young, V. (2016). A Review of 3D Printing Techniques and the Future in Biofabrication of Bioprinted Tissue. Cell Biochem. Biophys. *74*, 93–98. 10.1007/s12013-016-0730-0.

56. Pourchet, L.J., Thepot, A., Albouy, M., Courtial, E.J., Boher, A., Blum, L.J., and Marquette, C.A. (2017). Human Skin 3D Bioprinting Using Scaffold-Free Approach. Adv. Healthc. Mater. *6*. 10.1002/adhm.201601101.

57. El Ghalbzouri, A., Commandeur, S., Rietveld, M.H., Mulder, A.A., and Willemze, R. (2009). Replacement of animal-derived collagen matrix by human fibroblast-derived dermal matrix for human skin equivalent products. Biomaterials *30*, 71–78. 10.1016/j.biomaterials.2008.09.002.

58. Andreadis, S.T., Hamoen, K.E., Yarmush, M.L., and Morgan, J.R. (2001). Keratinocyte growth factor induces hyperproliferation and delays differentiation in a skin equivalent model system. FASEB J. Off. Publ. Fed. Am. Soc. Exp. Biol. *15*, 898–906. 10.1096/fj.00-0324com.

59. Jevtić, M., Löwa, A., Nováčková, A., Kováčik, A., Kaessmeyer, S., Erdmann, G., Vávrová, K., and Hedtrich, S. (2020). Impact of intercellular crosstalk between epidermal keratinocytes and dermal fibroblasts on skin homeostasis. Biochim. Biophys. Acta BBA - Mol. Cell Res. *1867*, 118722. 10.1016/j.bbamcr.2020.118722.

60. Brancati, G., Treutlein, B., and Camp, J.G. (2020). Resolving Neurodevelopmental and Vision Disorders Using Organoid Single-Cell Multi-omics. Neuron *107*, 1000–1013. 10.1016/j.neuron.2020.09.001.

61. Chen, J., Lau, B.T., Andor, N., Grimes, S.M., Handy, C., Wood-Bouwens, C., and Ji, H.P. (2019). Single-cell transcriptome analysis identifies distinct cell types and niche signaling in a primary gastric organoid model. Sci. Rep. *9*, 4536. 10.1038/s41598-019-40809-x.

62. Serra, D., Mayr, U., Boni, A., Lukonin, I., Rempfler, M., Meylan, L.C., Stadler, M.B., Strnad, P., Papasaikas, P., Waldt, A., et al. (2019). Self-organization and symmetry breaking in intestinal organoid development. Nature *569*, 66–72. 10.1038/s41586-019-1146-y.

63. van den Brink, S.C., Alemany, A., van Batenburg, V., Moris, N., Blotenburg, M., Vivié, J., Baillie-Johnson, P., Nichols, J., Sonnen, K.F., Martinez Arias, A., et al. (2020). Single-cell and spatial transcriptomics reveal somitogenesis in gastruloids. Nature *582*, 405–409. 10.1038/s41586-020-2024-3.

64. Cheng, J.B., Sedgewick, A.J., Finnegan, A.I., Harirchian, P., Lee, J., Kwon, S., Fassett, M.S., Golovato, J., Gray, M., Ghadially, R., et al. (2018). Transcriptional Programming of Normal and Inflamed Human Epidermis at Single-Cell Resolution. Cell Rep. *25*, 871–883. 10.1016/j.celrep.2018.09.006.

65. Maruguchi, T., Maruguchi, Y., Suzuki, S., Matsuda, K., Toda, K., and Isshiki, N. (1994). A new skin equivalent: keratinocytes proliferated and differentiated on collagen sponge containing fibroblasts. Plast. Reconstr. Surg. *93*, 537–544; discussion 545-546.

66. Ross, S., Spencer, S.D., Lasky, L.A., and Koeppen, H. (2001). Selective Expression of Murine Prostate Stem Cell Antigen in Fetal and Adult Tissues and the Transgenic Adenocarcinoma of the Mouse Prostate Model of Prostate Carcinogenesis. Am. J. Pathol. *158*, 809–816. 10.1016/S0002-9440(10)64028-X.

67. Cao, J., Spielmann, M., Qiu, X., Huang, X., Ibrahim, D.M., Hill, A.J., Zhang, F., Mundlos, S., Christiansen, L., Steemers, F.J., et al. (2019). The single-cell transcriptional landscape of mammalian organogenesis. Nature *566*, 496–502. 10.1038/s41586-019-0969-x.

68. Wang, S., Karikomi, M., MacLean, A.L., and Nie, Q. (2019). Cell lineage and communication network inference via optimization for single-cell transcriptomics. Nucleic Acids Res. *47*, e66. 10.1093/nar/gkz204.

69. Bergen, V., Lange, M., Peidli, S., Wolf, F.A., and Theis, F.J. (2020). Generalizing RNA velocity to transient cell states through dynamical modeling. Nat. Biotechnol. *38*, 1408–1414. 10.1038/s41587-020-0591-3.

70. Jin, S., Guerrero-Juarez, C.F., Zhang, L., Chang, I., Ramos, R., Kuan, C.-H., Myung, P., Plikus, M.V., and Nie, Q. (2021). Inference and analysis of cell-cell communication using CellChat. Nat. Commun. *12*, 1088. 10.1038/s41467-021-21246-9.

71. Kim, J., Kong, J., Chang, H., Kim, H., and Kim, A. (2016). EGF induces epithelial-mesenchymal transition through phospho-Smad2/3-Snail signaling pathway in breast cancer cells. Oncotarget *7*, 85021–85032. 10.18632/oncotarget.13116.

72. Aharonov, A., Shakked, A., Umansky, K.B., Savidor, A., Genzelinakh, A., Kain, D., Lendengolts, D., Revach, O.-Y., Morikawa, Y., Dong, J., et al. (2020). ERBB2 drives YAP activation and EMT-like processes during cardiac regeneration. Nat. Cell Biol. *22*, 1346–1356. 10.1038/s41556-020-00588-4.

73. Eapen, M.S., Sharma, P., Thompson, I.E., Lu, W., Myers, S., Hansbro, P.M., and Sohal, S.S. (2019). Heparin-binding epidermal growth factor (HB-EGF) drives EMT in patients with COPD: implications for disease pathogenesis and novel therapies. Lab. Invest. *99*, 150–157. 10.1038/s41374-018-0146-0.

74. Liu, S., Ye, D., Xu, D., Liao, Y., Zhang, L., Liu, L., Yu, W., Wang, Y., He, Y., Hu, J., et al. (2016). Autocrine epiregulin activates EGFR pathway for lung metastasis via EMT in salivary adenoid cystic carcinoma. Oncotarget *7*, 25251–25263. 10.18632/oncotarget.7940.

75. Shostak, K., Zhang, X., Hubert, P., Göktuna, S.I., Jiang, Z., Klevernic, I., Hildebrand, J., Roncarati, P., Hennuy, B., Ladang, A., et al. (2014). NF-κB-induced KIAA1199 promotes survival through EGFR signalling. Nat. Commun. *5*, 5232. 10.1038/ncomms6232.

76. Wang, L., Wang, L., Zhang, H., Lu, J., Zhang, Z., Wu, H., and Liang, Z. (2020). AREG mediates the epithelial-mesenchymal transition in pancreatic cancer cells via the EGFR/ERK/NF-κB signalling pathway. Oncol. Rep. *43*, 1558–1568. 10.3892/or.2020.7523.

77. Yu, C.-Y., Chang, W.-C., Zheng, J.-H., Hung, W.-H., and Cho, E.-C. (2018). Transforming growth factor alpha promotes tumorigenesis and regulates epithelial-mesenchymal transition modulation in colon cancer. Biochem. Biophys. Res. Commun. *506*, 901–906. 10.1016/j.bbrc.2018.10.137.

78. Okada, Y., Takahashi, N., Takayama, T., and Goel, A. (2021). LAMC2 promotes cancer progression and gemcitabine resistance through modulation of EMT and ATP-binding cassette transporters in pancreatic ductal adenocarcinoma. Carcinogenesis *42*, 546–556. 10.1093/carcin/bgab011.

79. Pei, Y.-F., Liu, J., Cheng, J., Wu, W.-D., and Liu, X.-Q. (2019). Silencing of LAMC2 Reverses Epithelial-Mesenchymal Transition and Inhibits Angiogenesis in Cholangiocarcinoma via Inactivation of the Epidermal Growth Factor Receptor Signaling Pathway. Am. J. Pathol. *189*, 1637–1653. 10.1016/j.ajpath.2019.03.012.

80. Bacigalupo, M.L., Manzi, M., Espelt, M.V., Gentilini, L.D., Compagno, D., Laderach, D.J., Wolfenstein-Todel, C., Rabinovich, G.A., and Troncoso, M.F. (2015). Galectin-1 triggers epithelial-mesenchymal transition in human hepatocellular carcinoma cells. J. Cell. Physiol. *230*, 1298–1309. 10.1002/jcp.24865.

81. Li, H., Zhong, A., Li, S., Meng, X., Wang, X., Xu, F., and Lai, M. (2017). The integrated pathway of TGFβ/Snail with TNFα/NFκB may facilitate the tumor-stroma interaction in the EMT process and colorectal cancer prognosis. Sci. Rep. *7*, 4915. 10.1038/s41598-017-05280-6.

82. Miyazaki, H., Takahashi, R., Prieto-Vila, M., Kawamura, Y., Kondo, S., Shirota, T., and Ochiya, T. (2018). CD44 exerts a functional role during EMT induction in cisplatin-resistant head and neck cancer cells. Oncotarget *9*, 10029–10041. 10.18632/oncotarget.24252.

83. Xu, H., Tian, Y., Yuan, X., Wu, H., Liu, Q., Pestell, R.G., and Wu, K. (2015). The role of CD44 in epithelial–mesenchymal transition and cancer development. OncoTargets Ther. *8*, 3783–3792. 10.2147/OTT.S95470.

84. Medici, D., Hay, E.D., and Olsen, B.R. (2008). Snail and Slug Promote Epithelial-Mesenchymal Transition through β-Catenin–T-Cell Factor-4-dependent Expression of Transforming Growth Factor-β3. Mol. Biol. Cell *19*, 4875–4887. 10.1091/mbc.E08-05-0506.

85. Rheinwald, J.G., and Green, H. (1977). Epidermal growth factor and the multiplication of cultured human epidermal keratinocytes. Nature *265*, 421–424. 10.1038/265421a0.

86. Haensel, D., and Dai, X. (2018). Epithelial-to-mesenchymal transition in cutaneous wound healing: Where we are and where we are heading. Dev. Dyn. Off. Publ. Am. Assoc. Anat. *247*, 473–480. 10.1002/dvdy.24561.

87. Jung, A.R., Jung, C.-H., Noh, J.K., Lee, Y.C., and Eun, Y.-G. (2020). Epithelial-mesenchymal transition gene signature is associated with prognosis and tumor microenvironment in head and neck squamous cell carcinoma. Sci. Rep. *10*, 3652. 10.1038/s41598-020-60707-x.

88. Brehm, M.A., and Shultz, L.D. (2012). Human allograft rejection in humanized mice: a historical perspective. Cell. Mol. Immunol. *9*, 225–231. 10.1038/cmi.2011.64.

89. Lawler, P.R., and Lawler, J. (2012). Molecular basis for the regulation of angiogenesis by thrombospondin-1 and -2. Cold Spring Harb. Perspect. Med. *2*, a006627. 10.1101/cshperspect.a006627.

90. Oike, Y., Yasunaga, K., and Suda, T. (2004). Angiopoietin-related/angiopoietin-like proteins regulate angiogenesis. Int. J. Hematol. *80*, 21–28. 10.1532/ijh97.04034.

91. Okabe, N., Ozaki-Kuroda, K., Nakanishi, H., Shimizu, K., and Takai, Y. (2004). Expression patterns of nectins and afadin during epithelial remodeling in the mouse embryo. Dev. Dyn. Off. Publ. Am. Assoc. Anat. *230*, 174–186. 10.1002/dvdy.20033.

92. Gilliver, S.C., Emmerson, E., Bernhagen, J., and Hardman, M.J. (2011). MIF: a key player in cutaneous biology and wound healing. Exp. Dermatol. *20*, 1–6. 10.1111/j.1600-0625.2010.01194.x.

93. Rodríguez-Enríquez, S., Carreño-Fuentes, L., Gallardo-Pérez, J.C., Saavedra, E., Quezada, H., Vega, A., Marín-Hernández, A., Olín-Sandoval, V., Torres-Márquez, M.E., and Moreno-Sánchez, R. (2010). Oxidative phosphorylation is impaired by prolonged hypoxia in breast and possibly in cervix carcinoma. Int. J. Biochem. Cell Biol. *42*, 1744–1751. 10.1016/j.biocel.2010.07.010.

94. Kur-Piotrowska, A., Bukowska, J., Kopcewicz, M.M., Dietrich, M., Nynca, J., Slowinska, M., and Gawronska-Kozak, B. (2018). Foxn1 expression in keratinocytes is stimulated by hypoxia: further evidence of its role in skin wound healing. Sci. Rep. *8*, 5425. 10.1038/s41598-018-23794-5.

95. Mieremet, A., Vázquez García, A., Boiten, W., van Dijk, R., Gooris, G., Bouwstra, J.A., and El Ghalbzouri, A. (2019). Human skin equivalents cultured under hypoxia display enhanced epidermal morphogenesis and lipid barrier formation. Sci. Rep. *9*, 7811. 10.1038/s41598-019-44204-4.

96. Mole, D.R., Blancher, C., Copley, R.R., Pollard, P.J., Gleadle, J.M., Ragoussis, J., and Ratcliffe, P.J. (2009). Genome-wide association of hypoxia-inducible factor (HIF)-1alpha and HIF-2alpha DNA binding with expression profiling of hypoxia-inducible transcripts. J. Biol. Chem. *284*, 16767–16775. 10.1074/jbc.M901790200.

97. Ngo, M.A., Sinitsyna, N.N., Qin, Q., and Rice, R.H. (2007). Oxygen-Dependent Differentiation of Human Keratinocytes. J. Invest. Dermatol. *127*, 354–361. 10.1038/sj.jid.5700522.

98. Evans, S.M., Schrlau, A.E., Chalian, A.A., Zhang, P., and Koch, C.J. (2006). Oxygen levels in normal and previously irradiated human skin as assessed by EF5 binding. J. Invest. Dermatol. *126*, 2596–2606. 10.1038/sj.jid.5700451.

99. Rezvani, H.R., Ali, N., Serrano-Sanchez, M., Dubus, P., Varon, C., Ged, C., Pain, C., Cario-André, M., Seneschal, J., Taïeb, A., et al. (2011). Loss of epidermal hypoxia-inducible factor-1α accelerates epidermal aging and affects re-epithelialization in human and mouse. J. Cell Sci. *124*, 4172–4183. 10.1242/jcs.082370.

100. Firth, J.D., Ebert, B.L., and Ratcliffe, P.J. (1995). Hypoxic regulation of lactate dehydrogenase A. Interaction between hypoxia-inducible factor 1 and cAMP response elements. J. Biol. Chem. *270*, 21021–21027. 10.1074/jbc.270.36.21021.

101. Augustin, C., Collombel, C., and Damour, O. (1997). Use of dermal equivalent and skin equivalent models for identifying phototoxic compounds in vitro. Photodermatol. Photoimmunol. Photomed. *13*, 27–36. 10.1111/j.1600-0781.1997.tb00105.x.

102. Gu, H., Zhu, Y., Jia, T., Li, X., Lu, Y., and Kaku, K. (2020). Development of a new eczema-like reconstructed skin equivalent for testing child atopic dermatitis-relieving cosmetics. J. Cosmet. Dermatol. *19*, 752–757. 10.1111/jocd.13069.

103. Ojeh, N., Akgül, B., Tomic-Canic, M., Philpott, M., and Navsaria, H. (2017). In vitro skin models to study epithelial regeneration from the hair follicle. PloS One *12*, e0174389. 10.1371/journal.pone.0174389.

104. Hirsch, T., Rothoeft, T., Teig, N., Bauer, J.W., Pellegrini, G., De Rosa, L., Scaglione, D., Reichelt, J., Klausegger, A., Kneisz, D., et al. (2017). Regeneration of the entire human epidermis using transgenic stem cells. Nature *551*, 327–332. 10.1038/nature24487.

105. Hammond, N.L., Dixon, J., and Dixon, M.J. (2019). Periderm: Life-cycle and function during orofacial and epidermal development. Semin. Cell Dev. Biol. *91*, 75–83. 10.1016/j.semcdb.2017.08.021.

106. Fischer, B., Metzger, M., Richardson, R., Knyphausen, P., Ramezani, T., Franzen, R., Schmelzer, E., Bloch, W., Carney, T.J., and Hammerschmidt, M. (2014). p53 and TAp63 promote keratinocyte

proliferation and differentiation in breeding tubercles of the zebrafish. PLoS Genet. *10*, e1004048. 10.1371/journal.pgen.1004048.

107. Subramanian, A., Sidhom, E.-H., Emani, M., Vernon, K., Sahakian, N., Zhou, Y., Kost-Alimova, M., Slyper, M., Waldman, J., Dionne, D., et al. (2019). Single cell census of human kidney organoids shows reproducibility and diminished off-target cells after transplantation. Nat. Commun. *10*, 5462. 10.1038/s41467-019-13382-0.

108. Fujii, M., Matano, M., Toshimitsu, K., Takano, A., Mikami, Y., Nishikori, S., Sugimoto, S., and Sato, T. (2018). Human Intestinal Organoids Maintain Self-Renewal Capacity and Cellular Diversity in Niche-Inspired Culture Condition. Cell Stem Cell *23*, 787-793.e6. 10.1016/j.stem.2018.11.016.

109. Velasco, S., Kedaigle, A.J., Simmons, S.K., Nash, A., Rocha, M., Quadrato, G., Paulsen, B., Nguyen, L., Adiconis, X., Regev, A., et al. (2019). Individual brain organoids reproducibly form cell diversity of the human cerebral cortex. Nature *570*, 523–527. 10.1038/s41586-019-1289-x.

110. Roger, M., Fullard, N., Costello, L., Bradbury, S., Markiewicz, E., O'Reilly, S., Darling, N., Ritchie, P., Määttä, A., Karakesisoglou, I., et al. (2019). Bioengineering the microanatomy of human skin. J. Anat. *234*, 438–455. 10.1111/joa.12942.

111. Reijnders, C.M.A., van Lier, A., Roffel, S., Kramer, D., Scheper, R.J., and Gibbs, S. (2015). Development of a Full-Thickness Human Skin Equivalent In Vitro Model Derived from TERT-Immortalized Keratinocytes and Fibroblasts. Tissue Eng. Part A *21*, 2448–2459. 10.1089/ten.TEA.2015.0139.

112. Mieremet, A., van Dijk, R., Boiten, W., Gooris, G., Bouwstra, J.A., and El Ghalbzouri, A. (2019). Characterization of human skin equivalents developed at body's core and surface temperatures. J. Tissue Eng. Regen. Med. *13*, 1122–1133. 10.1002/term.2858.

113. Botusan, I.R., Sunkari, V.G., Savu, O., Catrina, A.I., Grünler, J., Lindberg, S., Pereira, T., Ylä-Herttuala, S., Poellinger, L., Brismar, K., et al. (2008). Stabilization of HIF-1alpha is critical to improve wound healing in diabetic mice. Proc. Natl. Acad. Sci. U. S. A. *105*, 19426–19431. 10.1073/pnas.0805230105.

114. Gurtner, G.C., Werner, S., Barrandon, Y., and Longaker, M.T. (2008). Wound repair and regeneration. Nature *453*, 314–321. 10.1038/nature07039.

115. Liu, L., Sun, Q., Davis, F., Mao, J., Zhao, H., and Ma, D. (2022). Epithelial–mesenchymal transition in organ fibrosis development: current understanding and treatment strategies. Burns Trauma *10*, tkac011. 10.1093/burnst/tkac011.

116. Lu, J., Krepelova, A., Rasa, S.M.M., Annunziata, F., Husak, O., Adam, L., Nunna, S., and Neri, F. (2021). Characterization of an in vitro 3D intestinal organoid model by using massive RNAseq-based transcriptome profiling. Sci. Rep. *11*, 16668. 10.1038/s41598-021-96321-8.

117. Wiedemann, J., Billi, A.C., Bocci, F., Kashgari, G., Xing, E., Tsoi, L.C., Meller, L., Swindell, W.R., Wasikowski, R., Xing, X., et al. (2023). Differential cell composition and split epidermal differentiation in human palm, sole, and hip skin. Cell Rep. *42*, 111994. 10.1016/j.celrep.2023.111994.

118. Andor, N., Maley, C.C., and Ji, H.P. (2017). Genomic Instability in Cancer: Teetering on the Limit of Tolerance. Cancer Res. *77*, 2179–2185. 10.1158/0008-5472.CAN-16-1553.

119. Maeshima, K., Iino, H., Hihara, S., and Imamoto, N. (2011). Nuclear size, nuclear pore number and cell cycle. Nucleus *2*, 113–118. 10.4161/nucl.2.2.15446.

120. Eriksson, M., Brown, W.T., Gordon, L.B., Glynn, M.W., Singer, J., Scott, L., Erdos, M.R., Robbins, C.M., Moses, T.Y., Berglund, P., et al. (2003). Recurrent de novo point mutations in lamin A cause Hutchinson-Gilford progeria syndrome. Nature *423*, 293–298. 10.1038/nature01629.

121. Broers, J.L.V., Ramaekers, F.C.S., Bonne, G., Yaou, R.B., and Hutchison, C.J. (2006). Nuclear Lamins: Laminopathies and Their Role in Premature Ageing. Physiol. Rev. *86*, 967–1008. 10.1152/physrev.00047.2005.

122. Van de Vosse, D.W., Wan, Y., Wozniak, R.W., and Aitchison, J.D. (2011). Role of the nuclear envelope on genome organization and gene expression. Wiley Interdiscip. Rev. Syst. Biol. Med. *3*, 147–166. 10.1002/wsbm.101.

123. Kim, Y.-S., Yi, B.-R., Kim, N.-H., and Choi, K.-C. (2014). Role of the epithelial–mesenchymal transition and its effects on embryonic stem cells. Exp. Mol. Med. *46*, e108–e108. 10.1038/emm.2014.44.

124. Kalluri, R., and Weinberg, R.A. (2009). The basics of epithelial-mesenchymal transition. J. Clin. Invest. *119*, 1420–1428. 10.1172/JCI39104.

125. D'Arcy, C., and Kiel, C. (2021). Cell Adhesion Molecules in Normal Skin and Melanoma. Biomolecules *11*, 1213. 10.3390/biom11081213.

126. Chen, P., Xie, H., and Wells, A. (1996). Mitogenic signaling from the egf receptor is attenuated by a phospholipase C-gamma/protein kinase C feedback mechanism. Mol. Biol. Cell *7*, 871–881.

127. Kitchens, D.L., Snyder, E.Y., and Gottlieb, D.I. (1994). FGF and EGF are mitogens for immortalized neural progenitors. J. Neurobiol. *25*, 797–807. 10.1002/neu.480250705.

128. Bikle, D.D., Xie, Z., and Tu, C.-L. (2012). Calcium regulation of keratinocyte differentiation. Expert Rev. Endocrinol. Metab. *7*, 461–472. 10.1586/eem.12.34.

129. Lu, C.-C., Chu, P.-Y., Hsia, S.-M., Wu, C.-H., Tung, Y.-T., and Yen, G.-C. (2017). Insulin induction instigates cell proliferation and metastasis in human colorectal cancer cells. Int. J. Oncol. *50*, 736–744. 10.3892/ijo.2017.3844.

130. Gallagher, E.J., and LeRoith, D. (2010). The Proliferating Role of Insulin and Insulin-Like Growth Factors in Cancer. Trends Endocrinol. Metab. TEM *21*, 610–618. 10.1016/j.tem.2010.06.007.

131. Son, H., Park, I., Kim, J.Y., Kim, D.K., Illeperuma, R.P., Bae, J.Y., Lee, D.Y., Oh, E., Jung, D., Williams, D.R., et al. (2015). A Distinct Role for Interleukin-6 as a Major Mediator of Cellular Adjustment to an Altered Culture Condition. J. Cell. Biochem. *116*, 2552–2562. 10.1002/jcb.25200.

132. Bharati, K., and Ganguly, N.K. (2011). Cholera toxin: A paradigm of a multifunctional protein. Indian J. Med. Res. *133*, 179–187.

133. Straus, D.S. (1984). Growth-stimulatory actions of insulin in vitro and in vivo. Endocr. Rev. *5*, 356–369. 10.1210/edrv-5-2-356.

134. Kang, S., Song, J., Kang, H., Kim, S., Lee, Y., and Park, D. (2003). Insulin can block apoptosis by decreasing oxidative stress via phosphatidylinositol 3-kinase- and extracellular signal-regulated protein kinase-dependent signaling pathways in HepG2 cells. Eur. J. Endocrinol. *148*, 147–155. 10.1530/eje.0.1480147.

135. Seiberg, M. (2001). Keratinocyte-melanocyte interactions during melanosome transfer. Pigment Cell Res. *14*, 236–242. 10.1034/j.1600-0749.2001.140402.x.

136. Ahmed jan, N., and Masood, S. (2023). Vitiligo. In StatPearls (StatPearls Publishing).

137. Lee, A.-Y. (2012). Role of Keratinocytes in the Development of Vitiligo. Ann. Dermatol. *24*, 115–125. 10.5021/ad.2012.24.2.115.

138. Li, Y., Kuhn, M., Zukowska-Kasprzyk, J., Hennrich, M.L., Kastritis, P.L., O'Reilly, F.J., Phapale, P., Beck, M., Gavin, A.-C., and Bork, P. (2021). Coupling proteomics and metabolomics for the unsupervised identification of protein-metabolite interactions in Chaetomium thermophilum. PloS One *16*, e0254429. 10.1371/journal.pone.0254429.

139. Stuart, T., Butler, A., Hoffman, P., Hafemeister, C., Papalexi, E., Mauck, W.M., Hao, Y., Stoeckius, M., Smibert, P., and Satija, R. (2019). Comprehensive Integration of Single-Cell Data. Cell *177*, 1888-1902.e21. 10.1016/j.cell.2019.05.031.

140. Becht, E., McInnes, L., Healy, J., Dutertre, C.-A., Kwok, I.W.H., Ng, L.G., Ginhoux, F., and Newell, E.W. (2018). Dimensionality reduction for visualizing single-cell data using UMAP. Nat. Biotechnol. 10.1038/nbt.4314.

141. Jin, S., Guerrero-Juarez, C.F., Zhang, L., Chang, I., Ramos, R., Kuan, C.-H., Myung, P., Plikus, M.V., and Nie, Q. (2021). Inference and analysis of cell-cell communication using CellChat. Nat. Commun. *12*, 1088. 10.1038/s41467-021-21246-9.

142. Hao, Y., Hao, S., Andersen-Nissen, E., Mauck, W.M., Zheng, S., Butler, A., Lee, M.J., Wilk, A.J., Darby, C., Zager, M., et al. (2021). Integrated analysis of multimodal single-cell data. Cell *184*, 3573-3587.e29. 10.1016/j.cell.2021.04.048.

Appendix

Supplemental Figures

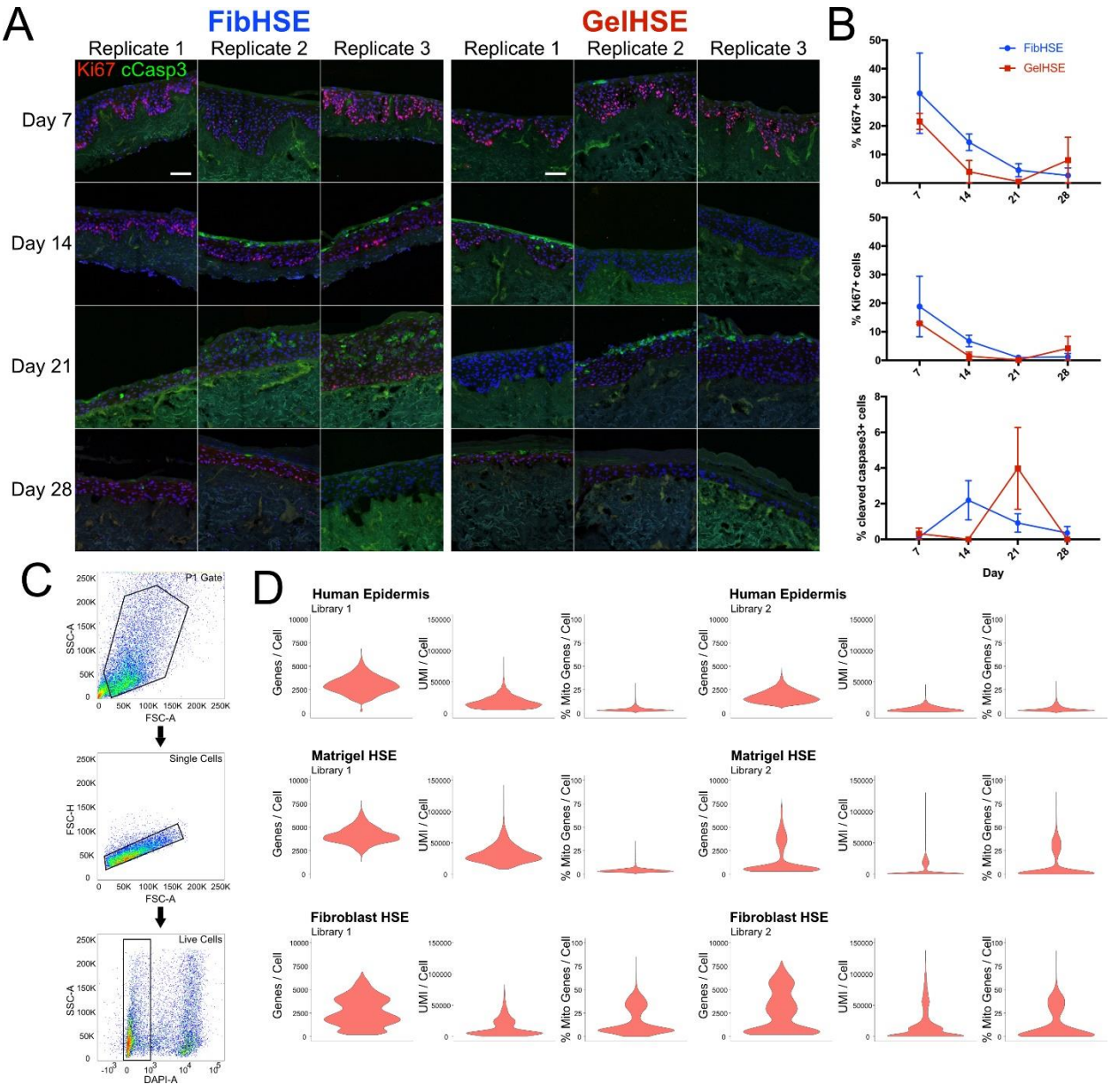

Supplemental Figure 1. FACS strategy and quality control metrics. Related to Figure 1. **A)** Immunostaining for Ki67 and cCASP3 for both FibHSEs and GelHSEs grown for 7, 14, 21, and 28 days. **B)** Quantification of the percentage of Ki67+ basal keratinocytes (left), Ki67+ total keratinocytes (middle), and percentage of cCASP3+ keratinocytes (right) across all 4 time points shown in panel A. Scale bar = 100 µm. **C)** Schematic of FACS strategy for physical sorting of live cells from human skin equivalents. SSC – A denotes side scatter area. FSC – A

denotes forward scatter area. FSC – H denotes forward scatter height. FITC – A denotes dead cells using SYTOX Blue. **D)** Violin plots showing genes per cell, percent mitochondrial (mito) genes per cell, and unique molecular identifiers (UMI) per cell for each *in vivo* (human epidermis), Matrigel HSE, and Fibroblast HSE libraries prior to quality control filtering.

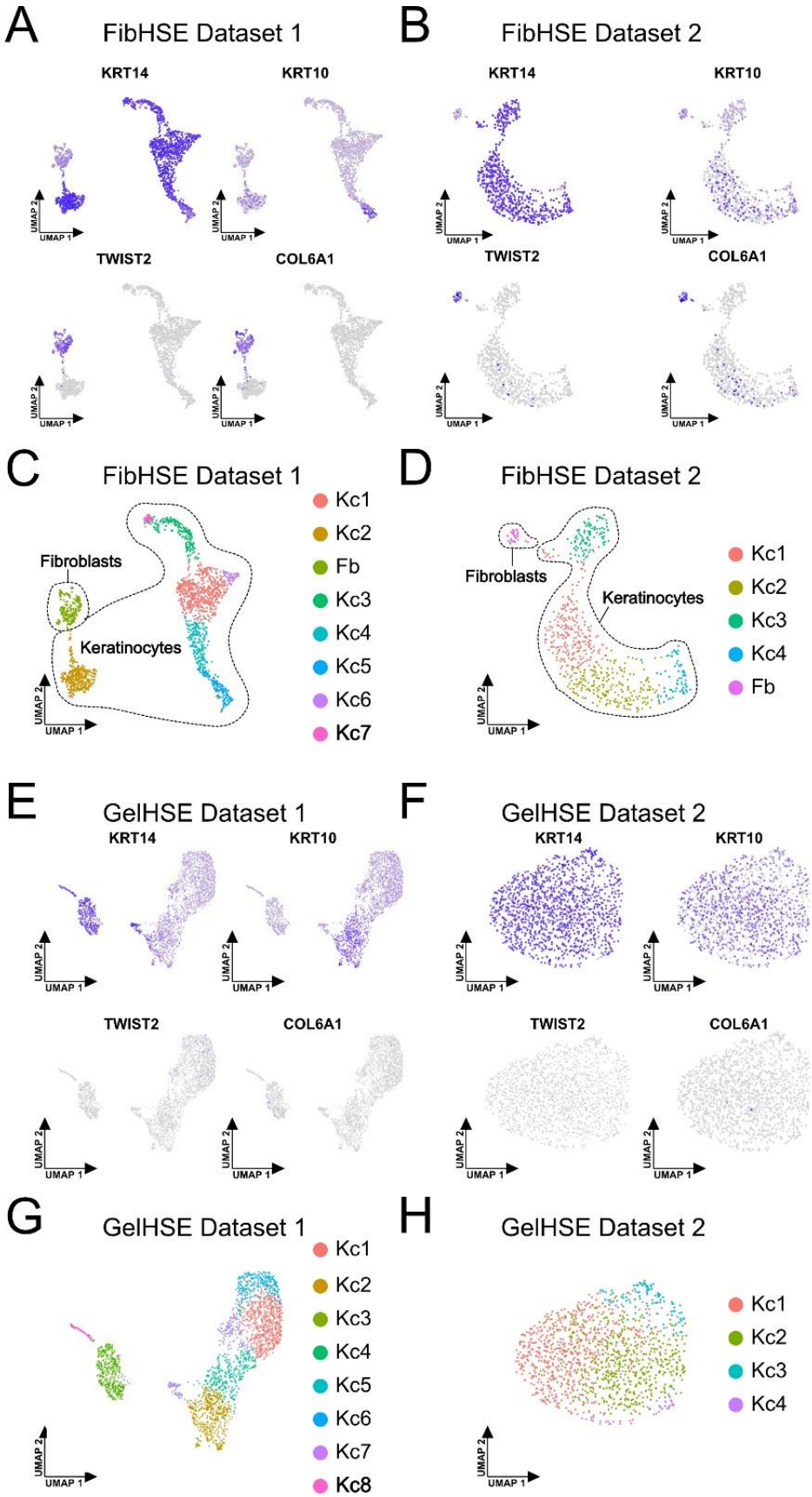
A
FibHSE Dataset 1
KRT14
KRT10
TWIST2
COL6A1
B
FibHSE Dataset 2
KRT14
KRT10
TWIST2
COL6A1
C
FibHSE Dataset 1
Fibroblasts
Keratinocytes
Kc1
Kc2
Fb
Kc3
Kc4
Kc5
Kc6
Kc7
D
FibHSE Dataset 2
Fibroblasts
Keratinocytes
Kc1
Kc2
Kc3
Kc4
Fb
E
GelHSE Dataset 1
KRT14
KRT10
TWIST2
COL6A1
F
GelHSE Dataset 2
KRT14
KRT10
TWIST2
COL6A1
G
GelHSE Dataset 1
Kc1
Kc2
Kc3
Kc4
Kc5
Kc6
Kc7
Kc8
H
GelHSE Dataset 2
Kc1
Kc2
Kc3
Kc4
UMAP 1
UMAP 2

Supplemental Figure 2. Identification of fibroblast populations in FibHSE datasets. Related to Figure 1. Feature plots showing the expression of keratinocyte markers *KRT14* and *KRT10* and fibroblast markers *TWIST2* and *COL6A1* for **(A)** FibHSE dataset 1, **(B)** FibHSE dataset 2, **(E)** GelHSE dataset 1, and **(F)** GelHSE dataset 2. Clustering of single cells isolated from **(C)** FibHSE dataset 1, **(D)** FibHSE dataset 2, **(G)** GelHSE dataset 1, and **(H)** GelHSE dataset 2 libraries displayed using UMAP embedding. Keratinocyte and fibroblast cell populations are outlined in **(C)** and **(D)**.

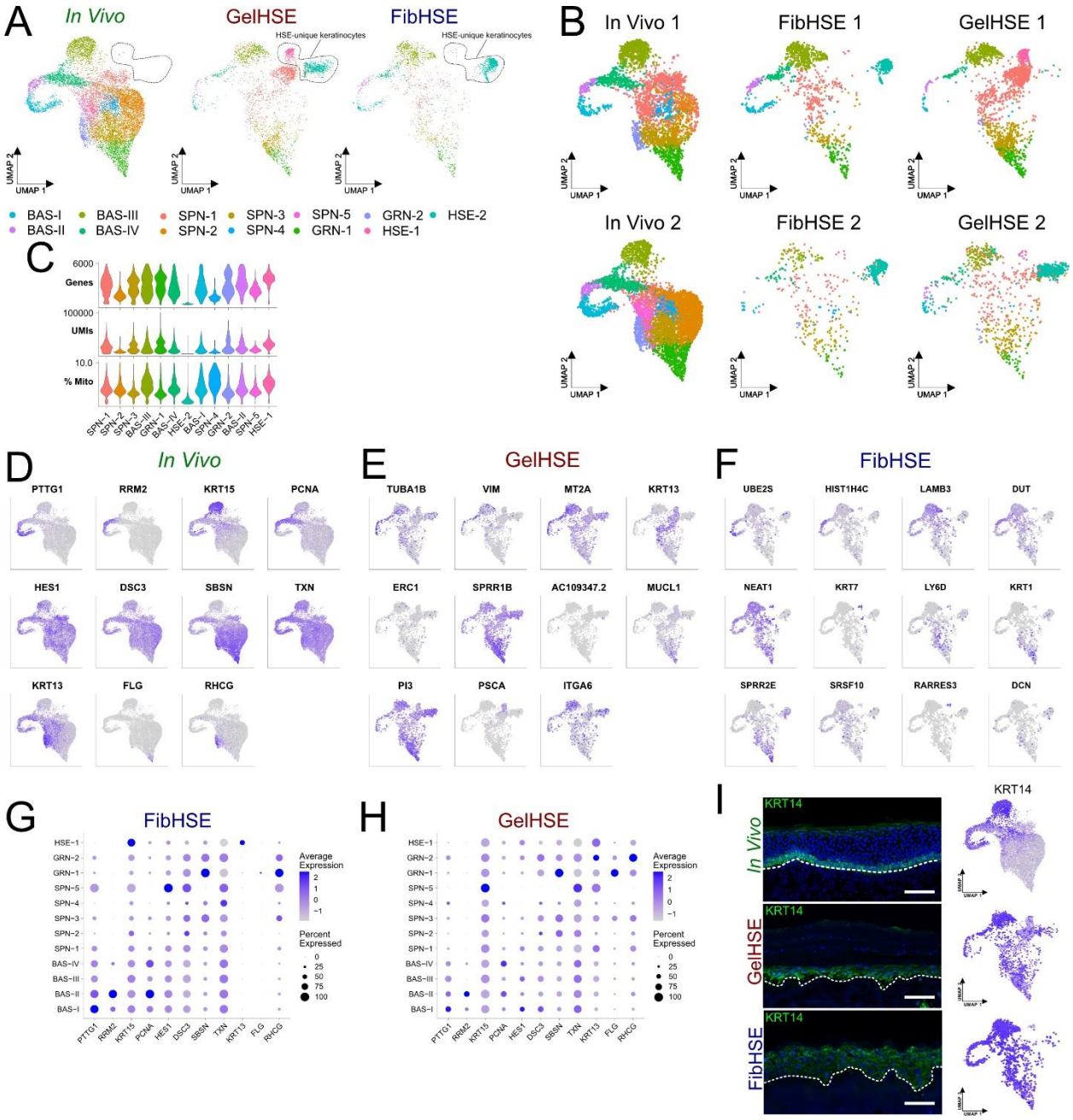

Supplemental Figure 3. Differential expression of key marker genes in the In Vivo and HSE samples. Related to Figures 1 and 2. **A)** Split UMAP plot showing the three sample types, individually, prior to removing HSE-2. **B)** Split UMAP plot showing the two *in vivo*, two GelHSE, and two FibHSE replicates, individually. **C)** QC metrics showing the number of genes detected (top), number of unique UMIs (middle), and percent mitochondrial genes (bottom) per cluster. Feature plots showing the expression of the top marker for each cluster of the **(D)** *in vivo*, **(E)** GelHSE, and **(F)** FibHSE datasets. Dot plots showing the top *in vivo* genes from Figure 1G for the **(G)** FibHSE and **(H)** GelHSE datasets. **I)** Immunostaining of KRT14 (left) in human neonatal

skin (top), day 28 GelHSE (middle), and day 28 FibHSE (bottom) and feature plots (right) showing the RNA expression of *KRT14* for each sample type. Scale bar = 100 μm.

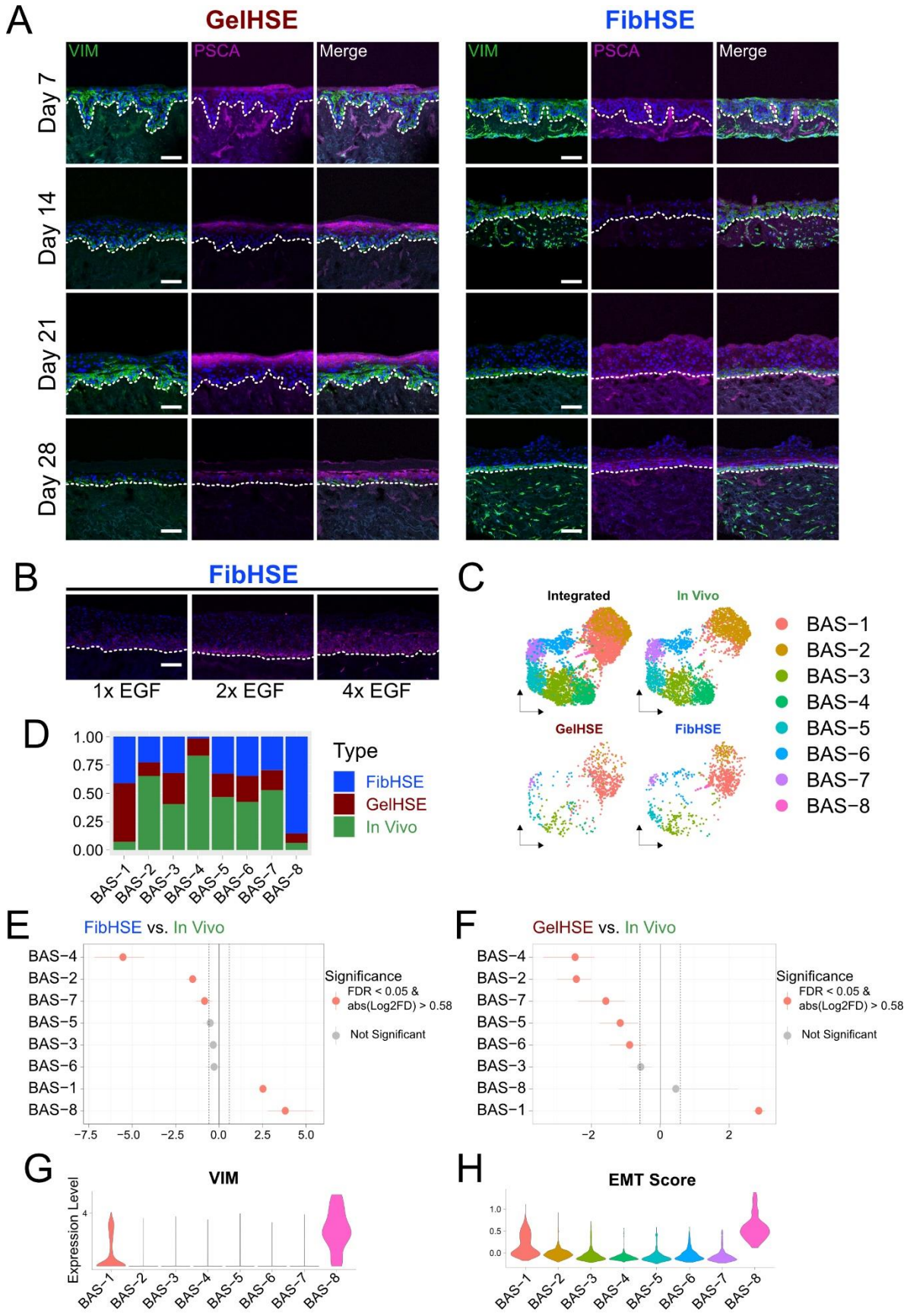
A
GelHSE
FibHSE
VIM
PSCA
Merge
Day 7
Day 14
Day 21
Day 28
B
FibHSE
1x EGF
2x EGF
4x EGF
C
Integrated
In Vivo
GelHSE
FibHSE
BAS−1
BAS−2
BAS−3
BAS−4
BAS−5
BAS−6
BAS−7
BAS−8
D
1.00
0.75
0.50
0.25
0.00
Type
FibHSE
GelHSE
In Vivo
E
FibHSE vs. In Vivo
Significance
FDR < 0.05 &
abs(Log2FD) > 0.58
Not Significant
F
GelHSE vs. In Vivo
G
VIM
Expression Level
H
EMT Score

Supplemental Figure 4. GelHSE and FibHSE altered cell states persist throughout culturing. Related to Figure 2 and 3. **A)** Immunostaining for VIM and PSCA for both FibHSEs and GelHSEs grown for 7, 14, 21, and 28 days. Dashed line denotes the epidermal-dermal junction. Scale bar = 100 µm. **B)** Vimentin immunostaining of day 14 FibHSEs supplemented with 1x (left), 2x (middle), or 4x (right) EGF. Scale bar = 100 µm. **C)** Subclustering of basal cells separates HSE and *in vivo*-specific basal populations. Split UMAP plots show the contribution of *in vivo*, GelHSE, and FibHSE cells to each basal subcluster. **D)** Bar plot showing the relative proportion of cells in the basal subclusters after adjusting for differences in the number of basal cells from each sample. **E-F)** Monte-Carlo permutation tests to determine the significance of the observed changes in basal populations for FibHSE relative to *in vivo* **(E)** or GelHSE relative to *in vivo* **(F)**. **G)** Violin plot of *VIM* expression in each of the different basal cell clusters. **H)** Violin plot of EMT gene module in each of the different basal cell clusters.

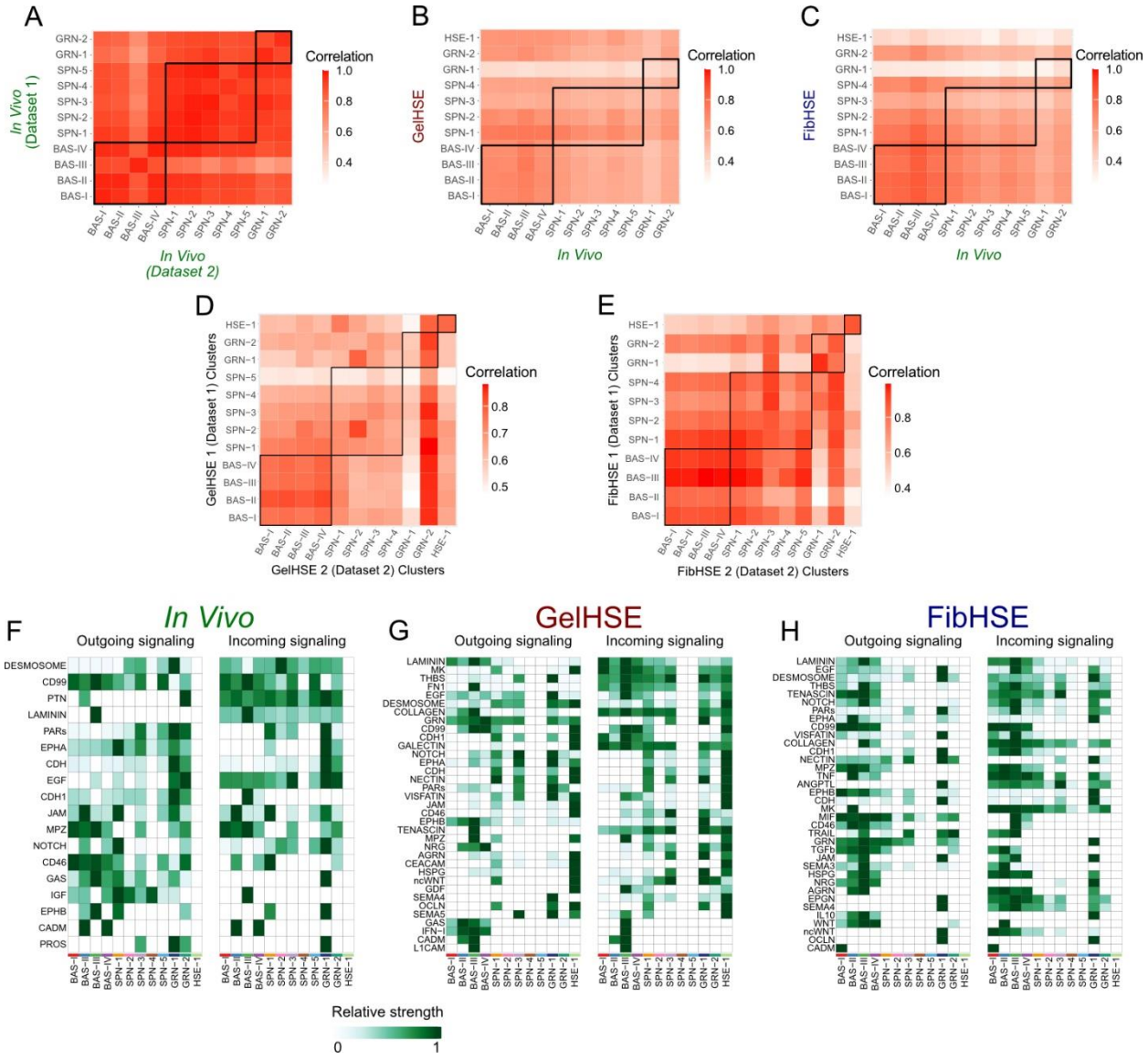

Supplemental Figure 5. Pearson correlation and signaling analysis. Related to Figure 2. **A-E)** Pearson correlation between average RNA expression of each cluster from the indicated datasets. **F-H)** Heatmap showing the relative strength of outgoing and incoming signals for all significant signaling pathways for the *in vivo*, GelHSE, and FibHSE datasets.

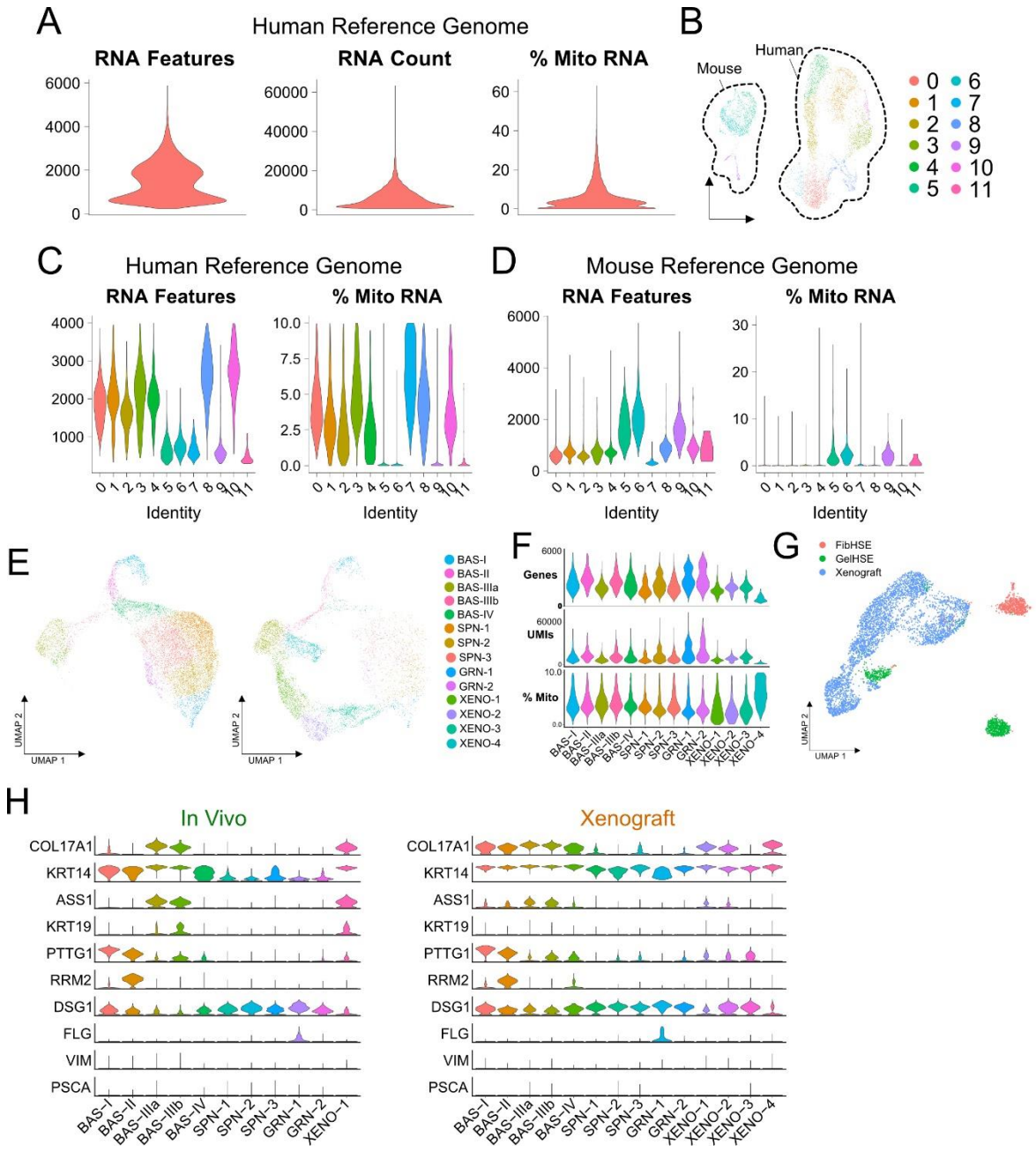

Supplemental Figure 6. Quality control metrics of xenografted HSE dataset. Related to Figure 4. **A)** Violin plots showing genes per cell, unique molecular identifiers (UMI) per cell, and percent mitochondrial (mito) genes per cell for the xenograft dataset aligned to the GRCh38 human reference genome. **B)** Clustering of single cells isolated from xenograft library displayed using UMAP embedding. Mouse cells and human cells are outline by dashed lines and labeled. **C-D)** Violin plots showing genes per cell and percent mitochondrial genes per cell for the xenograft dataset after clustering and aligning to the GRCh38 human reference genome **(C)** and mm10 mouse reference genome **(D)**. **E)** Split UMAP plot showing the two sample types,

individually, prior to removing XENO-4. **F)** QC metrics showing the number of genes detected (top), number of unique UMIs (middle), and percent mito genes (bottom) per cluster. **G)** Integration and clustering of HSE-unique populations, HSE-1 and HSE-2, along with xenograft-unique populations, XENO-1 through XENO-4, with sample type labels superimposed onto UMAP embedding. **H)** Violin plots showing RNA expression of the indicated genes in each cluster of the *in vivo* or xenograft datasets.

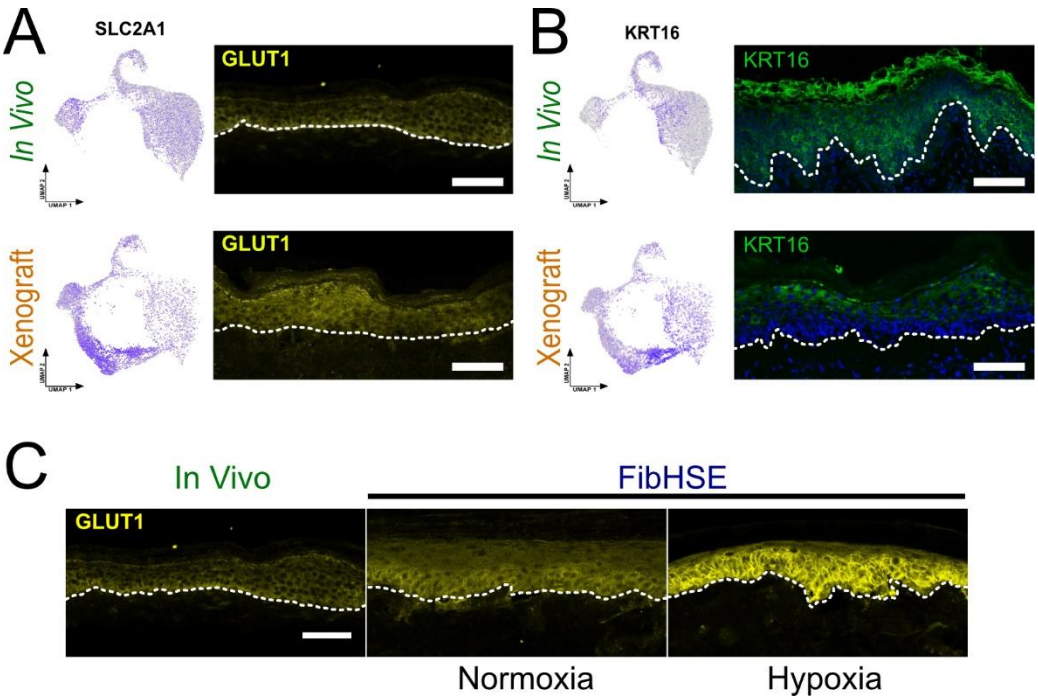

Supplemental Figure 7. GLUT1 and KRT16 expression patterns. Related to Figure 4 and 5. **A)** Feature plots (left) of *GLUT1* gene (*SLC2A1*) and immunostaining of GLUT1 (right) in both the *in vivo* samples (top) and xenograft samples (bottom). **B)** Feature plots (left) and immunostaining (right) of KRT16 in both the *in vivo* samples (top) and xenograft samples (bottom). Scale bar = 100 µm. **C)** Immunostaining of GLUT1 in neonatal human epidermis (In Vivo), FibHSEs grown under atmospheric oxygen levels (normoxia), and physiologically relevant hypoxic conditions.. Scale bar = 100 um. Dashed line denotes basal membrane.

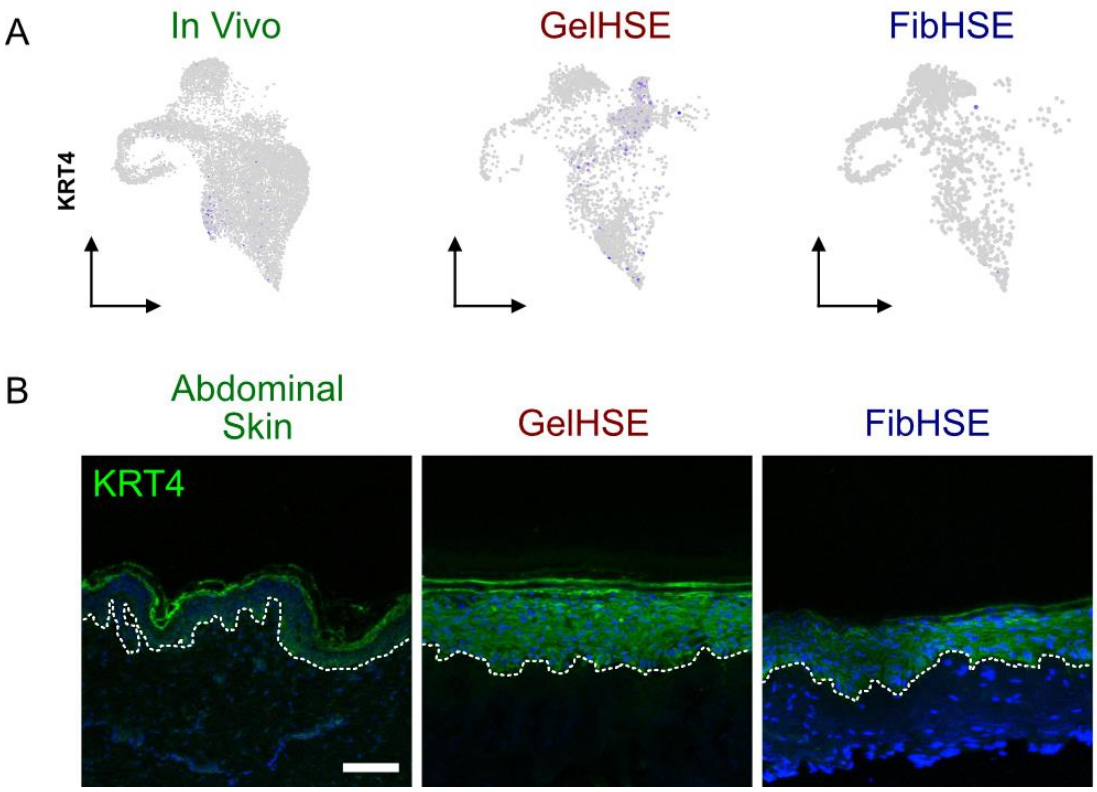

Supplemental Figure 8. Expression patterns of the periderm marker, KRT4. Related to Figure 2. **A)** Feature plots showing the expression of *KRT4* for the *in vivo* (left), GelHSE (middle), and FibHSE datasets (right). **B)** Immunostaining of KRT4 protein in human abdominal skin, GelHSE, and FibHSE samples.

STAR METHODS

Key resources table

REAGENT or RESOURCE	SOURCE	IDENTIFIER
Antibodies		
Chicken anti-KRT14	BioLegend	SIG-3476
Rabbit anti-KI67	Abcam	ab15580
Rabbit anti-COL17A1	One World Labs	ap9099c
Rabbit anti-KRT19	Cell signaling	13092
Mouse anti-KRT15	Santa Cruz	sc-47697
Rabbit anti-VIM	Cell Signaling	D21H3
Mouse anti-PSCA	Santa Cruz	sc-80654
Mouse anti-FLG	Santa Cruz	sc-66192
Mouse anti-DSG1	Santa Cruz	sc-137164
Mouse anti-SLUG	Santa Cruz	sc-166476
Rabbit anti-KRT16	Invitrogen	PA5-99172
Rabbit anti-cCASP3	Cell Signaling	9579T
Rabbit anti-KRT4	Fisher Scientific	16572-1-AP
Rabbit anti-GLUT1	Proteintech	218291AP
Rabbit anti-HIF1a	Proteintech	501733175
Rabbit anti-LOR	Abcam	ab85679
Alexa Fluor 488	Jackson ImmunoResearch	715-545-150, 711-545-152
Cy3 AffiniPure	Jackson ImmunoResearch	711-165-152, 111-165-003
Biological samples		
Human skin	New York Firefighters Skin Bank	http://www.cornellsurgery.org/pro/services/burn-surgery/skin-bank.html
Chemicals, peptides, and recombinant proteins		
PEN/STREP	GIBCO	15140-122
Keratinocyte Media (KCSFM)	Life Technologies	17005042
DMEM	GIBCO	11995
Ham's F12	Cambrex	12-615F
FBS	GIBCO	10437-028
Adenine	Sigma	A-9795
Cholera Toxin	Sigma	C-8052
Hydrocortisone	Calbiochem	3896

Insulin	Sigma	I-1882
EGF	Invitrogen	13247-051
Transferrin	Sigma	T-0665
Ciprofloxacin Hydrochloride	Serologicals	89-001-1
Matrigel	Corning	354234
Critical commercial assays		
Chromium Single Cell 3' Library & Gel Bead Kit v2	10x Genomics	PN-120237
Chromium Single Cell 3' Library & Gel Bead Kit v3	10x Genomics	PN-1000075
Chromium Single Cell A Chip Kits	10x Genomics	PN-120236
Chromium i7 Multiplex Kit	10x Genomics	PN-120262
Deposited data		
Raw scRNA-seq data	This paper	GEO: GSE190695
Experimental models: Cell lines		
Primary human keratinocytes	Hospital Maternity Ward	N/A
Primary human fibroblasts	Hospital Maternity Ward	N/A
Experimental models: Organisms/strains		
NSG Mouse	Jackson Laboratory	005557
Software and algorithms		
Cell Ranger 2.1.0	10x Genomics	https://support.10xgenomics.com/single-cell-geneexpression/software/downloads/latest
Cell Ranger 3.1.0	10x Genomics	https://support.10xgenomics.com/single-cell-geneexpression/software/downloads/latest
Seurat v3	Stuart et al. (2019)[139]	https://satijalab.org/seurat/articles/archive.html
scVelo v0.2.4	Bergen et al. (2020)[69]	https://scvelo.readthedocs.io/
UMAP	Becht et al. (2018)[140]	https://github.com/lmcinnes/umap

CellChatDB, CellChat v1.5	Jin et al. (2021)[141]	https://github.com/sqjin/CellChat
Monocle3	Cao and Spielmann et al. (2019)[67]	https://cole-trapnell-lab.github.io/monocle3/papers/
SoptSC	Wang, et al. (2019)[68]	https://github.com/WangShuxiong/SoptSC
Matlab	MathWorks	https://www.mathworks.com/products/new_products/release2019b.html
R	R core	https://www.r-project.org/
Python	Python Software Foundation	https://www.python.org/

RESOURCE AVAILABILITY

Lead contact

Further information and requests for resources and reagents should be directed to the lead contact, Scott Atwood (satwood@uci.edu).

Materials availability

This study did not generate new unique reagents.

Data and code availability

- The datasets generated during the current study have been deposited at GEO. These data are publicly available as of the date of publication. Accession numbers are listed in the key resources table.
- This paper does not report original code.
- Any additional information required to reanalyze the data reported in this paper is available from the lead contact upon request.

EXPERIMENTAL MODEL AND SUBJECT DETAILS

Human tissue samples

Human clinical studies were approved by the Ethics Committee of the University of California, Irvine. All human studies were performed in strict adherence to the Institutional Review Board (IRB) guidelines of the University of California, Irvine (2009-7083). We have obtained informed consent from all participants. All available discarded and deidentified tissues were used to generate primary cells for cell and organoid culturing. Each cohort of organoids initiated on separate days used cells from a distinct subject. Human cadaver skin from the New York Firefighters Skin Bank was devitalized and used as a scaffold for organoid culturing.

Cell Culture

Human primary keratinocytes and dermal fibroblasts were isolated from discarded neonatal foreskin. As such, all cells and organoids are of male origin. Primary human keratinocytes were cultured in Keratinocyte Serum Free Media supplemented with Epidermal Growth Factor 1-53 and Bovine Pituitary Extract. Primary human fibroblasts were maintained in DMEM with 10% FBS and 1% PEN/STREP. Cells were cultured in a 5% CO_2 incubator at 37˚C.

Animal Model Details

Female NOD scid gamma mice aged 12-14 weeks were used as the experimental model in this study. The NOD scid gamma mice were housed under standard conditions with ad libitum access to food and water. The mice were maintained in a temperature- and humidity-controlled environment with a 12-hour light/dark cycle. All maintenance, care, and experiments have been approved and abide by regulatory guidelines of the Institutional Animal Care and Use Committee of the University of California, San Diego.

Human Skin Equivalent Organoid Culture

Primary human keratinocytes were cultured in Keratinocyte Serum Free Media supplemented with Epidermal Growth Factor 1-53 and Bovine Pituitary Extract (Life Technologies; 17005042). Generation of organotypic skin cultures were performed as described in Li and Sen, 2015. Briefly, ~500K control cells were seeded on devitalized human dermis and raised to an air/liquid interface to induce differentiation and stratification over the indicated number of days with culture changes every two days. Prior to seeding keratinocytes, either Matrigel was applied to the underside of the devitalized dermis or primary human dermal fibroblasts were centrifuged into the devitalized dermis. To evaluate the effect of oxygen levels on 3D skin cultures, FibHSEs were cultured as previously described and exposed to either normoxia (18-20% oxygen) or hypoxia (3% oxygen) at the air-liquid interface for 14 days. To measure changes from EGF supplementation, culture

media was switch to Keratinocyte Serum Free Media supplemented with Bovine Pituitary Extract and variable concentrations of Epidermal Growth Factor 1-53 (Life Technologies; 17005042) after one week for one additional week of culturing.

Human Skin Equivalent Xenograft Model

Human neonatal epidermal keratinocytes (Thermo Fisher Scientific; C0015C) were maintained in Epilife media (Thermo Fisher: MEPI500CA) supplemented with HGKS (Thermo Fisher: S0015). To generate skin equivalents, 10^6 cells were seeded onto devitalized human dermis and maintained in an air-liquid interface for 7 days. Stratified epithelial tissue was then grafted onto 12-14 week old female NOD scid gamma mice (Jackson Laboratory: 005557). Bandages and sutures were removed 2 weeks after surgery and healthy grafts were harvested 10 days later.

METHOD DETAILS

Preparation of Devitalized Dermis

Cadaver human skin was acquired from the New York Firefighters Skin Bank (New York, New York, USA). Upon arrival at UC Irvine, the skin was allowed to thaw in a biosafety cabinet. Skin was then placed into PBS supplemented with 4X Pen/Strep, shaken vigorously for 5 minutes, and transferred to PBS supplemented with 4X Pen/Strep. This step was repeated two additional times. The skin was then placed into a 37°C incubator for 2 weeks. The epidermis was removed from the dermis using sterile watchmaker forceps. The dermis was washed 3 times in PBS supplemented with 4X Pen/Strep with vigorous shaking. The dermis was then stored in PBS supplemented with 4X Pen/Strep at 4°C until needed.

Primary Cell Isolation

Discarded and de-identified neonatal foreskins were collected during routine circumcision from UC Irvine Medical Center (Orange, CA, US). The samples were either processed for histological staining, single cell RNA-sequencing, or primary culture. No personal information was collected for this study. For primary cell isolation, fat from discarded and de-identified neonatal foreskins were removed using forceps and scissors and incubated with dispase epidermis side up for 2 hours at 37°C. The epidermis was peeled from the dermis, cut into fine pieces, and incubated in 0.25% Trypsin-EDTA for 15 minutes at 37°C and quenched with chelated FBS. Cells were passed through a 40µm filter, centrifuged at 1500rpm for 5 minutes, and the pellet resuspended in Keratinocyte Serum Free Media supplemented with Epidermal Growth Factor 1-53 and Bovine Pituitary Extract (Life Technologies; 17005042). Cells were either live/dead sorted using SYTOX

Blue Dead Cell Stain (ThermoFisher; S34857) for single cell RNA-sequencing or incubated at 37°C for culture.

Cell Sorting

Following isolation, cells were resuspended in PBS free of Ca^{2+} and Mg^{2+} and 1% BSA and stained with SYTOX Blue Dead Cell Stain (ThermoFisher; S34857). Samples were bulk sorted at 4ºC on a BD FACSAria Fusion using a 100µm nozzle (20 PSI) at a flow rate of 2.0 with a maximum threshold of 3000 events/sec. Following exclusion of debris and singlet/doublet discrimination, cells were gated on viability for downstream scRNA-seq.

Histology and Immunohistochemistry

Frozen tissue sections (10µm) were fixed with 4% PFA in PBS for 15 minutes. Following fixation, tissue sections were stained with Hematoxylin and Eosin following standard procedures. Sections were stained with Gill's III (Fisher Scientific; 22050203) for 5 minutes and Eosin-Y (Fisher Scientific; 22050197) for 1 minute. Tissue sections were visualized under a light microscope under 10x objective lens after mounting with Permount mounting media (Fisher Scientific; SP15-100). For immunostaining, tissue sections were fixed with 4% PFA in PBS for 15 minutes. 10% BSA in PBS was used for blocking. Following blocking, 5% BSA and 0.1% Triton X-100 in PBS was used for permeabilization. The following antibodies were used: chicken anti-KRT14 (1:500; BioLegend; SIG-3476), rabbit anti-KI67 (1:500; Abcam; ab15580), rabbit anti-COL17A1 (1:100; One World Labs; ap9099c), rabbit anti-KRT19 (1:250; Cell signaling; 13092), mouse anti-KRT15 (1:500; Santa Cruz; sc-47697), rabbit anti-VIM (1:500; Cell Signaling; D21H3), mouse anti-PSCA (1:500; Santa Cruz; sc-80654), mouse anti-FLG (1:500; Santa Cruz; sc-66192), mouse anti-DSG1 (1:500; Santa Cruz; sc-137164), mouse anti-SLUG (1:500; Santa Cruz; sc-166476), rabbit anti-KRT16 (1:500; Invitrogen; PA5-99172), rabbit anti-cCASP3 (1:500; Cell Signaling; 9579T), rabbit anti-KRT4 (1:500; Fisher Scientific; 16572-1-AP), rabbit anti-GLUT1 (1:500; Proteintech; 218291AP), rabbit anti-HIF1a (1:500; Proteintech; 501733175), and rabbit anti-LOR (1:500; Abcam; ab85679). Secondary antibodies included Alexa Fluor 488 (1:500; Jackson ImmunoResearch; 715-545-150, 711-545-152) and Cy3 AffiniPure (1:500; Jackson ImmunoResearch; 711-165-152, 111-165-003). Slides were mounted with Prolong Diamond Antifade Mountant containing DAPI (Molecular Probes; P36962). Confocal images were acquired at room temperature on a Zeiss LSM700 laser scanning microscope with Plan-Apochromat 20x objective or 40x and 63x oil immersion objectives. Images were arranged with ImageJ, Affinity Photo, and Affinity Designer.

Droplet-enabled Single Cell RNA-sequencing and Processing

Cell counting, suspension, GEM generation, barcoding, post GEM-RT cleanup, cDNA amplification, library preparation, quality control, and sequencing was performed at the Genomics High Throughput Sequencing Facility at the University of California, Irvine. Transcripts were mapped to the human reference genome (GRCh38) using Cell Ranger Version 3.1.0.

Quality Control Metrics Post-Cell Ranger Assessment

For downstream analyses, we kept cells which met the following filtering criteria per biological replicate per condition: >200 and <5000 genes/cell, and <10% mitochondrial gene expression. Genes that were expressed in less than 3 cells were excluded. Data were normalized with a scale factor of 10,000. Following downstream integration and clustering, one cluster in the In Vivo, GelHSE, and FibHSE integrated dataset, HSE-2, had an average of 469 unique genes expressed and 805 UMIs indicating that these are low quality cells. Similarly, one cluster in the In Vivo and Xenograft integrated dataset, XENO-4, had an average of 807 unique genes expressed and 1881 UMIs. This cluster was also excluded from downstream analysis.

Analysis and Visualization of Processed Sequencing Data

Seurat [142] and SoptSC [68] were implemented for analysis of scRNA-seq data in this study. Seurat was performed in R (version 4.2.1) and was applied to all the datasets in this study. To select highly variable genes (HVGs) for initial clustering of cells, we performed Principal Component Analysis on the scaled data for all genes included in the previous step. For clustering, we used the function FindClusters that implements Shared Nearest Neighbor modularity optimization-based clustering algorithm on 20 PC components. A nonlinear dimensionality reduction method, UMAP, was applied to the scaled matrix for visualization of cells in two-dimensional space using 20 PC components. The marker genes for every cluster compared with all remaining cells were identified using the FindAllMarkers function. For each cluster, genes were selected such that they were expressed in at least 25% of cells with at least 0.25-fold difference.

Pseudotime and Lineage Inference

Pseudotime and lineage analysis were performed using Monocle3 and SoptSC, respectively. Briefly, pseudotime was calculated as the shortest path distance between cells and root cell on the cell-to-cell graph constructed based on the similarity matrix. Root cell was identified by the user in Monocle3. Visualization of the cell trajectories was obtained using UMAP. Cell states were visualized using abstract lineage trees. Lineage trees are obtained by computing the minimum spanning tree of the cluster-to-cluster graph based on the shortest path distance between cells. Pseudotime was projected on the lineage tree such that the order of each state (cluster) was defined as the average distances between cells within the state and the root cell. The root cell for DPT was selected from the BAS-I cluster.

RNA Velocity

RNA velocity was estimated based on the spliced and unspliced transcript reads from the single-cell data. We followed the standard process of the velocyto pipeline to generate the spliced and unspliced matrices by applying velocyto.py to the data from the Cell Ranger output (outs) folder. Only interfollicular epidermal keratinocytes and the HSE unique keratinocytes were used to calculate velocity vectors. RNA velocity was estimated using the python package scVelo and then the velocity fields were projected onto the UMAP space produced by Seurat. Default settings were used for the rest of the parameters.

Probabilistic Cell-Cell Signaling Networks

The R package CellChat was used to infer, analyze, and visualize cell-cell communication from our scRNA-seq data. The preprocessed and normalized data from the Seurat objects were used as input for creating the CellChat objects. All known molecular interactions, including the core interaction between ligands and receptors with multi-subunit structure and additional modulation by cofactors, are integrated into a mass action-based model to quantify the communication probability between a given ligand and its cognate receptor. The signaling communication probability between two cell groups is modeled by considering the proportion of cells in each group across all sequenced cells. An option is provided for removing the potential artifact of population size when inferring cell-cell communication.

Cellular Entropy Estimation

Cellular Entropy (ξ) measures the likelihood that a cell will transition to a new state (i.e., from one cluster to another). Lower entropy values indicate that the cell remains in a steady state, while higher entropy values imply the cell inherits multiple state properties and is more likely to transition to a new state. Via the non-negative matrix factorization step in SoptSC, the probability of each cell assigned to each cluster is calculated.

EMT & Hypoxia Gene Modules

Gene modules were created using Seurat's AddModuleScore function and visualized using the FeaturePlot function. The genes used in each gene module were manually curated from literature with a focus on gene expression studies involving keratinocytes. All of the genes used in both gene modules along with the citations for the specific study that characterizes the gene's role in EMT and hypoxia can be found in Table S2.

QUANTIFICATION AND STATISTICAL ANALYSIS

Data are presented as the mean ± standard error of mean (SEM), as indicated. The sample sizes in each plot have been listed in the Results section and Figure Legends where appropriate. For differential gene expression analysis between cell clusters and data represented as violin plots, two-tailed Wilcoxon rank sum test was performed using R (https://www.r-project.org/). For comparison of cell population changes, a permutation test was performed using R. A significance threshold of $p < 0.01$ was used for defining marker genes of each cell cluster. For data presented in box or bar plots, an unpaired two-tailed Student's t-test was used when comparing two groups and a one-way ANOVA followed by Tukey's HSD was used when comparing three or more groups.

COMPETING INTERESTS

The authors declare no competing interests.